FH Aachen
University of Applied Sciences

Faculty of Aerospace Engineering

Master Thesis

Analysis of NEO Deflection Using Planetary Sunshade Sailcraft for Planetary Defence

Fabienne Seibert
3073229

supervised by
Prof. Dr.-Ing. Bernd Dachwald
co-supervised by
Dipl.-Ing. Jan Thimo Grundmann

August 21, 2023

Acknowledgements

I extend my sincere gratitude to my supervisors, Professor Bernd Dachwald and Mr. Thimo Grundmann, for their guidance and the freedom they granted during my research. Their support has not only greatly influenced the direction of this thesis but has been particularly significant due to our shared research interests, which made the realisation of this work possible.

My deepest and most sincere gratitude goes to my parents, Stefanie Lingstädt and Jörg Seibert, for their enduring support and unconditional love throughout my life. Your continuous belief in my choices have been fundamental to my journey, and I am profoundly thankful for your guidance and care.

I am also grateful for the incredible support of my dear friends, Tonya Quientes, Benedikt Geiben and Jonas Kremer. Your constant presence, encouragement, and shared moments of joy have been a lifeline throughout this journey. Your friendship has kept me grounded and inspired, and I am truly grateful for it.

Abstract

In response to the urgent climate crisis, the Planetary Sunshade Foundation envisions deploying a high number sunshade sailcraft, ranging from hundreds of millions to 1.5 billion units, near Sun-Earth Lagrange point 1. Assuming these sunshade sailcraft are already deployed in interplanetary space, this space-based geoengineering initiative, holds potential not only for addressing climate concerns but also for deflecting potentially hazardous asteroids by applying the *kinetic impactor energy* technique.

This study focuses on designing deflection mission scenarios for these sailcraft arrangements. The primary objective is to determine the required sailcraft mass and quantity within a specific time frame to achieve a deflection distance of two Earth radii. Target body for the analysis is the asteroid 2023 PDC, a fictitious asteroid which is designed for the scenario within the 8^{th} Planetary Defence Conference 2023. A hybrid approach is employed to find the best sailcraft trajectories among the analysed scenarios. Initial deflection simulations using *Poliastro*, a Python library for astrodynamics, while InTrance, integrating neural networks, drives the optimisation process. This methodology is applied to two distinct sunshade sailcraft configurations introduced by Fuglesang et al. in [32].

The findings demonstrate a deflection efficiency of 10 metres per kilogram impacting sail mass for the first sailcraft arrangement and 5 metres per kilogram for the second. In contrast the analytically approximated case achieves an efficiency of 1.5 metres per kilogram. This investigation underscores the substantial impact of the applied launch window analysis beyond extended deflection time on enhancing efficiency. Therefore the significant mass in interplanetary space, a result of the planetary sunshade deployment, provides a strategic edge for the kinetic energy impactor technique.

Zusammenfassung

Angesichts der drängenden Klimakrise plant die Planetary Sunshade Foundation die Ausbringung einer großen Anzahl von Sonnensegeln, die von mehreren hundert Millionen bis zu 1,5 Milliarden Einheiten reicht, nahe dem Sonne-Erde-Lagrange-Punkt 1. Angenommen, diese Sonnensegel sind bereits im interplanetaren Raum im Einsatz, birgt diese weltraumbasierte Geoengineering-Initiative nicht nur das Potenzial, Klimaprobleme anzugehen, sondern auch potenziell gefährliche Asteroiden durch Anwendung der *Kinetic Energy Impactor* Methode abzulenken.

Diese Studie konzentriert sich darauf, Abwermissionen für diese Sonnensegel-Anordnungen zu entwerfen. Das Hauptziel ist es, die erforderliche Masse und Anzahl der Sonnensegel innerhalb eines bestimmten Zeitraums zu bestimmen, um eine Ablenkungsdistanz von zwei Erdradien zu erreichen. Zielkörper für die Analyse ist der Asteroid 2023 PDC, ein fiktiver Asteroid, der für das Szenario der 8. Planetary Defence Conference 2023 entworfen wurde.

Ein hybrider Ansatz wird verwendet, um die besten Transferbahnen für die Segel zu finden. Anfängliche Ablenkungssimulationen werden unter Verwendung von *Poliastro*, einer Python-Bibliothek für Astrodynamik, durchgeführt, während *InTrance*, das neuronale Netzwerke integriert, den Optimierungsprozess vorantreibt. Diese Methodik wird auf zwei verschiedene Segelkonfigurationen angewendet, die von Fuglesang et al. in [32] vorgestellt wird.

Die Ergebnisse zeigen eine Ablenkungseffizienz von 10 Metern pro Kilogramm einschlagende Segelmasse für die erste Segelanordnung und 5 Meter pro Kilogramm für die zweite. Im Gegensatz dazu erzielt der analytisch approximierte Fall eine Effizienz von 1.5 Metern pro Kilogramm. Diese Untersuchung unterstreicht die erhebliche Auswirkung der angewendeten Bahnanalyse über die verlängerte Ablenkungszeit hinaus auf die Steigerung der Effizienz. Daher bietet die signifikante Masse im interplanetaren Raum, die aufgrund der Bereitstellung der Sonnensegel entsteht, einen strategischen Vorteil für die Abwehr von potenziell gefährlichen Asteroiden.

Contents

List of Figures

List of Tables

Nomenclature

Latin letters

A	m^2	area
a	m	semi-major axis
a	m/s^2	acceleration
a_c	m/s^2	characteristic acceleration
B	[-]	non-Lambertian coefficient
C_3	m^2/s^2	hyperbolic excess energy
d	[m]	diameter
e	[-]	eccentricity
e	[-]	coefficient of restitution
E	J	orbital energy
F	N	thrust force
$\boldsymbol{f}$	[-]	thrust force unit vector
f	[°]	true anomaly
H	[-]	absolute magnitude
h	m^2/s	specific angular momentum
I	Ns	momentum transferred to the asteroid
i	[-]	inclination
M	kg	asteroid mass
M	[°]	mean anomaly
m	kg	S/C or sailcraft mass
$\boldsymbol{n}$	[-]	sailcraft normal vector
P	s	orbit period
P	N	solar radiation pressure
p	Ns	momentum induced by the S/C
Q	W/m^2	solar radiation flux
r	m	solar distance
S	[d]	synodic period
s	[-]	specular reflection coefficient
T	K	sailcraft temperature
t	s	time
v	m/s	velocity
v_∞	m/s	hyperbolic excess velocity

Greek letters

α	[°]	light incidence angle
β	[-]	momentum enhancement factor
γ	[°]	thrust clock angle
δ	[°]	sailcraft clock angle
ϵ	[-]	emissivity
θ	[°]	elevation Angle
θ	[°]	transfer Angle
λ	[-]	lightness Number
ζ	[°]	thrust cone angle
η	[-]	sailcraft efficiency parameter
μ	m^3/s^2	gravitational parameter
ξ	m	deflection distance
ρ	kg/m^3	density
ρ	[-]	reflection coefficient
σ	[-]	sailcraft loading
τ	[-]	reflectivity
φ	[°]	azimuth angle
Ψ	[-]	reflection function
Ω	[°]	longitude of the ascending node
ω	[°]	argument of perigee

Subscripts

$(\,)_{\mathrm{A}}$	asteroid
$(\,)_{\mathrm{b}}$	back side
$(\,)_{\mathrm{E}}$	Earth
$(\,)_{\mathrm{e}}$	asteroid surface ejecta
$(\,)_{\mathrm{eff}}$	effective
$(\,)_{\mathrm{f}}$	front side
$(\,)_{\mathrm{i}}$	inner body
$(\,)_{\mathrm{imp}}$	impact
$(\,)_{\mathrm{G}}$	gravitational
$(\,)_{\mathrm{o}}$	outer body
$(\,)_{\mathrm{PDC23}}$	asteroid 2023 PDC
$(\,)_{\mathrm{PL}}$	payload
$(\,)_{\mathrm{S}}$	Sun
$(\,)_{\mathrm{s}}$	sailcraft structure
$(\,)_{\mathrm{sail}}$	solar sailcraft
$(\,)_{\mathrm{sc}}$	spacecraft
$(\,)_{\mathrm{shade}}$	planetary sunshade arrangement

Constants

au	=	$149597870.6934\,\mathrm{km}$	astronomical unit
c	=	$299792.458\,\mathrm{km/s}$	speed of light in vacuum
g_0	=	$9.80665\,\mathrm{m/s^2}$	Gravitational acceleration
$\mathcal{G}$	=	$6.6743 \times 10^{-20}\,\mathrm{km^3/(kg\,s^2)}$	gravitational constant
μ_S	=	$132\ 712\ 439\ 935\,\mathrm{km^3/s^2}$	gravitational parameter of the Sun
$R_\oplus$	=	$6.96342 \times 10^6\,\mathrm{m}$	Radius of the Earth
S_0	=	$1368\ \mathrm{W/m^2}$	solar constant
$\tilde{\sigma}$	=	$5.67051\ \times 10^{-8}\,\mathrm{W/(m^2K^4)}$	Stefan-Boltzmann constant

Acronyms & Abbreviations

DART	Double Asteroid Redirection Test
DLR	German Aerospace Centre
DES	Differential Equation System
EMB	Earth-Moon Barycentre
ESA	European Space Agency
IDR	Ideal Reflection Model
InTrance	Intelligent Trajectory optimisation using neurocontroller evolution
KEI	Kinetic Energy Impactor
$\mathrm{L_1}$	Sun-Earth Lagrange Point 1
MOID	Minimum Orbital Intersection Distance
MJD	Modified Julian Date
NEA	Near Earth Asteroid
NED	Nuclear Explosive Device
NEO	Near Earth Object
NPR	Non-Perfect Reflection
PDC	Planetary Defence Conference
PHA	Potentially Hazardous Asteroids
PSF	Planetary Sunshade Foundation
CDR	Carbon Dioxide Removal
S/C	Spacecraft
SNPR	Simplified Non-Perfect Reflection
SOI	Sphere Of Influence
SRM	Solar Radiation Management
SRP	Solar Radiation Pressure
TRL	Technology Readiness Level

Chapter 1

Introduction

1.1 Motivation

The pressing issue of climate change has reached a critical juncture, demanding immediate and innovative solutions to mitigate its far-reaching impacts. Rising temperatures, extreme weather events, and the accelerated loss of biodiversity pose significant challenges for the future of our planet [29]. According to the latest IPCC report, it is unlikely that the +1.5°C target for the limitation of global warming can be achieved by the reduction of emissions on the ground alone [37]. In this context, novel technologies and approaches including *space-based geoengineering* are being explored.

One such concept gaining attention is the deployment of solar radiation management from space to address the severe effects of climate change on Earth without direct interference with the planet's atmosphere and ecosystems [35, 52]. For this purpose, the *Planetary Sunshade Foundation* has proposed a plan to counteract global warming by deploying over one billion sunshield sailcraft, each roughly the size of a football field, as a large "occulting disk" [63]. These sailcraft would be positioned near the Sun-Earth Lagrange point 1 (L_1) [32]. In addition to their primary purpose of mitigating the effects of global warming, this deployment offers the potential for an additional benefit: serving as a viable option for planetary defence by deflecting *potentially hazardous asteroids* (PHA).

Beside global warming, asteroid impacts represent an ongoing danger and - according to their size - could cause severe damage to our planet. A notable example of a PHA is (99942) Apophis, which is expected to have a Earth-flyby in 2029, passing even closer than the orbit of geostationary satellites. This close approach could result in orbital resonance with respect to the Earth, raising concerns about its future trajectory and potential impact risk [2]. In general, the number of known PHAs located in the solar system amounts to roughly 2000 [49]. Therefore the implementation of the planetary sunshade sailcraft might not only be useful for the fight against global warming but also represents a promising approach for the protection of planet Earth from asteroids.

Assuming that a planetary sunshade has already been successfully deployed, the high mass already present in interplanetary space provides a significant advantage for the

application of the *kinetic energy impactor* (KEI) technique. Since many "impact-sails" are available, a high impact success rate per sail is not mandatory, which significantly relaxes requirements regarding sailcraft control right before the impact. The high available mass also allows relaxations concerning the specific impact energy required per sail, reducing the lead time, and consequently shortening the overall trajectory. This approach allows a deviation from the conventional design paradigms that prioritise minimal start mass and enhanced energy efficiency, underscoring the transformative nature of using a substantial mass of sunshade sailcraft for kinetic energy impactor missions.

This work analyses the influence of re-directing a large number of sunshade sailcraft as kinetic impactors towards a fictitious asteroid, 2023 PDC, within the scenario created for the *Planetary Defence Conference 2023* (PDC 2023).

The interconnected research areas of climate control and PHA defence, among other critical areas, play a fundamental role in the preservation of humanity's only known habitat to date - planet Earth.

1.2 Objectives

This study focuses on designing deflection mission scenarios for two distinct sunshade sailcraft configurations introduced by Fuglesang et al. in [32]. The primary objective is to determine the required sailcraft mass and quantity within a specific time frame to achieve a deflection distance of two Earth radii. Target body for the analysis is the asteroid 2023 PDC, a fictitious asteroid which is designed for the scenario within the 8th Planetary Defence Conference 2023. A hybrid approach is employed to find the best sailcraft trajectories among the analysed scenarios. Initial deflection simulations using *Poliastro*, a Python library for astrodynamics, while InTrance, integrating neural networks, drives the optimisation process.

Combining the capabilities of the Poliastro library with the neural network-based optimsation approach employed by InTrance, sailcraft trajectories, which entail an enhanced deflection efficiency, can be efficiently explored and identified. This approach increases the deflection capabilities and reduces mission constraints. It enables to unlock the full potential of the planetary sunshade sailcraft as a means of effective asteroid deflection, contributing to the ongoing efforts in planetary defence and safeguarding our planet from potentially hazardous asteroids.

Chapter 2

The Physics Behind Solar Sailing

In general, solar sails are innovative propulsion systems that utilise lightweight and reflective materials, like aluminised Mylar, to capture and reflect light, generating a small yet constant thrust force. This unique propulsion approach is classified as a *low-thrust propulsion* technique [19, 51, 78]. Although the concept of solar sails traces back to the 17^{th} century, remarkable progress has been made in recent decades. Notable experimental missions, such as Japan's IKAROS and The Planetary Society's LightSail projects, have demonstrated the feasibility and potential of solar sailing [43, 75].

When it comes to employing solar sails for asteroid deflection, the initial crucial step is to approach the target asteroid. Therefore, a fundamental requirement for designing and analysing trajectories for such missions is a comprehensive understanding of the physical and dynamic principles underlying solar sailing. This chapter deals with the fundamental physical background of solar sailing, providing insights essential for successful asteroid deflection missions.

2.1 Solar Radiation Pressure

To begin with, solar sailcraft are propulsion systems using *solar radiation pressure* (SRP) to propel spacecraft through space. Instead of relying on traditional rocket engines that require fuel, solar sailcraft harness the momentum imparted by photons on the sail. Therefore, the total acceleration vector $\ddot{\boldsymbol{r}}$ of the solar sailcraft is determined by the combined effects of two significant factors: the acceleration vector $\boldsymbol{a}_{\text{SRP}}$ induced by the SRP and the gravitational acceleration vector $\boldsymbol{a}_{\text{G}}$ exerted by the Sun (or other perturbing bodies) in a two body problem [20, 16].

$$\ddot{\boldsymbol{r}} = \boldsymbol{a}_{\text{SRP}} + \boldsymbol{a}_{\text{G}}. \tag{2.1}$$

Consequently, in order to accurately determine the orbital motion of a solar sailcraft, it is necessary to identify the corresponding acceleration induced by the SRP, as well as the underlying physical principles governing this phenomenon.

Similar to other forms of spacecraft propulsion, solar sail technology is founded upon Newton's third law, which states that for every action, there is an equal and opposite

reaction. [16] This is achieved via the SRP generated by the incoming photons from solar radiation. These photons impinge upon the highly reflective sailcraft surface, transferring their momentum to the sail and inducing a continuous acceleration [51]. When denoting the solar radiation flux as Q and the speed of light in vacuum as c, the transfer of momentum through the solar radiation pressure through absorption P can be expressed as

$$P = \frac{Q}{c} \tag{2.2}$$

In addition, the radiation flux of a point light source is inversely proportional to the square of the distance. Equation (2.3) defines the SRP exerted at a distance r from the Sun,

$$P = \frac{S_0}{c}\left(\frac{r_0}{r}\right)^2 = 4.563\,\mu N/\mathrm{m}^2 \cdot \left(\frac{r_0}{r}\right)^2 \tag{2.3}$$

where $r_0 = 1\,\mathrm{au}$ is the mean solar distance of Earth and S_0 is the solar constant which equals $1368\,\mathrm{W/m^2}$ [19, 51].

2.1.1 Sailcraft Orientation & Force Vector

In order to establish a robust framework that enables a precise understanding of the sailcraft motion and behaviour in response to the SRP-induced acceleration, two unit vectors are introduced: the *sail normal vector* ($\boldsymbol{n}$) and the *thrust force unit vector* ($\boldsymbol{f}$) [20, 19]. The sailcraft normal vector, denoted as $\boldsymbol{n}$, is a unit vector that is perpendicular to the surface of the sailcraft and points away from the Sun. In Figure 2.1, the definition of $\boldsymbol{n}$ can be observed, which relies on two key parameters: the *sail cone angle* (α) and the *sail clock angle* (δ). The sail cone angle, determines the angle between the radial

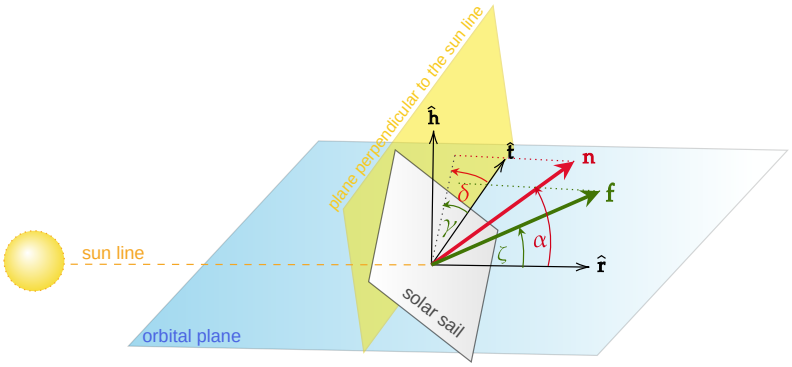

Figure 2.1: The visualisation based on the representation in [19] and shows the sail normal vector $\boldsymbol{n}$ and the thrust force unit vector $\boldsymbol{f}$ on a non-perfectly reflecting solar sail.

unit vector $\hat{\boldsymbol{r}}$ (and the Sun-line) and the sail normal vector. On the other hand, the sail clock angle is measured between the projection of $\boldsymbol{n}$ and the transversal unit vector $\hat{\boldsymbol{t}}$. The latter lies on the plane perpendicular to the Sun-line, see Figure 2.1. [51, 19] This combined information allows a precise definition of the sailcraft's orientation using the

sail normal vector [20, 51]. The thrust unit vector points along the direction of the thrust force and is similar defined like the sail normal vector. The angles which determine the direction of $\boldsymbol{f}$ are called the *thrust cone angle* (ζ) and the *thrust clock angle* (γ) [20]. If the sail normal vector and the thrust force unit vector point into the same direction ($\boldsymbol{f} = \boldsymbol{n}$) then the sail clock angle and the thrust clock angle coincide ($\delta = \gamma$), and similarly, the sail cone angle and the thrust cone angle are also identical ($\alpha = \zeta$) [20]

2.1.2 Different Solar Radiation Pressure Force Models

Within the field of SRP force modelling, various approaches have been developed, with three models emerging as particularly significant: the *ideal reflection model* (IDR), the *simplified non-perfect reflection model* (SNPR) and the *non-perfect reflection model* (NPR) [19]. All three models are distinguished according to their reflection efficiency and briefly described in this section [19].

Ideal Reflection Model

The IDR model serves as a simplified approximation, as it assumes the solar sail to be an ideal reflector. In Figure 2.2, it can be seen that by considering the light incidence angle α, the resulting force vector from the incoming solar radiation and its reflection can be divided into two components: the force vector $\boldsymbol{F}_{\text{SRP}}$ resulting from the incident radiation, denoted as $\boldsymbol{F}_{\text{i}}$, and the force vector resulting from the reflected radiation, denoted as $\boldsymbol{F}_{\text{r}}$. Consequently, the thrust force vector can be determined by equation (2.2)

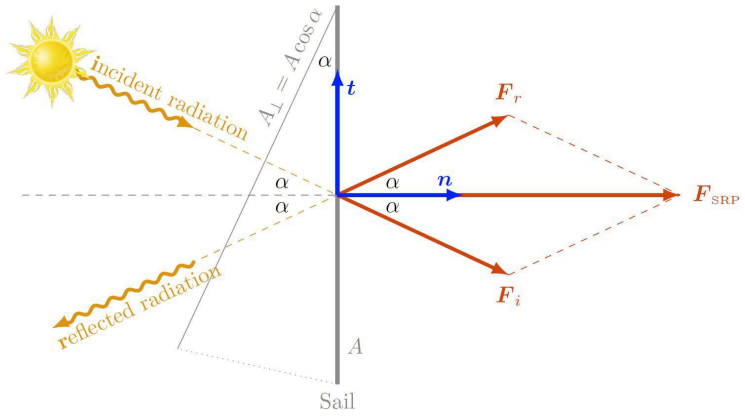

Figure 2.2: Representation of the SRP force on an ideal solar sail [19].

$$\boldsymbol{F}_{\text{SRP}} = 2PA\cos^2\alpha\,\boldsymbol{n}\,, \tag{2.4}$$

where P is the corresponding solar radiation pressure which is multiplied by the factor 2 due to the fact that the incoming photons are absorbed and then re-emitted as reflected photons, resulting in a double transfer of momentum. In the particle model, this process

involves absorbing the energy of the incoming photon and using it to generate the energy of the outgoing reflected photon, effectively transferring momentum twice from the photons. Furthermore, A defined as the area of the sailcraft [19, 20]. Important to note, for the IR case, the thrust force unit vector points always in the same direction as the sail normal vector ($\boldsymbol{f} = \boldsymbol{n}$) [20].

Non-Perfect Reflection Model

In reality, a solar sail is never a perfect reflector. Therefore, the NPR model provides a more precise depiction of the optical characteristics of the sailcraft. By considering coefficients describing the reflection, absorption, emission, and transmission behaviour specific to the sailcraft, calculations using the NPR approach yield significantly more accurate results. These optical parameters, along with their interrelationships governing the determination of $\boldsymbol{F}_{\mathrm{SRP}}$, are derived and discussed in [20] with comprehensive detail. Figure 2.3 shows the SRP on a non-perfectly reflecting solar sail, where ϕ is the centre line angle between the thrust force vector $\boldsymbol{f}$ and the sail normal vector $\boldsymbol{n}$. [19] When $\mathcal{P} =$

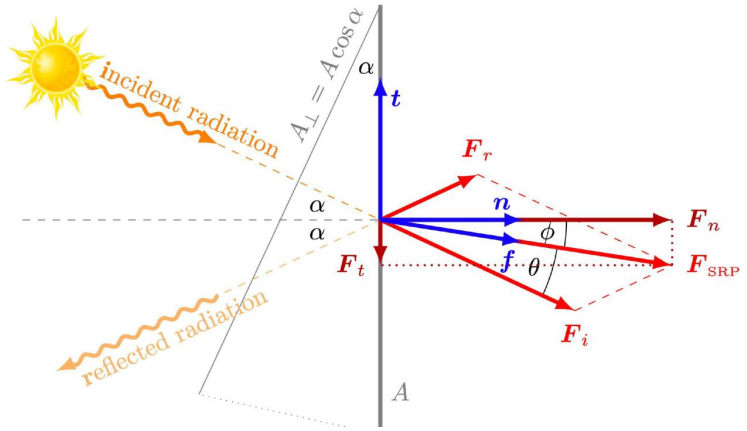

Figure 2.3: Representation of the SRP force on a non-perfectly reflecting solar sail [19].

$(\rho, s, \epsilon_{\mathrm{f}}, \epsilon_{\mathrm{b}}, B_{\mathrm{f}}, B_{\mathrm{b}})$ represents the set of corresponding optical parameters, the function $\Psi(\alpha, \mathcal{P})$ incorporates these parameters with α and can be employed to determine the thrust force resulting from SRP [26]. The reflection coefficient is denoted by ρ, and the specular reflection-factor is represented by s. The emission coefficients (ϵ) of the front and back sides are indicated by "f" and "b", respectively. Additionally, B_{f} and B_{b} represent the non-Lambertian coefficients[1] of the front and back sides, respectively, which describe the angular distribution of the emitted and diffusely reflected photons[2].

$$\boldsymbol{F}_{\mathrm{SRP}} = 2PA\cos\alpha\Psi(\alpha, \mathcal{P})\boldsymbol{f} \tag{2.5}$$

[1]The non-Lambertian coefficient describes how light is reflected unevenly from a given surface compared to the idealised Lambertian model [47].

[2]The parameters and their labelling are taken over from [26]

To describe the corresponding reflection behaviour accurately, the function Ψ can be separated in a transversal and a normal component, characterised with the indices "n" and "t" [20].

$$\Psi(\alpha, \mathcal{P}) = \sqrt{\Psi_n^2(\alpha, \mathcal{P}) + \Psi_t^2(\alpha, \mathcal{P})} \tag{2.6}$$

The single components of ψ can be expressed with the optical parameters and the sail cone angle as follows:

$$\Psi_n = \frac{1}{2}(1 + s\rho)\cos\alpha + \frac{1}{2}\left(B_\mathrm{f}(1-s)\rho + (1-\rho)\frac{\epsilon_\mathrm{f}B_\mathrm{f} - \epsilon_\mathrm{b}B_\mathrm{b}}{\epsilon_\mathrm{f} + \epsilon_\mathrm{b}}\right) \tag{2.7}$$

$$\Psi_t = \frac{1}{2}(1 - s\rho)\sin\alpha \tag{2.8}$$

Simplified Non-Perfect Reflection Model

Regarding the SNPR model, the calculations compensate the imperfect reflection through the use of a global sail efficiency parameter η (equation (2.9)). While this simplifies the analysis, it does not account for the optical properties of the sail as precisely as the NPR model. [20]

$$\boldsymbol{F}_\mathrm{SRP} = 2\eta PA\cos^2\alpha\,\boldsymbol{n} \tag{2.9}$$

Model Comparison

To illustrate the distinctions among the three aforementioned force models, the concept of "SRP force bubbles" is employed, see Figure 2.4. This visualisation, introduced by Dachwald in [20], offers a graphical representation of the evaluation of the SRP force vector based on the orientation of the sailcraft. The endpoint of the thrust vector is restricted to reside within a boundary known as the "SRP force bubble" [19]. It can be observed that the simplified model shares the same overall shape as the ideal model, leading to identical trajectory analyses between the two models. The decrease in η for the SNPR case simply results in an offset, which can be compensated by adjusting the sail area accordingly. However, the non-perfectly reflecting model exhibits a different "bubble-shaped" profile, setting it apart from the other two models. As a result, the SNPR and IR models are considered as representatives of *ideal sails*, while the NPR model represents the application of *non-ideal sails*. [20]

In the ideal sail model, the transverse component of the SRP thrust force is disregarded, resulting in the thrust force unit vector and the sail normal vector pointing in the same direction. This assumption implies that the thrust cone angle is presumed to be perfectly aligned with the sail cone angle, as discussed earlier in Section 2.1.1. However, as the light incidence angle increases, deviations between these angles become more significant. Consequently, for the NPR model, the thrust force vector is additionally constrained concerning its direction. [20] Considering the limitations inherent in the simplified and ideal SRP force models, it is advisable to utilize them only during the initial stages of mission analysis. Therefore, the NPR SRP force model is employed for the calculations within *InTrance* in Section 6.4 [20]. An overview of the three different SRP force models can be taken from Table 2.1.

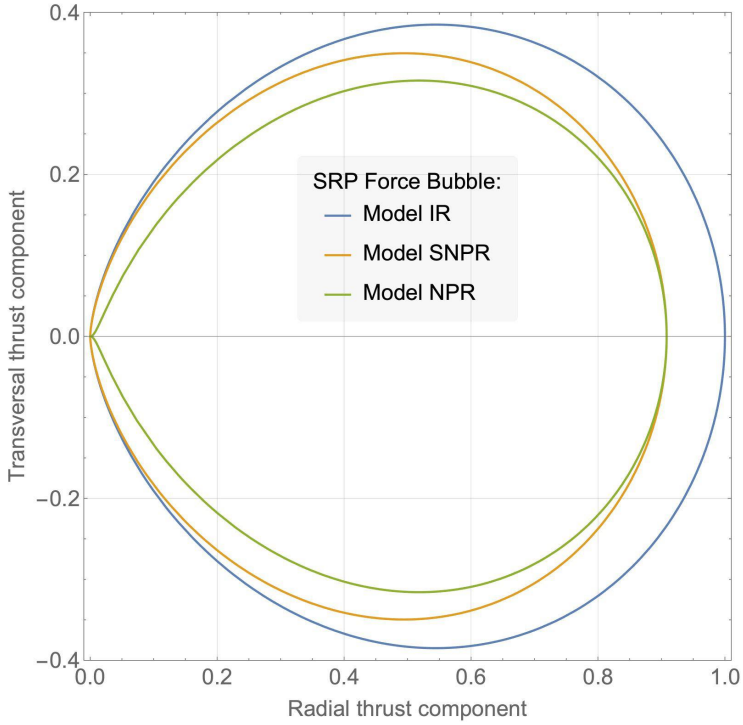

Figure 2.4: The SRP force bubble representation for the IR, SNPR and the NPR model. [19, 20]

Table 2.1: Overview of the different SRP force models [19, 20]

Ideal Reflection Model (IR)	Simplified Non-Perfect Reflection Model (SNPR)	Non-Perfect Reflection Model (SNPR)
$\boldsymbol{F}_{\mathrm{SRP}} = 2PA\cos^2\alpha\,\boldsymbol{n}$	$\boldsymbol{F}_{\mathrm{SRP}} = 2\eta PA\cos^2\alpha\,\boldsymbol{n}$	$\boldsymbol{F}_{\mathrm{SRP}} = 2PA\cos\alpha\Psi\boldsymbol{f}$
• highly simplified model, assuming a perfect reflector • just for early preliminary studies	• global reflection efficiency factor η • just for early preliminary studies	• consideration of optical parameters of the sail by the function $\Psi(\alpha, \mathcal{P})$ • appropriate for a precise trajectory analysis

2.2 Metrics for Sailcraft Design & Performance

When considering the parameters relevant to solar sailcraft performance, one of the most fundamental component is the *characteristic acceleration* (a_c). This parameter plays a crucial role in determining the transfer time to a specific target object, as well as establishing the feasibility of achieving certain classes of orbits [51]. The characteristic

acceleration represents the solar radiation pressure acceleration encountered by a solar sail when it is aligned perpendicular to the Sun-line ($\boldsymbol{n} = \hat{\boldsymbol{r}}$) at a solar distance of one astronomical unit (au) [51]. The value of a_c can be determined with equation (2.10), where P_eff represents the *effective* SRP acting on the sail. In other words, the magnitude of P_eff includes all relevant optical parameters of the sail within the scope of the NPR model [20].

$$a_\mathrm{c} = \frac{2P_\mathrm{eff}}{\sigma} \tag{2.10}$$

Here, σ represents the *sailcraft loading*, which depends on the total sailcraft mass m and its area A (Equation (2.11)).

$$\sigma = \frac{m}{A} \tag{2.11}$$

The total mass of the sailcraft can be further divided into the mass of the sailcraft assembly, denoted as m_S, and the payload mass, defined as m_PL, which represents the remaining mass attributed to the sail and yields [19]

$$\sigma = \frac{m_\mathrm{S} + m_\mathrm{PL}}{A} = \sigma_\mathrm{S} + \frac{m_\mathrm{PL}}{A} \tag{2.12}$$

Consequently, $\sigma_\mathrm{S} = \frac{m_\mathrm{S}}{A}$ is the assembly loading, which includes the propulsion system of the sailcraft and therefore the sail film and all necessary devices for its storage and deployment [20, 51]. Another important parameter for the performance assessment of a solar sailcraft is the *lightness number* λ. The lightness number represents the relationship between the characteristic acceleration of the sail and the gravitational acceleration of the Sun at 1 au ($a_0 = \frac{\mu_\mathrm{S}}{r_0^2}$), see equation (2.13) [51, 20].

$$\lambda = \frac{a_\mathrm{c}}{a_0} \tag{2.13}$$

2.2.1 Sailcraft Temperature

The successful implementation of an interplanetary mission using a solar sailcraft relies significantly on the material properties of the sail membrane. Critical among these factors is the consideration of temperature limits to ensure the sail's optimal performance and structural integrity during the mission. In this regard, polyimide films like Kapton® have emerged as a promising option for the double-sided coating of solar sailcraft due to their notable radiation resistance [86, 20].

To ensure the long-term viability of the solar sail, it is imperative to maintain its temperature within a specific and well-defined range. Typically, a temperature range of 520 K to 570 K is deemed suitable for safe operation [86]. This temperature constraint also has implications for the sailcraft's closest distance to the Sun, as exceeding the specified temperature limits may lead to material degradation or mechanical failures [22]. The equilibrium temperature (T) of the sailcraft at a given distance from the Sun (r) can be calculated using the Stefan-Boltzmann constant ($\tilde{\sigma} = 5.67051 \times 10^{-8}\,\mathrm{W/(m^2 K^4)}$) and the

following equation [22].

$$T = \left(\frac{1-\rho}{(\epsilon_{\mathrm{f}} + \epsilon_{\mathrm{b}})} \left(\frac{S_0}{\tilde{\sigma}} \right) \left(\frac{r_0}{r} \right)^2 \cos\alpha \right)^{\frac{1}{4}} \tag{2.14}$$

The light incidence angle α within the equation reveals that the temperature of a solar sailcraft's surface also depends on its orientation relative to the Sun [19]. This aspect requires consideration in steering and attitude control to optimise mission performance and longevity. Various strategies, such as thermal coatings and active cooling systems, are used to manage temperature fluctuations and ensure successful solar sail missions. Therefore, understanding the specific thermal load on the sailcraft throughout its interplanetary journey enables the optimisation of the sailcraft's trajectory and orientation.

2.3 Solar Sailcraft Orbital Dynamics

According to equations (2.5) and (2.13), the SRP force acting on a sailcraft can also be derived as

$$\boldsymbol{F}_{\mathrm{SRP}} = \lambda \frac{\mu_{\mathrm{S}} m}{r^2} \cos^2\alpha \boldsymbol{n} \tag{2.15}$$

Dividing this force by the sailcraft mass yields the corresponding acceleration a_{SRP} [20, 19]. Upon substituting the detailed expressions of a_{SRP} and a_{G} into equation (2.1), the total resulting acceleration can be determined as follows:

$$\ddot{\boldsymbol{r}} = \lambda \frac{\mu_{\mathrm{S}}}{r^2} \cos^2\alpha\, \boldsymbol{n} - \frac{\mu_{\mathrm{S}}}{r^2} \hat{\boldsymbol{r}} \tag{2.16}$$

which represents the respective *equation of motion* (EoM) for the NPR sail model. [51, 20] By solving for n using the unit vectors $\hat{\boldsymbol{r}}$, $\hat{\boldsymbol{h}}$, and $\hat{\boldsymbol{t}}$ it can be deduced

$$\boldsymbol{n} = \cos\alpha \hat{\boldsymbol{r}} + \cos\delta \sin\alpha \hat{\boldsymbol{t}} + \sin\delta \sin\alpha \hat{\boldsymbol{h}} \tag{2.17}$$

and the direction of the thrust force unit vector is then given by equation (2.17) [51].

$$\boldsymbol{f} = \cos\zeta \hat{\boldsymbol{r}} + \cos\gamma \sin\zeta \hat{\boldsymbol{t}} + \sin\gamma \sin\zeta \hat{\boldsymbol{h}} \tag{2.18}$$

2.3.1 Equations of Motion for Solar Sailcraft

The vector equation of motion can now be decomposed into scalar components using a suitable coordinate system, such as spherical polar coordinates [51]. In this context, the radial position vector $\boldsymbol{r}$, the elevation angle θ, and the azimuth angle ϕ are introduced (see Appendix A.2) [51, 20]. The resulting equations of motion can be expressed as follows:

$$\ddot{r} = r\dot{\theta}^2 + r\dot{\varphi}^2 \cos^2\theta - \frac{\mu_{\mathrm{S}}}{r^2} + \lambda \frac{\mu_{\mathrm{S}}}{r^2} \cos^3\alpha \tag{2.19}$$

$$\ddot{\varphi} = -\frac{2\dot{r}\dot{\varphi}}{r} + 2\dot{\varphi}\dot{\theta}\tan\theta + \lambda\frac{\mu_{\mathrm{S}}}{r^3\cos\theta}\cos^2\alpha\sin\alpha\sin\delta \tag{2.20}$$

$$\ddot{\theta} = -\frac{2\dot{r}\dot{\theta}}{r} - \dot{\varphi}^2\sin\theta\cos\theta + \lambda\frac{\mu_{\mathrm{S}}}{r^3}\cos^2\alpha\sin\alpha\cos\delta \tag{2.21}$$

As a result, the motion of an ideal reflecting solar sailcraft in spherical polar coordinates is described by these three second-order differential equations (DES) [20].

2.3.2 Interplanetary Trajectories

To reach PHAs, a fundamental understanding of the orbital dynamics governing interplanetary trajectories is essential. The interplanetary mission design to reach the asteroid is primarily defined by the initial position of the departure body relative to the target asteroid [18]. The optimal scenario arises when the target asteroid is positioned directly opposite the departure location, leading to the shortest possible time of flight (TOF). This outcome is influenced by the fact that transfers exhibiting the *Hohmann* geometry demand the least energy for their execution. The time between such constellations can be described using the synodic period S, which is calculated as:

$$S = \left(\frac{1}{P_{\mathrm{i}}} - \frac{1}{P_{\mathrm{o}}}\right)^{-1} \tag{2.22}$$

where P_{i} is the orbital period of the inner body (e.g., Earth), and P_{o} is the orbital period of the outer body (e.g., the asteroid) [18, 16]. It's worth noting that for near-Earth asteroids with orbital sizes close to Earth's (semi-major axis ≈ 1 au), the synodic period S can become very long.

Additionally, three trajectory types are distinguished based on the transfer angle $\Delta\theta$. A trajectory is classified as type I if the transfer angle is greater than 180°, type II if it is below 180°, and type III if $\Delta\theta > 360°$ [18] (Figure 2.5). When considering a solar sail starting in an initial orbit around Earth, it must leave Earth's sphere of influence (SOI) to achieve an interplanetary transfer to the asteroid. The velocity with which the sail leaves Earth's SOI is known as the *hyperbolic excess velocity* $\boldsymbol{v}_\infty$ [18]. It is defined as the heliocentric velocity difference between the departure planet (Earth in this example) $\boldsymbol{v}_{\mathrm{E}}$ and the velocity of the sailcraft in the transfer ellipse $\boldsymbol{v}_{\mathrm{sc}}$.

$$\boldsymbol{v}_\infty = \boldsymbol{v}_{\mathrm{sc}} - \boldsymbol{v}_{\mathrm{E}} \tag{2.23}$$

Consequently, the hyperbolic excess energy is given by $C_3 = |\boldsymbol{v}_\infty|^2$, reflecting the specific energy associated with the sailcraft's escape from Earth's gravitational influence [18]. C_3 is generally provided by the launch vehicle, which brings the according spacecraft into the transfer orbit [18]. Furthermore, during an interplanetary mission, the trajectory can be analytically approximated using the *patched conic approximation*[3] [18]. This approximation divides the trajectory into different segments, each governed by the

[3]See Appendix B.1 for a further explanation of orbit and trajectory shapes.

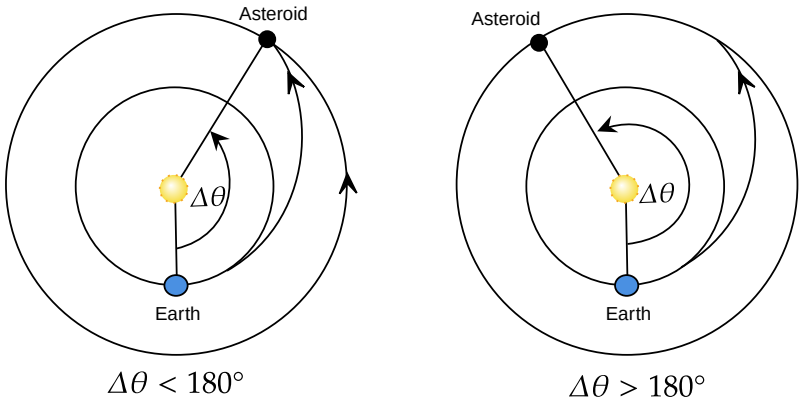

Figure 2.5: Visualisation of the transfer angle for two orbital constellations, adapted from [18].

gravitational influence of a specific celestial body. Initially, the sailcraft operates within Earth's SOI, where Earth's gravitational force dominates the trajectory. Once the sailcraft leaves Earth's SOI with an *hyperbolic* orbit and enters interplanetary space, it is primarily influenced by the gravitational field of the Sun, and the trajectory can be approximated as an *elliptical* orbit around the Sun, known as a *Hohmann transfer* orbit [18]. To optimise the mission design, factors like the specific launch window, positions of the target asteroid and Earth, and propulsion availability for trajectory adjustments must be carefully considered. Solar sails introduce the complexity of solar radiation pressure, which significantly affects the spacecraft's acceleration and trajectory.

Chapter 3

Planetary Sunshield: Space-Based Geoengineering for Climate Control

3.1 Space Based Geoengineering: Advantages & Moral Classification

Space-based geoengineering is an emerging field of research that aims to mitigate the impacts of climate change by modifying Earth's climate system from outer space. This approach always involves the implementation of a system outside the Earth's atmosphere, aimed at achieving an occultation effect to counteract the impacts of greenhouse gas emissions [3, 69]. Scientists have proposed various space-based geoengineering methods, such as dust clouds or earth rings [4, 5, 68]. This thesis primarily focuses on the application of a large multi-sailcraft sunshield near the Sun-Earth Lagrange point 1 (L_1). While this concept is still largely theoretical, it has attracted significant attention due to its potential advantages and ethical implications [3, 7]. One key characteristic of space-based geoengineering is that it refrains from directly modifying Earth's ecosystem, distinguishing it from carbon dioxide removal (CDR) methods. This mitigates the risk of negative side effects on terrestrial, oceanic, and atmospheric systems that may arise from CDR techniques [3]. By regulating solar radiation without directly altering the ecosystem, space-based geoengineering offers a significant advantage in terms of avoiding the need for complex predictions of collateral damage associated with Earth's atmospheric composition and processes [3].

Another advantage of space-based solar radiation management (SRM) is its potential for a rapid reduction in solar radiation flux reaching Earth compared to the slower decarbonisation processes involved in CDR methods. This makes SRM a potentially valuable "last resort" solution in addressing the pressing climate crisis [69].

However, one major criticism of space-based geoengineering is that it does not address the root cause of climate change. Critics argue that implementing such projects may inadvertently discourage necessary behavioural changes and reductions in greenhouse gas emissions [3]. To address this concern, advocates emphasise the importance of properly classifying space-based geoengineering efforts as complementary to other climate change

mitigation strategies. Ideally, a comprehensive approach should combine both space-based geoengineering and emission reduction efforts to achieve the desired climate goals [3, 46].

However, despite ongoing efforts to reduce greenhouse gas emissions, the current strategies and initiatives to combat climate change have not been effective enough to meet the ambitious targets set for mitigating global warming [37]. Consequently, alongside moral considerations regarding humanity's awareness of greenhouse gas emissions, missions like the planetary sunshade project may be necessary when other approaches prove insufficient [3].

3.2 The Planetary Sunshade Foundation

The *Planetary Sunshade Foundation* (PSF) was established in 2021 with the objective of enhancing and complementing existing efforts to mitigate the impacts of the climate crisis. Recognising that current decarbonisation initiatives and concepts alone are insufficient to ensure Earth's habitability, the PSF emphasises the need for a space-based SRM strategy. As part of their plan, the PSF intends to deploy a large occulting disk near the Sun-Earth Lagrange point 1 (L_1). With over one billion sailcraft working in unison, the occulting disk forms a barrier to intercept and redirect solar radiation [32]. Figure 3.1 represents an artist impression of a possible arrangement of these solar sailcraft. By blocking a

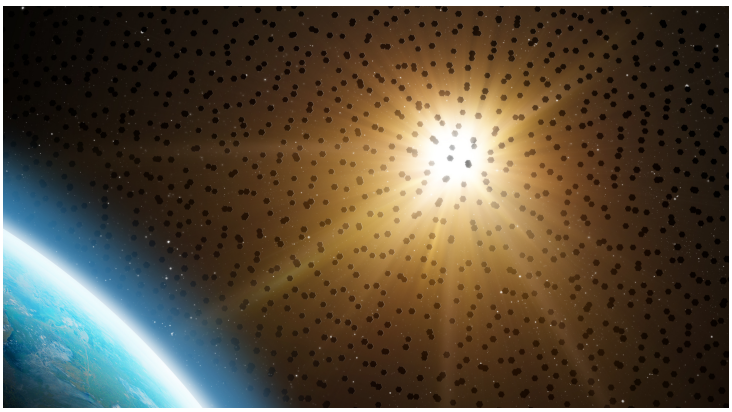

Figure 3.1: Possible arrangement of the planetary sunshade sailcraft (artist impression) [63].

significant portion of solar radiation before it reaches Earth, the aim is to regulate and reduce the amount of heat absorbed by our planet, ultimately working towards achieving the ambitious +1.5°C temperature target [63].

3.2.1 Sunshade Position at L_1

When it comes to addressing global warming, Seifritz proposed in 1989 a solution that involved the placement of thin reflective aluminium screens at the Sun-Earth Lagrange point, a semi-stable position requiring reduced propulsion effort to cast a shade on Earth

[71]. Important to note is that L_1 rotates around the Sun at the same angular speed as Earth, ensuring that the sunshade remains positioned between the Earth and the Sun at all times, effectively blocking incoming radiation [69], see Figure 3.2. However, it is

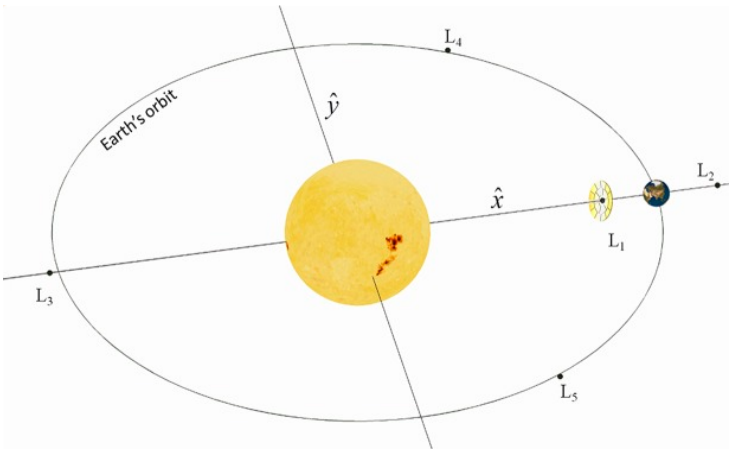

Figure 3.2: Location of the occulting disk near to L_1 [69].

important to consider the optimal occultation effect and the influence of solar radiation pressure, as they affect the ideal position of the sunshield-disk. Research conducted by McInnes et al. indicates that the most suitable location for the sunshade sailcraft is approximately 2.4 million kilometres closer to the Sun from Earth. This adjusted position serves as the departure point for trajectory optimisation and deflection analysis, allowing for precise manipulation of the sailcraft's path [69].

3.2.2 Feasibility

Numerous studies have explored various configurations of sunshade sailcraft, considering factors such as reflection efficiency, sail area, and mass [35, 32, 69]. Achieving the required global shading of approximately 1.7 % presents a challenge, requiring a careful balance between the size and number of sunshades deployed and their impact on Earth's climate [35]. Researchers have proposed several theoretical solar shield concepts located at the L_1, aiming to achieve the desired global shading [69, 35]. For example, McInnes et al. designed a mass-optimised configuration expected to improve global warming by two degrees with a total mass of around 10^{11} kg [52]. However, this work focuses on the two sunshield sailcraft constellations introduced by Fuglesang et al. in [32] (see Section 3.2.3).

The application of solar sailing technology faces a significant challenge due to the low technology readiness level (TRL) of solar sailcraft propulsion. Most planned bus components reach a TRL of 9, while solar sailing projects are only at TRL 3 to 6 [32]. For instance, the DLR & ESA *GOSSAMER-1* project has achieved a TRL of 5 [36]. In this work, the two analysed arrangements assume a TRL between 3 and 4 [32]. Therefore, considerable research investment is needed to advance solar sailing technology to an adequate level within approximately 15 years [32]. Regarding the worst-case scenario of the two chosen constellations (see Table 3.1 sunshade arrangement 2), the estimated cost

of manufacturing and launching the entire system would be around US$5–$10^{12}$. However, further advancements in sail-film technology could significantly reduce these costs [32]. Over a twenty-year deployment, the expenses would likely be substantially lower compared to the potential damages resulting from the projected increase in global temperatures [32].

In summary, while the concept of a global sunshade holds promise as a potential climate mitigation strategy, it is currently faces various challenges that need to be addressed and thoroughly evaluated before implementation. Further research and collaboration among scientists, engineers, and policymakers are necessary to assess the feasibility, potential risks, and benefits of such a large-scale geoengineering project.

3.2.3 Sunshade Sailcraft Properties

As mentioned before, the purpose of the planetary sunshade sailcraft is to operate as one large sunshield placed close to L_1 (Figure 3.2). The individual sailcraft are intended to form a loose constellation and a discontinuous occulting disk (Figure 3.1). Furthermore, the desired occultation effect does not necessarily presuppose the occurrence of umbral shadows [32]. In the study conducted by Fuglesang et al., two distinct sunshade sailcraft arrangements with different levels of reflection efficiency are presented to fulfil the required global shading of roughly 1.7 % [35, 53]. These arrangements can be adapted for KEI missions, where the sailcraft would act as kinetic impactors to deflect hazardous asteroids. The first arrangement involves a characteristic acceleration of $a_c = 0.9\,\mathrm{mm/s^2}$ and a sailcraft area of 9000 $\mathrm{m^2}$, resulting in a mass of 81 kg. Implementing this configuration would require substantial development and research, estimated to take about 20 years to realise [32]. On the other hand, the second arrangement presented by Fuglesang et al. represents a more state-of-the-art version with a characteristic acceleration of $0.21\,\mathrm{mm/s^2}$. However, it features a sail area of $2500\,\mathrm{m^2}$, which currently places it at a TRL of approximately 4. The total system mass for this arrangement is 8.35×10^{10} kg and the corresponding mass per sail is 55 kg [32]. It is worth noting that the TRL of 4 is primarily attributed to the sail area of $2500\,\mathrm{m^2}$ rather than the characteristic acceleration. The characteristic acceleration of $0.21\,\mathrm{mm/s^2}$ is indeed considered feasible for the mission by concerning current technology standards. An overview of the physical properties concerning the two sunshade sailcraft arrangements can be taken form Table 3.1. The physical properties of both sailcraft arrangements are the initial inputs for further calculations and analyses related to the deflection analysis and trajectory optimisation, discussed in Chapter 6.

Table 3.1: General data of the two chosen planetary sunshade arrangements [32].

Sunshade Arrangement 1

specification per sail	sail mass (m)	81 kg
	sail area (A)	9000 m^2
	lightness number (λ)	0.151
	characteristic acceleration (a_c)	0.9 mm/s^2
total sunshade system	sail number	4.1×10^8
	system mass	3.4×10^{10} kg
	average heliocentric distance	0.98396 au

Sunshade Arrangement 2

specification per sail	sail mass (m)	55 kg
	sail area (A)	2500 m^2
	lightness number (λ)	0.035
	characteristic acceleration (a_c)	0.21 mm/s^2
total sunshade system	sail number	1.5×10^9
	system mass	8.4×10^{10} kg
	average heliocentric distance	0.98396 au

Chapter 4

Planetary Defence & Solar Sails

4.1 Introduction to Planetary Defence

The impact of celestial bodies within our solar system is evident in the numerous impact crater formations on various planetary surfaces. Even on Earth, we experience a continuous influx of small objects. Fortunately, these objects are typically compact in size and pose no significant threat. However, smaller objects with higher impact frequencies can still have dangerous consequences, particularly due to explosive effects during atmospheric entry. [28] Furthermore, the presence of a *potentially hazardous asteroid* (PHA) with a diameter up to two kilometres can result in severe global damage [10]. Although collisions with PHAs of this size are statistically rare, the risk of impact remains ever-present. One notable event that raised global awareness was the Tunguska event in 1908 when a massive explosion occurred in a remote region of Siberia. The impact, believed to be caused by an asteroid or comet, devastated over 2000 square kilometres of forest. [33]

Despite extensive efforts to monitor near-Earth objects (NEOs), early detection of all potential hazards is not guaranteed due to challenges such as sky brightness and the faintness of objects caused by large phase angles [56]. Additionally, predicting the trajectory of a PHA accurately is challenging, primarily due to the influence of the Yarkovsky and YORP effects [10]. Furthermore, the number of registered PHAs within our solar system amounts to approximately 2000, see Figure 4.1.

In this context, planetary defence refers to the strategies and measures taken to protect our planet from the threats emerging from PHAs. One of the primary focuses of planetary defence is the detection and tracking of NEOs [73]. Observatories and space-based telescopes continuously monitor the skies, searching for potentially hazardous objects. By tracking their orbits and predicting their future trajectories, scientists can identify objects that may pose a risk to Earth [73].

In the event that a PHA is identified, various methods are being explored for asteroid deflection[1] [44]. One of the techniques being investigated is the kinetic energy impactor approach, where a spacecraft is intentionally directed to collide with an asteroid to alter

[1]Further deflection techniques are discussed in Appendix C.

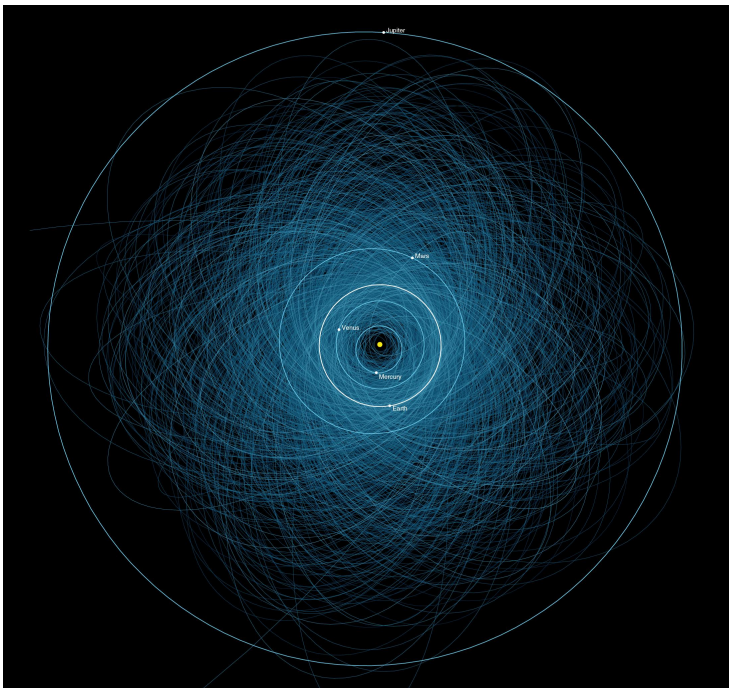

Figure 4.1: Orbits of known potentially hazardous asteroids [49].

its trajectory, see Section 4.2.2 [44]. The reference *safe deflection distance* in this context amounts to one Earth diameter ($2R_{\oplus} = 12742\,\text{km}$). Significant organisations dedicated to addressing the risks of planetary defence are the *Planetary Defense Coordination Office* (PDCO), which was established by NASA in 2016 [11] as well as ESA's *Near-Earth Objects Coordination Centre* (NEOCC) [1]. Furthermore, the first and only successfully executed planetary defence mission, testing the kinetic impactor technique, is called DART and was applied in September 2022, see Section 4.2.3.

4.1.1 Potentially Hazardous Asteroids

In the context of planetary defence, *small solar system bodies* (SSSB) encompass objects that do not achieve self-rounding due to their own gravitational forces and are also not classified as moons. Self-rounding refers to the process by which an object's gravitational forces are not strong enough to shape it into a nearly spherical form [39]. These small bodies can be categorised in various ways, but the most relevant for planetary defence research are Near-Earth Asteroids (NEAs), particularly those classified as *Potentially Hazardous Asteroids* (PHAs). NEAs are a subset of small bodies that have a perihelion distance of less than 1.3 astronomical units (au) from the Sun, which brings them in relatively close proximity to Earth's orbit [49]. PHAs, on the other hand, are a specific subset of NEAs that meet additional criteria for potential hazard.

The *Minimum Orbit Intersection Distance* (MOID) is the minimum distance between the orbit of an asteroid and the orbit of Earth. If an asteroid's MOID is less than 0.05 au (approximately 7.5 million kilometres), it is considered a PHA. This indicates a potential

for close approaches to Earth in the future. A further classification parameter is the absolute magnitude (H)[2] of an asteroid, which is a measure of its brightness as observed from a standard distance of 1 au. Asteroids with an absolute magnitude of 22.0 or brighter fall into the PHA category. Larger asteroids tend to have brighter absolute magnitudes, and these can potentially cause more significant consequences upon impact [49].

It is crucial to differentiate between asteroids and comets, as they have different characteristics and origins. Comets are primarily composed of ice and dust and are typically formed in the colder outer regions of the solar system. When they approach the Sun, they develop a glowing coma and, in some cases, a tail due to the sublimation of the icy components [24]. On the other hand, asteroids are rocky bodies that predominantly exist in the inner solar system.

Understanding the characteristics of NEAs and PHAs is of high importance for planetary defence. By identifying and monitoring these small bodies, researchers can assess potential impact risks and develop strategies to mitigate any potential threats they may pose to Earth. Planetary defence efforts depend on accurate data and continuous observation to detect and track these celestial objects, ultimately ensuring the safety and security of our planet.

4.1.2 The Planetary Defence Conference

The *Planetary Defence Conference* (PDC) is a significant international event that gathers scientists, engineers, policymakers, and experts from around the world to address the critical topic of planetary defence against potential asteroid and comet impacts. This conference serves as a prominent platform for sharing the latest scientific research, technological innovations, and mission proposals related to planetary defence strategies. [42] Through presentations, panel discussions, and workshops, attendees collaborate to tackle various aspects of planetary defence, including asteroid characterization, impact modelling, mitigation techniques, mission planning, international cooperation, and risk assessment. By fostering interdisciplinary dialogue and fostering global collaboration, the PDC plays a crucial role in advancing our understanding of near-Earth objects and developing effective defence measures to protect our planet. Additionally, the conference contributes to raising public awareness about the potential risks and consequences of asteroid impacts, engaging the broader community in the efforts towards planetary defence. [42]

In order to achieve this objective, the Planetary Defense Conference introduces a new fictitious asteroid impact scenario every two years, providing scientists with a platform to test and refine their deflection and risk mitigation strategies. The scenario developed for the PDC in 2023 serves as an example-case study for this research, further discussed in Chapter 5.

[2]The absolute magnitude H of an asteroid measures its inherent brightness, as if observed from a distance of 1 au where the Sun, asteroid, and observer align in a straight line (zero phase angle) [55].

4.2 Asteroid Deflection Implementation

This section deals with the practical aspects of asteroid deflection, exploring the fundamental orbital dynamics essential for successful deflection missions. The focus lies on the kinetic impactor technique, which is one of the most straightforward methods for altering an asteroid's trajectory. While this method provides a solid foundation for deflection, it is worth noting that other techniques based on various physical principles can be found in Appendix C for achieving the required impulse transfer. Understanding and implementing these deflection strategies are vital steps towards safeguarding our planet from potential impact threats.

4.2.1 Asteroid Impact Trajectories

Understanding the trajectory of a PHA is critical for effective impact threat mitigation. This knowledge enables the determination of the required deflection strategy's intensity and type. Once a potential hazardous asteroid is detected, the projected impact location can be visualized on a projection plane [59]. This projection plane, known as the *b-plane*, typically corresponds to Earth's plane at the predicted impact time [59]. The b-plane is centred at Earth's core and is perpendicular to the incoming asteroid trajectory's asymptote [85], as depicted in Figure 4.2. If an intersection results in the plotted, potential

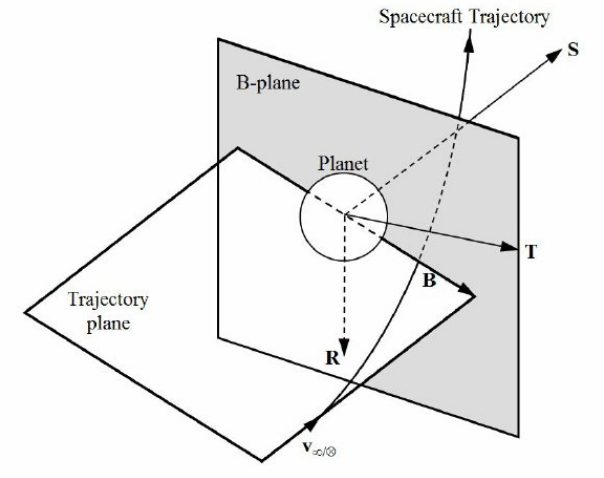

Figure 4.2: Visualisation of the b-plane [15].

impact region and the Earth's capture cross section, a collision is possible [85]. Albeit, an impact is not impossible, if no intersection occurs. The so-called *keyholes* are narrow ranges within the b-plane, which lead the asteroid into a resonant return trajectory[3], due to Earth's gravitational perturbation [85]. The required orbit alteration, resulting from the deflection process, depends on the distance between asteroid and Earth's surface [85].

[3]Orbital resonance is defined between two bodies where the orbital periods of asteroid and Earth are related by small integers [16].

In his 2009 publication, Izzo expresses the required deflection for a successfully completed deflection mission with the *deflection formula* (4.1) [17]. The *safe deflection distance* is defined as roughly one Earth diameter ($\Delta\xi \approx 2R_\oplus$) from Earth surface [84].

$$\Delta\xi = -\frac{3a\boldsymbol{v}_\mathrm{E}(t_\mathrm{s}\sin\theta)}{\mu_\mathrm{S}}\int_{t_0}^{t_\mathrm{f}}(t_\mathrm{s}-t)(\boldsymbol{v}_\mathrm{A}(t)\cdot\boldsymbol{a}_\mathrm{A}(t))dt \tag{4.1}$$

The equation used to compute the achieved deflection on the b-plane at time t_s involves several key parameters. These parameters include the heliocentric velocity $\boldsymbol{v}_\mathrm{A}$ and heliocentric semi-major axis a of the asteroid, as well as the velocity $\boldsymbol{v}_\mathrm{E}$ at which it approaches Earth at time t_f [17, 59]. The acceleration $\boldsymbol{a}_\mathrm{A}$ imparted to the PHA is provided by the chosen deflection method [17]. Additionally, the angle θ is defined as the angle between Earth's heliocentric velocity and the relative velocity of the asteroid [59]. The parameter μ_S represents the gravitational parameter of the Sun.

4.2.2 The Kinetic Energy Impactor Technique

Asteroid deflection and impact mitigation involve various approaches. These include slow-push/pull methods, kinetic impact missions, and nuclear detonations [72]. The latter two techniques are considered quasi-instantaneous, while slow-push and pull methods require a longer time frame to achieve the desired deflection.

In the context of this thesis, the focus is mainly on the *kinetic energy impactor* (KEI) technique, which will be discussed in more detail in this section. As mentioned previously, the KEI falls under the category of quasi-instantaneous techniques. It represents the simplest implementation to deflect an asteroid [26]. The deflection occurs through a collision between the impact spacecraft (S/C) and the NEA. The efficiency of the KEI technique depends on the transferred momentum resulting from the impact and the ejected material [54].

Principle of Operations

Taking into account Newton's first two laws, equation (4.2) [83] expresses the transfer of impact momentum.

$$I_\mathrm{A} = M\Delta v = p_\mathrm{sc} + p_\mathrm{e} > p_\mathrm{sc} \tag{4.2}$$

In this equation, p_sc represents the momentum of the S/C, while p_e denotes the additional momentum generated by ejected surface material. I_A is defined as the absolute change in momentum of the asteroid [83]. Figure 4.3 visualises the fundamental process of momentum transfer during a collision between celestial bodies. The increase in momentum due to p_e can be quantified using the *momentum enhancement-factor* β [38].

Momentum Transfer Efficiency

Assuming, a spacecraft (S/C) with mass the m is impacting an asteroid with the mass M at a relative impact velocity $\boldsymbol{v}_\mathrm{imp}$. In this scenario, the resulting change in the target

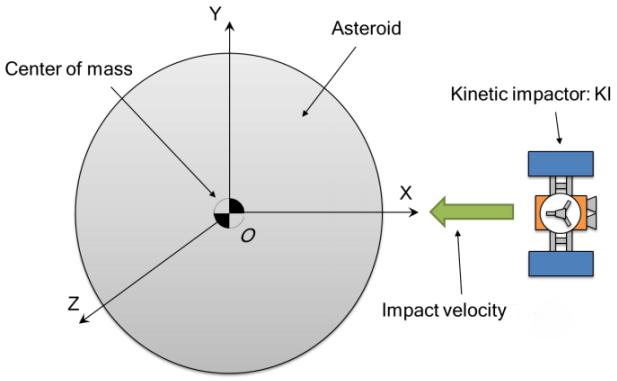

Figure 4.3: A simplified visualisation of the KEI technique, by considering the impactor colliding with the asteroid at a specific impact velocity v_{imp} (adapted from [84]).

asteroid's orbit velocity ($\Delta \boldsymbol{v}$) multiplied with M yields the collision induced momentum transfer to the asteroid. [31, 13]

$$M\Delta \boldsymbol{v} = m\boldsymbol{v}_{\text{imp}} + (\beta - 1)(\boldsymbol{n} \cdot \boldsymbol{v}_{\text{imp}})\boldsymbol{n} \tag{4.3}$$

Here $\boldsymbol{n}$ represents the normal unit vector from the asteroid's surface [13]. A complex surface structure of the target asteroid could lead to a non-collinearity of the initial and the transferred momentum vectors ($M\Delta \boldsymbol{v}$ and $m\boldsymbol{v}_{\text{imp}}$). This effect occurs due to the spatial distribution of the ejecta, which is influenced by uneven surface structures [13]. However, this non-collinearity is not considered in this thesis.

Derived from equation (4.3) the momentum enhancement factor β, is basically defined by the ratio of the asteroid momentum change (I_{A}) after the collision and the relative KEI momentum (p_{sc}) with respect to the asteroid's momentum before the impact (p_{A}) [38, 62].

$$\beta = \frac{|\boldsymbol{I}_{\text{A}}|}{|\boldsymbol{p}_{\text{sc}}|} = 1 + \frac{|\boldsymbol{p}_{\text{e}}|}{m|\boldsymbol{v}_{\text{imp}}|} \tag{4.4}$$

The variation of β depends on the additional momentum due to the ejecta, which escapes from the asteroid along the "impact-line" [41]. The rotation of an asteroid generates a tangential component to the ejecta velocity, which however, is not included in the vertical component [40]. Considering, that solely the component of the incident momentum vector along the orbital motion direction ($\boldsymbol{e}_{\text{t}}$) induces the transverse momentum transfer, the determination of β can be more precisely implemented by the following equation [13].

$$\beta = \frac{M|\Delta \boldsymbol{v}|}{m\boldsymbol{v}_{\text{imp}} \cdot \boldsymbol{e}_{\text{t}}} \tag{4.5}$$

Material that does not achieve the required velocity to escape the gravitational force of the asteroid, returns back to the surface after the ejection. Therefore, this procedure does not induce an additional push ($\beta = 1$) [41, 70].

Significant for any case of orbit alteration is the magnitude of the velocity change (Δv). Equation (4.6) shows the resulting Δv as a function of the β-factor [62].

$$\Delta v = \beta \frac{p_{sc}}{M} \tag{4.6}$$

When introducing e as the coefficient of restitution, then for the case $\beta < 1$ and $e < 0$, it implies a *subplastic* or *perforating* collision [62]. This type of collision occurs when a small, dense object like a bullet penetrates a larger, less dense object [62]. On the other hand, a *plastic* or *perfectly inelastic* collision ($\beta = 1$, $e = 0$) results in the transformation of kinetic energy into work or heat, leading to deformation of the colliding objects [62]. In a *perfectly elastic* collision ($\beta = 2$, $e = 1$), kinetic energy is conserved, and the two bodies will separate with the same relative speed as before the collision [62]. In some cases, the value of β can significantly increase, indicating a *superelastic* collision that may result in an explosion due to exoergic reactions.

Determining the value of β depends significantly on factors such as impact velocity, impact geometry, target internal structure, and material properties, as demonstrated by previous research [62]. These factors play a crucial role in accurately assessing the momentum enhancement during the collision process [64]. The results from the DART mission (see Section 4.2.3) demonstrate the significant influence of the β-factor on the momentum transfer efficiency, which can in some cases be higher than the impact-induced momentum itself [14]. Moreover, the characterisation of momentum enhancement due to ejecta plays a crucial role in investigating and understanding asteroid deflection using KEI applications in greater detail. However, it is essential to acknowledge that the specific effects of ejecta development on solar sail impacts in asteroids have not been extensively studied. While some research exists on the effects of high-velocity impacts on asteroids, it is challenging to directly infer the corresponding consequences of a solar sail impact. The unique dynamics of the interaction between a solar sail and an asteroid's surface, coupled with the complex nature of ejecta generation during such an event, warrant dedicated investigations. Given that solar sail materials are generally designed to be lightweight, featuring thin and flexible structures, it is reasonable to anticipate that β would be close to 1 in many scenarios. This assumption implies that the momentum transferred to the asteroid during the solar sail impact would be approximately equal to the sail's momentum. However, it is crucial to recognize that real-world conditions may introduce complexities that could affect the actual value of β.

Asteroid Fragmentation Hazard

Important to note is that the ejected material resulting from the impact has implications beyond the momentum transfer intensity. The impact event can give rise to a meteorite stream, which may potentially reach Earth and contribute to further pollution concerns. [81] A comprehensive analysis conducted by Wiegert et al. [81] evaluated the risk of fragmentation hazards associated with the DART mission applied to the Didymos system. Fortunately, in this specific case, no significant hazards were identified. However, when considering larger impactors and asteroids, the trajectory becomes a crucial factor. The

generation of substantial material ejections under such circumstances could pose a genuine threat.

4.2.3 The Double Asteroid Redirection Test (DART)

The *Asteroid Impact & Deflection Assessment* (AIDA) represents a pioneering planetary defence mission jointly conducted by the ESA and NASA. It aims to investigate asteroid deflection through the KEI technique (further discussed in the upcoming section) [12]. The primary target of this mission is the secondary body of the binary asteroid (65803) Didymos, which is called Dimorphos. AIDA comprises two distinct missions known as the *Double Asteroid & Redirection Test* (DART) and *Hera*[4]. DART, led by NASA, involves a spacecraft colliding with Dimorphos, resulting in an adjustment of its orbital period around the primary body [12]. The DART impactor hit the asteroid with a velocity of approximately 6 km/s in September 2022, coinciding with Didymos' close approach to Earth during that time frame [14]. The highly successful hyper-velocity impact of DART resulted in an immediate reduction of Dimorphos's along-track orbital velocity component by approximately 2.70 mm/s. This significant decrease indicates enhanced momentum transfer caused by the impact-generated ejecta streams, resulting in a momentum enhancement of $\beta \approx 3.6$ [14]. The success of the DART mission shows the effectiveness of the kinetic impactor technique, in mitigating the threat of asteroid strikes. Combining this technique with the application of the planetary sunshade sailcraft therefore offers another promising approach to planetary defence strategies.

4.3 Introducing Solar Sails as Asteroid Deflectors

Solar sails have garnered significant attention in asteroid deflection research. While some research is exploring the potential of solar sails as gravity tractors [80] or solar collectors [44], most studies focus on the KEI technique. This approach involves trajectories close to the Sun to strategically accelerate the sailcraft, resulting in an amplified final momentum transfer to the asteroid. For instance, Matloff's study in 2006 deals with the use of solar sails for deflecting NEOs [50] by the application of the KEI technique. The research investigated the effectiveness of solar sails in altering the orbit of a hypothetical NEO threat. The findings demonstrated that solar sails can efficiently deflect asteroids, offering a promising approach for planetary defence. Following the AIDA collaboration, another interesting study investigated solar sails as an alternative mission concept to the DART mission for planetary defence [65]. The investigation also aims to start from L_1, aiming for low-cost transfers to asteroids, broadening the prospects of solar sail applications in future missions.

Additionally, Dachwald et al. conducted an analysis of a mission design involving the deflection of asteroid 99942 Apophis using a solar sail as a kinetic impactor. In

[4]Hera, scheduled for launch in 2024, aims to investigate the geophysical structure and surface properties of Dimorphos, showcase deep-space communication capabilities, and document the outcomes of the DART impact [66].

the study neural networks are used for trajectory optimisation through a program called InTrance, an abbreviation for "Intelligent Trajectory optimisation using neurocontroller evolution" (see Section 6.4) [26]. The research results show that by concerning 100×168 kg solar sailcraft KEIs, a retrograde impact trajectory could achieve significant momentum transfer, leading to a sufficient deflection distance of Apophis with respect to the Earth.

However, it's worth noting that achieving a retrograde impact orbit may not always be feasible in certain scenarios, as demonstrated in the 1st ACT global trajectory optimization competition organized by ESA, where prograde impact orbits were explored. Despite challenges such as advanced trajectory optimization and efficient sail deployment mechanisms, these investigations underscore the promising potential of solar sails in asteroid deflection. Their passive nature, continuous thrust without the need for propellant, and utilization of solar radiation pressure for propulsion make them a viable and scalable option for realistic asteroid deflection scenarios.

Chapter 5

Example Case: Scenario Design of the PDC 2023

In this chapter, the focus shifts to an example case scenario specifically designed for the Planetary Defence Conference in 2023. During the conference, a hypothetical scenario was introduced, featuring the discovery of a fictional asteroid by an international team, using the Dark Energy Camera (DECam) on 10 January 2023. This asteroid's trajectory is projected to intersect with Earth, posing a potential collision threat on 22 October 2036 [42]. The significance of the 2023 PDC scenario lies in its role as a tool for advancing our understanding of planetary defence strategies and enhancing our preparedness for potential asteroid impact events. While the scenario is fictional, the scientific and technical principles employed to study and respond to it are very real and serve as a valuable framework for addressing actual threats in the future. This scenario not only provides a platform for addressing actual threats in the future, but it also simulates the initial uncertainties regarding the asteroid's orbit and characteristics, and their refinement over time through the best possible observations.

Since this scenario is selected as the example case for the application within this work, the following sections delve into a more detailed description of the given PDC scenario and explore various aspects related to the asteroid's orbital and physical properties as well as the respective impact-trajectory characteristics.

5.1 Physical Characteristics of 2023 PDC

The focal point of the scenario designed for the PDC 2023 is a fictional asteroid referred to as *2023 PDC*. Beginning with its physical properties, 2023 PDC is highly likely to be classified as a C-type asteroid. C-type asteroids represent one of the most common types found in our solar system and are predominantly situated in the main asteroid belt between Mars and Jupiter. They derive their name from their carbonaceous composition and typically possess dark surfaces, reflecting only a small fraction of sunlight. This characteristic aligns with the given magnitude of 19.4 ± 0.3 for 2023 PDC [42].

Additionally, the current estimated diameter of 2023 PDC falls within the range of

550 to 860 meters, suggesting an average diameter of approximately 700 metres [42]. Determining the exact mass of asteroids poses considerable challenges. Therefore, a volume determination for a triaxial ellipsoid, a common shape modelling method for asteroids [74], is applied using the aforementioned diameter of 700 meters and the average density of a C-type asteroid ($\rho = 1.7$ g/cm^3) [76]. This calculation yields an estimated mass of 3.0 $\times 10^{11}$ kg for 2023 PDC. Table 5.1 shows the relevant physical information concerning 2023 PDC. In addition, it is noteworthy that 2023 PDC stands out in terms

Table 5.1: Physical characteristics of 2023 PDC [42, 57].

Physical characteristics of 2023 PDC	
classification	C-type
mass m_{PDC23} [kg]	3.0 $\times 10^{11}$
density ρ [g/cm^3]	1.7
diameter d [m]	700
absolute magnitude H [-]	19.4 $\pm$ 0.3

of its mass when compared to the average size and mass of asteroids in the main belt [76].

5.2 Orbital Characteristics of 2023 PDC

2023 PDC follows an orbit around the Sun that has resemblance to Earth's, which leads to a high synodic period of almost 60 years. It is characterised by a low eccentricity ($e \approx 0.09$) and a heliocentric distance to the Sun comparable to that of Earth. At its closest approach, 2023 PDC is located at a distance of 0.90 au from the Sun, while at its farthest point, it extends to approximately 1.07 au. The orbital period of the asteroid amounts to 359 days and is therefore slightly shorter than that of the Earth [60]. As can be seen in Figure 5.1, the orbit of 2023 PDC is inclined by 10 degrees relative to the ecliptic plane [57]. In relation to Earth, 2023 PDC moves at a very slow velocity, gradually approaching our planet [60]. Figure 5.2 illustrates the orbit of 2023 PDC within the inner Solar System, showing its gradual approach to Earth over the course of four months until the collision in October 2036. The orbital characteristics, including the Keplerian orbital elements[1], from the NASA Horizon[2] system can be taken from table 5.2. Due to these specific orbital characteristics, reaching 2023 PDC poses a considerable challenge. To visualise the impact trajectory of 2023 PDC on the b-plane (Figure 5.3), the *NASA/JPL NEO Deflection App* offers a valuable tool[3]. Figure 5.3 depicts the b-plane view of the asteroid's impact trajectory, with the Earth represented by the blue circle. The red circles mark the deflection distances given in Earth radii. The green dot marks the intersection

[1] See Appendix B.1

[2] The JPL Horizons on-line solar system data and ephemeris computation service grants users access to solar system data and facilitates the generation of ephemerides for various solar system objects [57].

[3] This software allows modeling and simulating potential deflection scenarios for NEOs, aiding in the assessment of various deflection strategies for planetary defence [58].

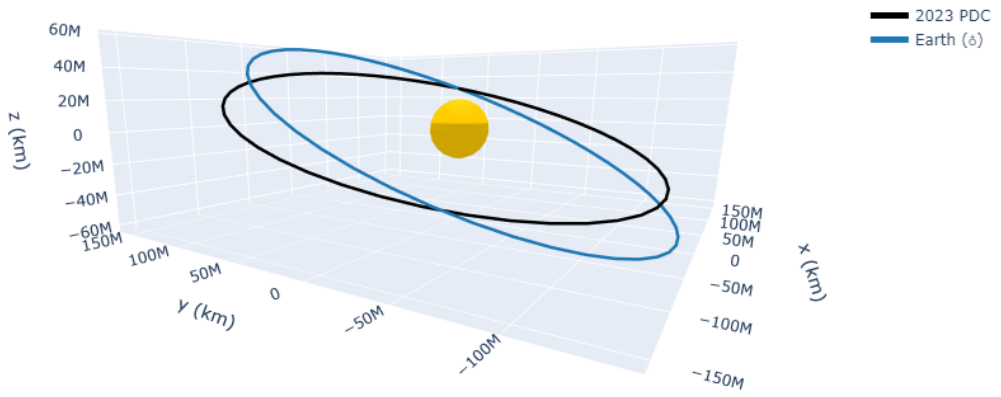

Figure 5.1: Three dimensional view of the heliocentric orbit of 2023 PDC (black orbit) and the Earth (blue orbit) with the equatorial plane as reference.

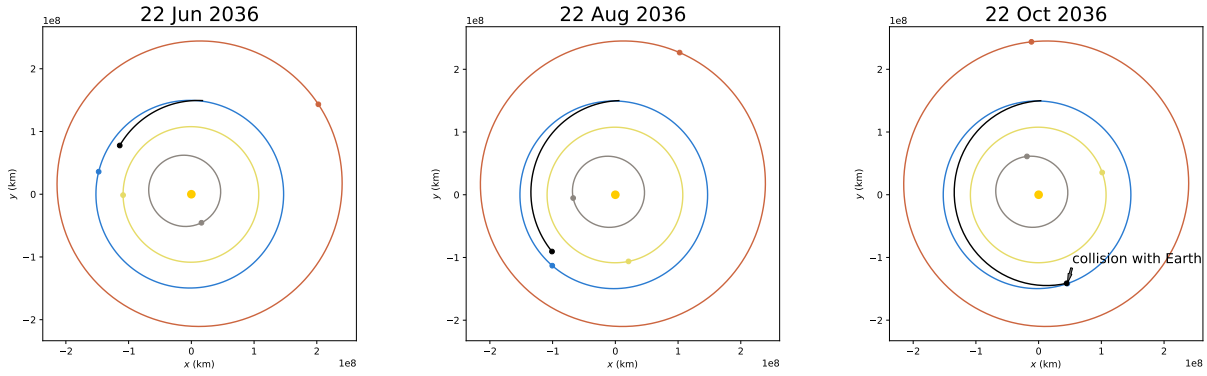

Figure 5.2: The orbit of 2023 PDC within the inner Solar System is simulated over four months, illustrating its approaching trajectory towards Earth until the impact on 22 October 2036.

Table 5.2: The heliocentric orbital characteristics describing the orbit of 2023 PDC [42, 57].

Orbital Characteristics of 2023 PDC	
MJD	2460218.5
heliocentric orbital period P [d]	359
synodic period S [yr]	59.83
perihelion distance r_{p} [au]	0.901626
aphelion distance r_{a} [au]	1.079943
semi-major axis a [au]	0.9223913
eccentricity e	0.0899877
inclination i [°]	10.204
argument of pericenter ω [°]	86.929
longitude of the ascending node Ω [°]	209.4019
mean anomaly M [°]	343.434

of the asteroid's trajectory with the b-plane. Furthermore, the depiction on the b-plane shows, that the asteroid is projected to hit within the African countries Nigeria or Benin [42].

5.3 Impact Consequences & Deflection Issues

The potential local hazard of a large ground impact involving asteroid 2023 PDC could lead to a highly destructive blast wave and thermal fireball upon entry and impact. The consequences of such an event would be significant, with blast damage ranging from levels that are unsurvivable to causing shattered windows and structural damage over extensive areas. Moreover, the thermal damage is also expected to be substantial, with an extremely high probability (greater than 99 %) of reaching unsurvivable levels [48].

While thermal damage regions generally tend to be smaller compared to the corresponding blast areas, the largest impactors may create larger critical and unsurvivable thermal damage zones. As for the estimated range of possible damage sizes, the most likely outer damage radius is projected to be around 150–230 kilometres. However, in the case of the largest outer damage areas, they could extend over a radius of 330 kilometres [48, 42].

Based on the latest modelling of the impact scenario of 2023 PDC, the probability of global effects resulting from impacts with the largest estimated asteroid energies is extremely low, at approximately 0.02 %. Should such an event occur, the total average population affected by these global effects is estimated to be around 20 000 people, considering all potential impactor sizes, including sub-global ones. However, in the worst-case scenario, the maximum estimated population affected by global effects could reach up to approximately 80 million individuals [48].

Asteroid 2023 PDC could be deflected by applying a small velocity change to alter its

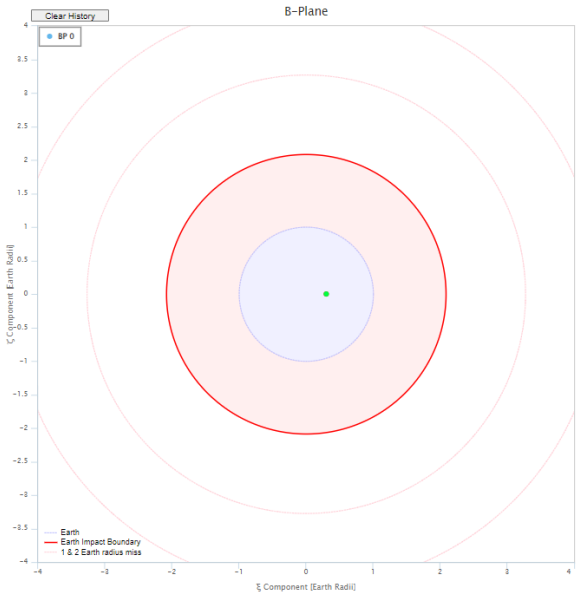

Figure 5.3: The impact trajectory of 2023 PDC visualised on the b-plane [58].

path away from collision. Chodas et al. consider two deflection techniques for this specific case: the kinetic impactor method and the Standoff Nuclear approach, where a nuclear explosive device (NED) is detonated near the asteroid's surface, causing vaporisation and recoil [60]. Furthermore, the schedule for deflection could be challenging due to the growing Δv requirement over time and the time needed to develop, launch, and deliver deflection spacecraft [60].

Chapter 6

Simulation Methodology

6.1 Implementation of the Kinetic Energy Impacts

In the context of the deflection strategy, momentum transfer to the asteroid is accomplished through accumulated collisions between the sailcraft and the asteroid, effectively employing the sails as KEIs. For the theoretical implementation, these kinetic impacts are assumed to occur in the prograde direction relative to the heliocentric orbital motion of 2023 PDC. According to equation 4.6, the change in 2023 PDC's velocity ($\Delta \boldsymbol{v}$) can be determined follows

$$\Delta \boldsymbol{v} = \beta \frac{m_{\text{sail}}}{M_{\text{PDC23}}} (\boldsymbol{v}_{\text{sail}} - \boldsymbol{v}_{\text{PDC23}}) \tag{6.1}$$

where $\boldsymbol{v}_{\text{sail}}$ and $\boldsymbol{v}_{\text{PDC23}}$ are the tangential velocity vectors of sailcraft and asteroid during the impact [26]. The momentum enhancement factor β is set to one for further calculations, considering that the sunshade sails are primarily composed of a thin and lightweight film. Therefore, the analysis does not account for momentum enhancement caused by impact ejecta, and the deflection distance relies solely on the collision-induced momentum transfer to the asteroid. Additionally, this study assumes a perfectly conducted impact between the sail and asteroid, where the entire mass of the sail is used for the momentum transfer. In order to determine the achieved deflection distance from the impacts both orbits are propagated: the orbit of the non-deflected asteroid and the orbit of the deflected asteroid.

6.2 Orbit Propagation

In this study, the simulation methodology involves the use of the Danby solver, a symplectic integrator known for its accuracy and stability in celestial mechanics simulations [27]. The Danby solver is implemented within the application of Poliastro, a Python library for celestial mechanics and astrodynamics, which provides the necessary tools for orbit propagation and analysis.

The initial conditions for the propagation are obtained from the Horizons system, which provides precise orbital information for both the asteroid and Earth. Through trajectory simulations, the motion of the asteroid and Earth can be effectively tracked over time. The simulation process continues until the estimated collision date with Earth (22 October 26), and the distances of both asteroids from Earth are recorded at this point. To compensate for numerical inaccuracies, the difference in distances between the deflected and non-deflected 2023 PDC from Earth is calculated. This approach helps account for any errors that may arise during the orbit propagation process. By comparing the distances of both asteroid positions from Earth at the estimated collision date on 22 October 36, the achieved deflection distance $\Delta\xi$ can be assessed. If the final position of the deflected asteroid is denoted as $\boldsymbol{r}_{\mathrm{PDC23\ def}}$ and the position of the non-deflected asteroid as $\boldsymbol{r}_{\mathrm{PDC23}}$, then the deflection distance $\Delta\xi$ at the respective collision date can be determined using the formula

$$\Delta\xi = \Big|\ |\ \boldsymbol{r}_{\mathrm{PDC23}} - \boldsymbol{r}_{\mathrm{E}}\ | - |\ \boldsymbol{r}_{\mathrm{PDC23\ def}} - \boldsymbol{r}_{\mathrm{E}}\ |\ \Big| \tag{6.2}$$

where pos_{E} represents the position of Earth at the estimated collision date. This approach enables to evaluate the effectiveness of the kinetic impact deflection strategy and its ability to alter the trajectory of the asteroid, potentially preventing a collision with Earth.

6.3 Analytical Approximation of Possible Impact-Trajectories

To assess the feasibility of deflecting 2023 PDC, an analytical approach is employed to generate exemplary sail-impact orbits. These orbits serve as the basis for a primary deflection analysis aimed at determining the specific sailcraft velocities in relation to 2023 PDC. It is important to note that this analytical method does not involve deriving trajectories from the initial launch position near L_1. Instead, these trajectories offer an overview of potential KEI designs within the feasible range of the sunshade sailcraft's capability to achieve the desired impact velocity on 2023 PDC.

The orbits are designed to intercept the asteroid at the sailcraft's solar apoapsis, ensuring that it aligns with the solar distance of 2023 PDC at the specified impact time (as depicted in Figure 6.1). To adhere to the temperature limitations of the sunshade sailcraft assembly, a perihelion distance of 0.4 au is chosen [26, 32]. When r_{PDC23} is the respective solar distance of the asteroid 2023 PDC and a_{sail} is the corresponding semi-major axis of the sailcraft, then the sailcraft velocity v_{sail} is determined by

$$v_{\mathrm{sail}} = \sqrt{\frac{2\mu_{\mathrm{S}}}{r_{\mathrm{PDC23}}} - \frac{\mu_{\mathrm{S}}}{a_{\mathrm{sail}}}} \tag{6.3}$$

Figure 6.1 illustrates three exemplary impact scenarios, each represented by a distinct kinetic impact orbit. For instance, Impact Scenario 1 (blue orbit) involves a kinetic impact at the asteroid's perihelion. Analysing these impact scenarios and their corresponding sailcraft orbits enables the determination of the sailcraft's velocity at the time of impact.

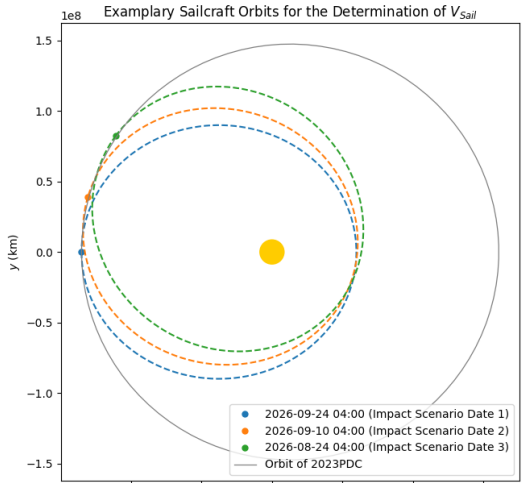

Figure 6.1: Three exemplary impact scenarios and the corresponding sailcraft orbits to determine the sail velocity at impact.

This information is used for calculating the momentum transfer according to Equation 6.1 and assessing the effectiveness of the KEI strategy in altering 2023 PDC's trajectory. Important to note, this first calculation provides just a preliminary overview and does not include any optimisation processes.

6.4 Trajectory Optimisation with InTrance

This section deals with the methodology used to achieve the objective of reaching the asteroid with optimised trajectories. The approach is based on the use of the trajectory optimisation program "InTrance" (Intelligent Trajectory Optimisation using Neurocontroller Evolution), which is developed by Dachwald in [20]. InTrance is a method designed specifically for optimising spacecraft trajectories that employ very-low-thrust propulsion systems. The primary objective of InTrance is to enhance the efficiency and performance of space missions by finding optimal paths for sailcraft, taking advantage of continuous, low-thrust propulsion [20].

6.4.1 InTrance Key Features

InTrance is a *smart global trajectory optimisation method* (GTOM), which means it is able to find optimal trajectories on a near-global scale. An advantage is that InTrance operates with minimal inputs, specifically requiring only information about the target body and the corresponding initial condition intervals [21], which are defined in Section 6.5.1. Figure 6.2 is adapted from [21] and shows the low-thrust trajectory optimisation process within InTrance. Furthermore, the key feature of InTrance lies in the fusion of two cutting-edge techniques: evolutionary algorithms and neural networks. Evolutionary algorithms emulate the process of natural selection, where the most promising solutions

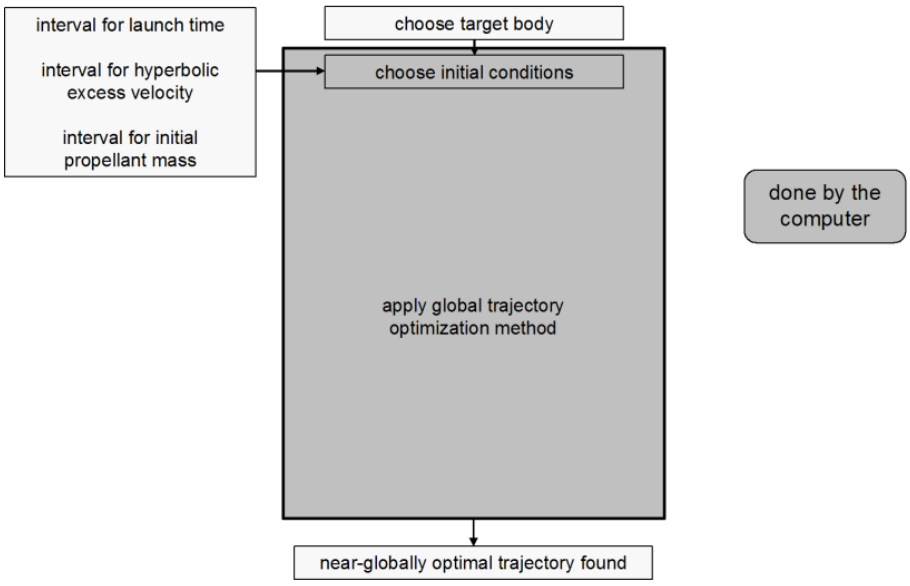

Figure 6.2: Representation of the smart global trajectory optimisation within InTrance with the respective initial condition intervals and the target body as input (adapted from [21]).

are retained and used to generate new ones. This enables an optimisation process without the requirement of an initial guess or the experience of a trajectory optimisation expert [21]. Complementing the evolutionary algorithms, neural networks play a crucial role in the optimisation process. Neural networks are adaptive systems capable of learning from the sailcraft's environment and previous experiences. They enable the modelling and prediction of the effects of different thrust directions and magnitudes, which significantly aids in identifying trajectories that lead to efficient and effective mission outcomes [20, 26].

6.4.2 InTrance Workflow

The workflow of InTrance begins with the initialisation of a population of potential trajectories, each representing a unique combination of thrust profiles and directions. Evolutionary algorithms then evaluate these trajectories based on predefined fitness criteria, such as fuel efficiency and mission duration. The most promising trajectories are selected as the foundation for generating new trajectories [20].

As the optimisation progresses, neural networks come into play. They learn from the evaluated trajectories and refine their predictions, enabling more accurate assessments of the impact of various thrust profiles on the spacecraft's trajectory [20]. The trajectory optimisation process is iterative, with a feedback loop between the evolutionary algorithms and neural networks. The evolutionary algorithms use the neural networks' refined predictions to guide the generation of new trajectories through techniques like crossover and mutation [20, 23]. With each iteration, the trajectory selection process improves,

leading to the identification of increasingly efficient and better-performing trajectories. The optimisation process continues until convergence to near-globally optimal solutions is achieved [20].

InTrance's integration of evolutionary algorithms and neural networks allows for a comprehensive exploration of the vast solution space, facilitating the discovery of trajectories that enable the spacecraft to efficiently reach the asteroid while conserving fuel and minimising mission duration [23].

6.5 Reaching the Asteroid with Numerically Determined Trajectories

Although InTrance includes a function for calculating the maximum asteroid deflection, the version at hand does not feature this capability. Unfortunately, due to time constraints, implementing and adapting the program to determine the maximum impact velocity was not feasible. As an alternative strategy, the software computes TOF-optimised trajectories using InTrance, which are subsequently employed for further calculations. This approach ensures that despite the software's limitations, the analysis progresses effectively by using the available tools.

To compensate for this limitation and gain insights into the highest achievable impact velocity among the investigated TOF-optimised trajectories, a comprehensive analysis of several start dates is conducted. By varying the start dates, different departure opportunities and corresponding trajectories are explored to identify the impact velocities that result in the most significant deflection. This approach allows understanding a potential range of impact velocities and their corresponding deflection distances, for a given launch date. By focusing on impact velocity as a key parameter, the efficiency of the solar sailcraft can be evaluated in achieving the desired deflection, while also considering the associated mission duration. This approach provides a foundation for selecting the most suitable launch window and optimising the trajectory to accomplish effective asteroid deflection while minimising mission duration. Furthermore, various sailcraft characteristics and parameters are analysed in conjunction with the impact velocities to understand their combined influence on the overall deflection effectiveness. By integrating these factors into the simulation analysis, a comprehensive understanding of the solar sailcraft's performance and its ability to achieve the desired deflection objective is provided. This approach emphasises a broad coverage of a potentially complex optimisation space, prioritising exploration of various local optima over a search for absolute optima. This strategy recognises the location between these local optima and acknowledges the challenge of navigating a multi-dimensional optimisation range.

6.5.1 Input Parameters

Sailcraft Parameters

InTrance offers a diverse set of input arguments to define the optimisation problem. In this study, specifically a solar sailcraft is chosen based on the configurations described in Section 3.2.3 (Table 3.1). The input parameters include the lightness number and characteristic acceleration, while selecting the *non-ideal sail* option for more realistic results. This incorporates essential parameters such as maximum sail temperature, (specular) reflection coefficient, and back and front emissivity (Section 2.1.2), adopting values aligned with state-of-the-art research on solar sailcraft technology. This consistent set of the sailcraft parameters applied in this study are presented in Table 6.1. Furthermore, InTrance offers the capability to account for the ageing of sail properties by specifying an interval that characterises the range of sail behaviour concerning degradation.

Table 6.1: InTrance input parameters for the given analysis concerning the sailcraft membrane characteristics (non-ideal sail) [86, 20].

maximum sail temperature $T_{\max}$ [K]	513.15
reflection coefficient ρ	0.88
specular reflection coefficient s	0.94
front side emission coefficient ϵ_{f}	0.05
back side emission coefficient ϵ_{b}	0.55
front side non-Lambertian coefficient B_{f}	0.79
back side non-Lambertian coefficient B_{b}	0.55

Simulation Parameters

The simulation file of InTrance allows for various parameters to be inserted, defining the start position and start time of the sailcraft, as well as the number of integration steps and the size of the integration interval. The integration interval is set to 600 days for the first sailcraft arrangement, which also defines the maximum mission duration. Recognising that the sails in arrangement 2 require more time due to the reduced characteristic acceleration, the integration interval for this arrangement is extended to 1000 days. To ensure a sufficient resolution, the integration steps are selected to achieve one iteration step per day. Since the sunshade sailcraft have the same heliocentric angular velocity like the Earth, the starting location of the sunshade sailcraft can be defined as follows: Positioned 2.4 million kilometres sunward from Earth, this initial point is characterised using Keplerian heliocentric orbital elements. The determination of this position relies on ephemeris data sourced from NASA's Horizons system. The Cartesian state vectors are

then converted into spherical coordinates to modify Earth's position vector $\boldsymbol{r}_{\mathrm{E}}$ by

$$r_{\mathrm{shade}} = |\boldsymbol{r}_{\mathrm{E}}| - 2.4 \times 10^6\,\mathrm{km} \tag{6.4}$$

This modification ensures that the actual position of the sunshade sailcraft can be effectively modelled using the heliocentric position r_{shade}. An overview of the process to define the start position for the simulation input is depicted in Figure 6.3.

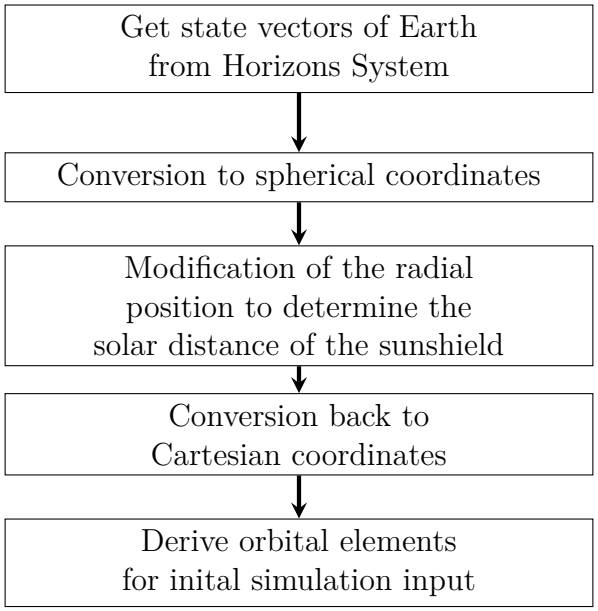

Figure 6.3: Procedure for defining the starting location of the sunshade sailcraft within the trajectory simulation.

Subsequently, the position, now including the newly determined coordinates, is converted back into Cartesian coordinates, followed by the derivation of specific orbital elements that depict the initial position of the planetary sunshade sailcraft for the simulation. Alongside this, the hyperbolic excess velocity (v_∞) of the sailcraft is included in the simulation. In the unique case of positioning the sails close to L_1, v_∞ represents the difference between the actual heliocentric velocity of the specific position of the sunshade sails and the angular velocity of Earth (or L_1). Defining Earth's orbital period (P_{E}) as

$$P_{\mathrm{E}} = 2\pi\sqrt{\frac{a_{\mathrm{E}}^3}{\mu_{\mathrm{S}}}} \tag{6.5}$$

allows for the establishment of the corresponding angular velocity of Earth (ω_{E}) as

$$\omega_{\mathrm{E}} = \frac{2\pi}{P_{\mathrm{E}}} \tag{6.6}$$

Subsequently, the velocity (v_{shade}) of the sunshield at the solar distance r_{shade} can be computed using the relationship

$$v_{\mathrm{shade}} = \omega_{\mathrm{E}} r_{\mathrm{shade}} \tag{6.7}$$

Moreover, the circular orbital velocity of the sunshade spacecraft (v_{orb}) is defined as $v_{\text{orb}} = \sqrt{\frac{\mu_{\text{S}}}{r_{\text{shade}}}}$ and, consequently, the value of v_∞ can be determined utilizing Equation 6.8.

$$v_\infty = v_{\text{orb}} - v_{\text{shade}} \tag{6.8}$$

Moreover, the optimisation goal within the simulation is set to a fly-by mission with the shortest time of flight. In the simulation, the differential equation system is solved using the Runge-Kutta-Fehlberg method, which has been chosen among the available options.

6.6 Implementation of An Exemplary Deflection Mission

To find a near-optimal deflection mission for 2023 PDC, a comprehensive approach is taken, combining the course of required momentum transfer for achieving the desired deflection distance with the impact velocities determined through InTrance calculations. The primary objective is to identify a realisable departure date that aligns with the fly-by trajectory derived from the InTrance simulations. The best trajectory, among the various trajectories analysed, is distinguished by its minimal requirement for impactor mass to achieve a successful deflection. This optimal scenario with the least impactor mass is derived from the following relationship:

$$m_{\text{sail}} = \frac{\Delta I}{v_{\text{imp}}} \tag{6.9}$$

This expression reveals that the lowest necessary impact mass corresponds to identifying a trajectory and its associated launch date that yields the smallest ratio between ΔI and v_{imp}. In simpler terms, the quest is to pinpoint a launch date from the array of analysed options where the required momentum transfer is possibly low while simultaneously attaining a high impact velocity.

By striking this balance between impact velocity and momentum transfer, the aim is to devise a highly efficient KEI deflection manoeuvre. This approach shall increase the overall efficiency of the deflection mission concerning 2023 PDC. To realise this, a analysis process is designed whose overview can be taken from Figure 6.4. The process involves iteratively exploring various launch dates and their corresponding trajectories to identify the most advantageous combination. The trajectory optimisation performed in InTrance allows for the identification of trajectories that result in the highest impact velocities, while considering the characteristics of the sailcraft and its propulsion system. Simultaneously, the momentum transfer required to achieve the desired deflection distance is calculated, considering the mass and relative velocity of the sailcraft and 2023 PDC. By varying the launch date, different fly-by trajectories and impact velocities are assessed, taking into account the sailcraft's position relative to L_1.

Through this integrated approach, the study aims to pinpoint the optimal launch date and trajectory that combine the advantages of high impact velocity and low ΔI, ensuring an effective and efficient kinetic impact deflection of 2023 PDC. The result is expected to

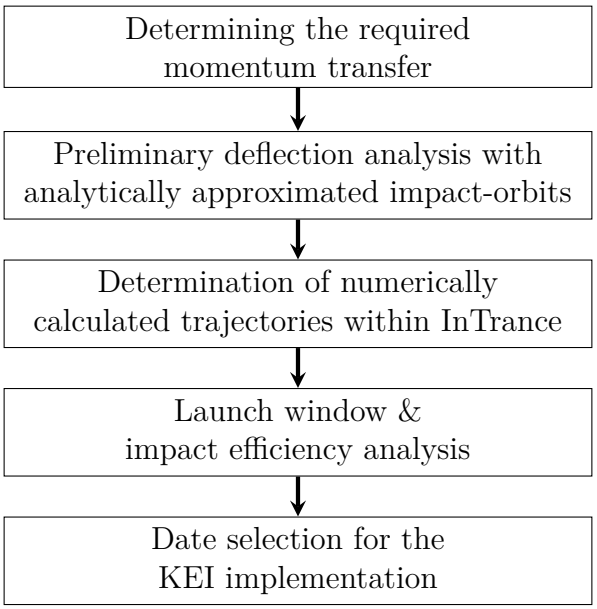

Figure 6.4: Simulation process for the KEI deflection mission.

yield valuable insights into the practical feasibility of the proposed deflection mission and provide valuable data for future planetary defence strategies.

Chapter 7

Results & Discussion

7.1 Initial Overview and Preliminary Deflection Analysis of 2023 PDC

This section is dedicated to providing a preliminary assessment of the feasibility and requirements for the successful deflection of 2023 PDC. The results are generated using the methodology outlined in Section 6.3, where exemplary sail impact orbits are approximated analytically to determine the respective impact velocities for each day. These initial results offer a rough overview of the potential deflection scenarios by considering the physical limitations of the sunshade sailcraft.

7.1.1 Determination of the Required Momentum Transfer

The selection of the best impact dates is significantly influenced by the required total change in the asteroid's momentum ($\Delta \boldsymbol{I}$) and thus by the required impactor mass (m_{sail}), which in turn determines the number of necessary impacting sailcraft. As mentioned earlier in Section 4.2.1, the minimum safe deflection distance for the analysis of the deflection efficiency is chosen as one Earth diameter or two Earth radii ($2R_{\oplus} \approx 12760$ km). Equation 6.1 yields the relation $\Delta \boldsymbol{I} = m_{\text{sail}} \boldsymbol{v}_{\text{imp}}$ where the impact velocity $\boldsymbol{v}_{\text{imp}}$ equals the difference between $\boldsymbol{v}_{\text{sail}}$ and $\boldsymbol{v}_{\text{PDC23}}$. Therefore, the impacting sail mass and velocity must be weighed up to realise a sufficient momentum transfer achievement for a given impact date. To assess the magnitude of the required momentum transfer, the deflected asteroid trajectory is simulated over various impact dates, ranging from October 2023 to October 2029, see Figure 7.1. The results, shown in Figure 7.1, reveal an exponential increase in the trend-line of the required ΔI over time. Consequently, optimising the deflection process entails striking a balance between achieving sufficient impact velocity and mass and identifying a suitable impact time. The latter is constrained by the time of flight (TOF) of the sailcraft from its launch location near L_1 to its arrival at the asteroid. In other words, as time progresses, the amount of momentum needed for a successful deflection significantly increases, indicating that prompt action is crucial in dealing with potentially hazardous asteroids. Therefore, also including the respective TOF, a scope of

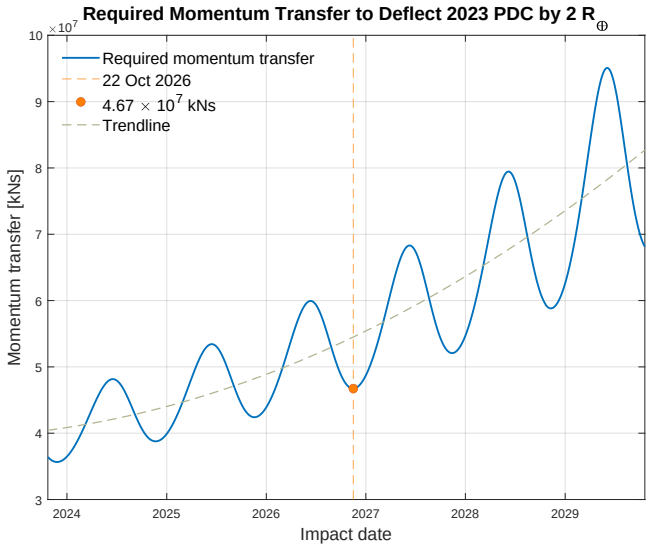

Figure 7.1: Magnitude of the required momentum transfer for the deflection of 2023 PDC, simulated over several impact dates (from 22 October 2023 to 22 October 2029).

departure dates for the trajectory analysis is set for the time range from April 1, 2023 to September 1, 2026.

Moreover, in Figure 7.1 the 22 October 2026 is marked, which is situated within a distinct local minimum range of the required ΔI. This particular date is selected as the impact date for the subsequent KEI implementation, forming the basis for a preliminary analytical deflection analysis in the subsequent section.

7.1.2 Deflection Efficiency

In general, the mass of the asteroid has a significant influence in determining the deflection efficiency of the KEI application. In order to comprehensively assess the efficiency of the KEI application, an analysis is conducted to quantify the relationship between asteroid mass and deflection efficiency within the context of the analytically approximated deflection scenario. The focus of this analysis is to understand how the deflection efficiency varies with different asteroid masses. By incrementally increasing the asteroid mass in the simulations, it can be observed how the achieved deflection distance per kilogramme of impacting sail mass evolves for this specific preliminary investigation.

To realise this investigation, a simulation approach is employed, where the deflection process is simulated by tracking the change in the asteroid's velocity resulting from an impact by a 1 kg heavy sailcraft. This calculation is performed across a spectrum of asteroid masses, systematically increasing the asteroid mass during the analysis and reporting the respective achieved deflection distance.

As evident from the relationship expressed in Equation 6.9, it becomes clear that the impact velocity, in addition to the asteroid mass, significantly influences deflection efficiency. On 22 October 2026, the impact velocity amounts to 3.27 km/s, derived from

the analytically approximated sailcraft impact orbit. In this context, Figure 7.2 illustrates the relationship between the deflection efficiency per kilogramme of impacting sail mass and the asteroid mass for the given impact date on 22 October 2026. The figure also shows

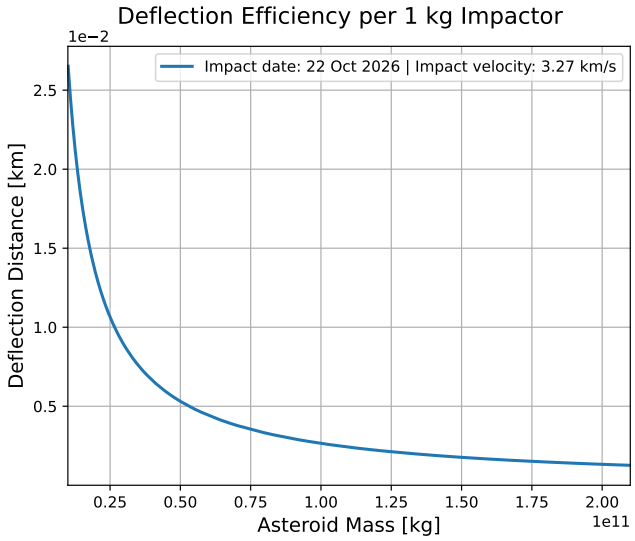

Figure 7.2: Achieved deflection distance $\Delta\xi$ over an increasing asteroid mass for a KEI application on 22 October 2026. The according analytically approximated impact velocity amounts to 3.27 km/s and the required momentum transfer to the asteroid is 4.67×10^7 kNs.

that the achieved deflection distance exhibits an inverse proportionality to the asteroid mass ($\Delta\xi \propto \frac{1}{M}$), which coincides with an analytical calculation by applying Equation (6.9). The analysis provides an insight into the concrete deflection outcomes attainable for an asteroid of the specific order of magnitude of 2023 PDC. The findings reveal an achieved deflection distance of approximately **1.5 m/kg** is conducted.

These established relationships and principles serve as fundamental building blocks for subsequent developments. By regarding the interplay between asteroid mass and deflection efficiency, this analysis contributes to a broader understanding of asteroid deflection dynamics. The goal for the upcoming investigations is to identify mission scenarios and their corresponding trajectories aimed at enhancing the mass-specific deflection efficiency for both sunshade sailcraft arrangements.

7.1.3 Accumulated Impacts over Time

Due to the significant number of planned sailcraft to be present in a future PSF sunshield arrangement, the planetary sunshade constellation offers the opportunity for a series of sequenced impacts spread over several days. Theoretically, the KEI sailcraft would be capable of launching directly, as they do not require a launch vehicle to escape Earth's SOI. However, conducting such a mission would likely involve an advanced study of the discovered PHA and time-consuming policy decisions. Considering a "delay" of one year

after the asteroid's discovery and a transfer time of two years, the 22 October 2026 emerges as a suitable date for the application of the KEI sails. As shown in Figure 7.1, this date corresponds to a local minimum in the required ΔI.

To simulate the accumulated KEI approach, as depicted in Figure 7.3a, the sailcraft's velocity at the respective impact date, and consequently, the corresponding impact velocity, is calculated using analytically approximated potential impact orbits (as detailed in Section 6.3). These orbits are configured, featuring a perihelion positioned at 0.4 au and an aphelion aligned with the orbital location of the 2023 PDC. This configuration serves a dual purpose: it approaches the asteroid while staying within the sailcraft's temperature limits. This balance ensures not only proximity to the target but also safeguards the integrity of the sailcraft within the demanding thermal environment concerning a close solar fly-by. The calculation entails an examination spanning multiple days, where the mass of multiple KEIs is evaluated. This assessment is intended to ascertain both the required impactor mass per day and the corresponding duration required to achieve a deflection of 2023 PDC by $2R\oplus$. Additionally, for each individual day within this time frame, the corresponding impact orbit is simulated. This simulation is performed to determine the sail and impact velocities pertinent to each day.

Assuming a sail mass of 81 kg, similar to sunshade arrangement 1 (Table 3.1), this scenario would entail deploying 4200 KEI sailcraft per day, allowing the desired safe deflection distance from Earth to be achieved within 45 days (see Figure 7.3a). In other words, this approach implies 175 sail-impacts per hour. The Figure 7.3a also shows that a number of 2000 impacting KEI per day would lead to a deflection of $1R\oplus$ after 45 days of the impact sequence.

One crucial factor in the calculation is the relatively high mass of the asteroid, which necessitates a larger number of KEI for successful deflection. For instance, if 2023 PDC had a mass comparable to asteroid 99942 Apophis, which is estimated to 4.67 $\times 10^{10}$ kg [26], 690 impactors per day would be required (29 impacts per hour) to achieve deflection within the same 45-day impact-period, see Figure 7.3b.

In other words, the results of this initial analytical approximation demonstrate the feasibility of deflecting a smaller (average) and more frequently Earth impacting asteroid, such as Apophis, using this method with a considerably reduced number of KEI. In contrast, the unusually high mass and size of 2023 PDC pose challenges, necessitating a larger number of sailcraft impacts for successful deflection.

Furthermore, concerning the curves depicting the achieved deflection over the impact duration, it becomes evident that the slope of the curves begins to flatten after approximately 30 days. This reduction in deflection efficiency can be attributed to a localised increase in the necessary momentum transfer (Figure 7.1), indicating a behaviour similar to saturation at this point. This behaviour constrains the impact duration in terms of deflection efficiency.

The benefits of using the planetary sunshade constellation in the context of an asteroid deflection mission are evident when addressing these challenges. With its capacity, estimated in the range of hundreds of millions to potentially over a billion[1]

[1]The precise count hinges on the specific sunshade sailcraft configuration.

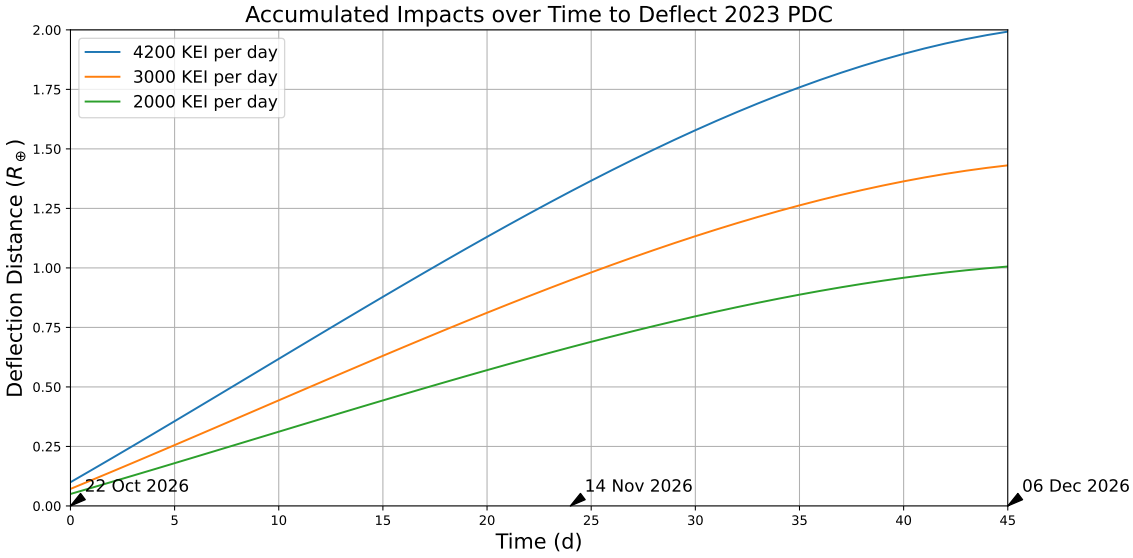

(a) Required KEI per day for the mass of 2023 PDC

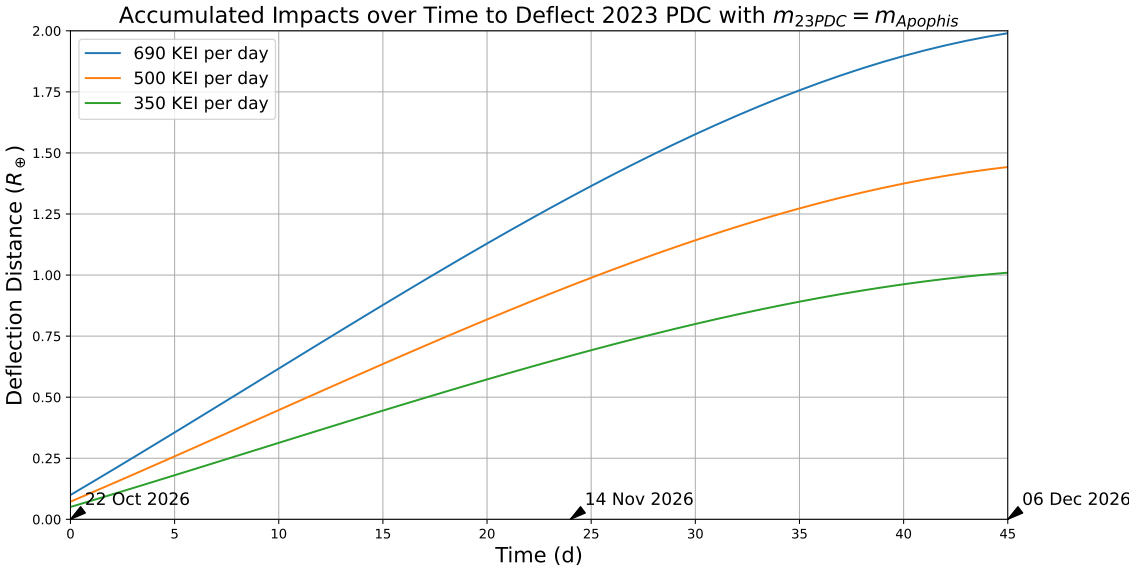

(b) Required KEI if 2023 PDC had the mass of Apophis.

Figure 7.3: A visual representation of accumulated impacts per day required to achieve the safe deflection distance. The analysis employs an analytically approximated impact velocity and assumes an impactor mass of 81 kilogrammes per sail. The first impact is projected for 22 October 2026.

sailcraft units, a practical application for effective asteroid deflection emerges. Even in the case of an asteroid like the 2023 PDC, the number of sailcraft units needed for deflection seems comparatively modest in relation to the resources available within the constellation. This revelation shows the robustness of the proposed strategy, demonstrating how the sunshade sailcraft concept possesses the adaptability for several asteroid deflection missions.

7.1.4 Discussion

The results from the preliminary analysis with analytically approximated impact orbits indicate that the time frame to apply the KEI mission is essential in dealing with potentially hazardous asteroids like 2023 PDC. The required momentum transfer for successful deflection increases exponentially over time, underscoring the importance of identifying suitable impact dates within the available time frame.

The results show that the deflection efficiency is inversely proportional to the asteroid mass, meaning that larger asteroids like 2023 PDC require a higher number of impacting sailcraft for successful deflection compared to smaller asteroids like Apophis. In this specific case, it becomes evident that a KEI deflection mission, designed by determining analytically approximated sail impact orbits, would result in a deflection distance of 1.5 metres per kilogramme of impactor mass, targeting an asteroid with the mass of 2023 PDC. Furthermore, also the analytically approximated impact velocity of 3.27 km/s for an impact date on 22 October 2026 has a significant influence on the achieved deflection distance per kilogramme.

In addition to the magnitude of impact velocity, flight time and asteroid mass, another crucial factor to consider is the influence of the specific impact trajectory, which directly affects the achievable impact velocity. This impact trajectory of the sailcraft is affected by the orbital characteristics of the asteroid, which consequently plays a significant role in determining the optimal launch window and impact conditions for a successful deflection mission. Therefore, a comprehensive analysis of these additional factors is essential to design a mission that enhances the deflection efficiency and ensures the successful outcome of the KEI mission aimed at deflecting 2023 PDC.

Moreover, owing to the substantial quantity of sunshade sailcraft available, the planetary sunshade constellation presents a promising avenue, concerning a sequence of impacts to attain successful deflection of 2023 PDC. To accomplish this for an impact date on 22 October 2026, over 4200 KEI sailcraft per day, each with a mass of 81 kg, would be essential for a time span of 45 days. While the coordination and navigation of such a fleet of sailcraft toward the asteroid poses considerable challenges, the high number of sailcraft within the sunshade constellation must not be overlooked. Having a large number of sailcraft in orbit provides a degree of redundancy and flexibility. In cases where the coordination or steering of individual sailcraft for a precise impact proves challenging or encounters difficulties, the surplus of sailcraft could be redirected towards the asteroid to compensate for any setbacks. This redundancy can mitigate the impact of potential failures in individual sailcraft control during the impact period.

Moreover, the findings from the analysis of accumulated impacts per day underscore

the also importance of the impactor's mass (or sailcraft mass). Therefore the following parameters have been identified as a significant influence on the deflection efficiency for a specific impact date:

- The required momentum transfer for the respective impact date.
- The achieved impact velocity for the respective impact date.
- The mass of the asteroid.
- The mass (and number) of the impacting sailcraft.
- The respective deflection time until the asteroid reaches. Earth

It is crucial to emphasise that the preceding findings serve as a fundamental overview, outlining the efficiency of a preliminary designed deflection mission. This mission revolves around a potential array of theoretical impact trajectories, assessed to determine an attainable impact velocity concerning an elliptic transfer orbit. Consequently, the analysed orbits just serve for the determination of v_{imp} and do not include a realistic transfer from L_1 to the asteroid. Therefore, the subsequent sections of this study, focus on the execution of advanced calculations, specifically aimed the numerical determination of trajectories within InTrance in order to create realistic, physical transfer trajectories from the initial sunshade position to the asteroid. Simultaneously, the development of a procedure is conducted to reveal the best trajectory from an array of possibilities. This, in turn, provides the corresponding launch window within the scope of the analysed mission scenarios. This will reveal whether the applied process offers an opportunity to significantly enhance the deflection efficiency.

7.2 Launch Window Analysis

In this section, the goal is to determine the best launch window, among the investigated mission scenarios, for the KEI mission aimed at deflecting 2023 PDC. The primary objective is to identify the most favourable departure dates among the investigated mission scenarios that result in the trajectories, which enable a successful deflection within a reasonable time frame. To achieve this, the previously discussed two different sunshade sailcraft arrangements are employed concerning the respective sailcraft characteristics. Therefore, the attributes of both sailcraft configurations are implemented into the InTrance calculation. This procedure yields a multitude of trajectories, each optimised by time of flight. Among these numerically calculated trajectories the most effective, in terms of deflection efficiency, shall be identified and subsequently aiding in finding the precise departure date that aligns with the distinctive sailcraft properties and physical limitations of this arrangement.

7.2.1 Sunshade Sailcraft Arrangement 1

To design an asteroid deflection mission aimed for 2023 PDC using the sunshade sailcraft arrangement 1, the initial step involves the selection of an adequate launch window, concerning the respective properties of the sailcraft constellation. This launch window shall provide the best deflection efficiency which can be achieved among the investigated scenarios.

The attributes of the first sailcraft configuration are implemented into the InTrance calculation. This procedure yields a multitude of trajectories, each optimised by time of flight. Among these numerically calculated trajectories the most effective, in terms of deflection efficiency, shall be identified and subsequently aiding in finding the precise departure date that aligns with the distinctive sailcraft properties and physical limitations of this arrangement.

For the first configuration of the sunshield sailcraft, a characteristic acceleration of $0.9\,\mathrm{mm/s^2}$ is given (Table 3.1). This is inserted within the InTrance input to calculate TOF-optimised fly-by trajectories to 2023 PDC starting from the sunshade location close to L_1. These trajectories are calculated with an interval of one month between the departure dates of the sunshade sailcraft and provide the according information concerning the magnitude of the respective impact velocities and the transfer times. These parameters are depicted in Figure 7.4, where the variation of both parameters over a range of departure dates is shown. During the time span of departure dates analysed

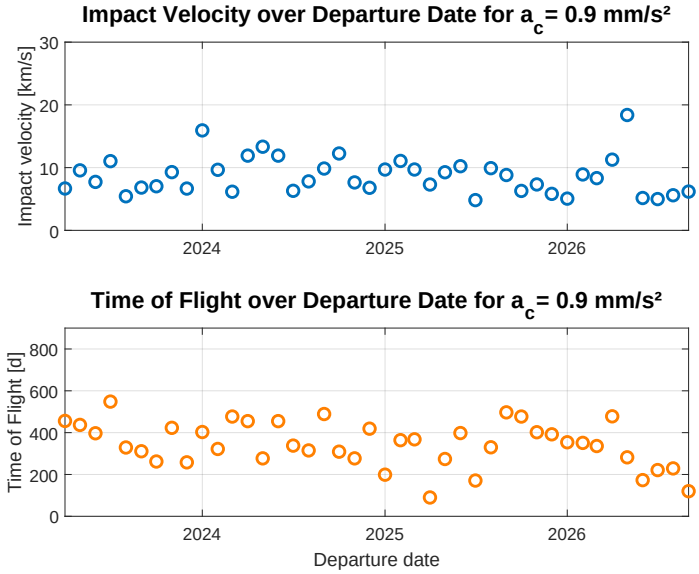

Figure 7.4: Visualisation of time of flight and impact velocity over several departure dates from April 2023 to September 2026 for the sunshade sailcraft arrangement 1 ($a_c = 0.9\ \mathrm{mm/s^2}$).

using InTrance, the impact velocities vary significantly between 4.8 km/s and 18 km/s. Additionally, the flight time required for these trajectories spans a range of 90 days to 548 days, which yields average values of 344 days for TOF and 8.67 km/s for v_{imp}. Despite the

highest impact velocity is achieved on 07 February 2027, this date does not align with an adequate amount of required momentum transfer. As shown in Figure 7.1, the required momentum transfer exhibits a value close to the local maximum on this date, indicating that it might not be the most suitable choice for the deflection mission. Therefore, in order to determine an appropriate launch window for the KEI mission based on the insights from Figure 7.4, a further analysis process is conducted. This process aims to identify the departure date that result in the best trajectory, considering both the impact velocities and the required momentum transfer for successful deflection.

Since the departure date is defined by the TOF and the required momentum transfer to the asteroid is determined by the departure (or impact) date, identifying an achievable launch window involves striking a balance between achieving the highest possible impact velocity and selecting a departure date that corresponds to a local minimum of the required momentum transfer. Figure 7.5 illustrates the range and distribution of the, by InTrance determined impact velocities, along with the corresponding required momentum transfer for the deflection of 2023 PDC. These values are overlaid and visualised depending on the

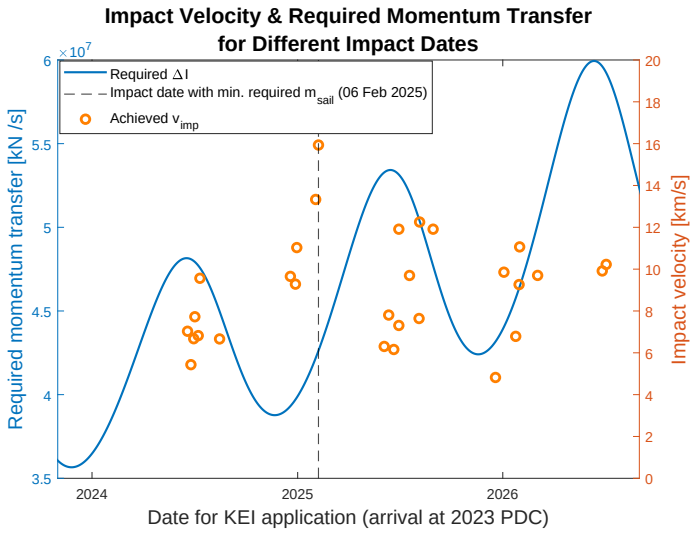

Figure 7.5: Visualisation of the variation of impact velocities determined from InTrance and the corresponding required momentum transfer to deflect 2023 PDC with $a_c = 0.9$ mm/s^2. The values are presented in relation to the impact (or arrival) date and the black line marks the impact date with the assigned lowest required impactor mass.

respective *impact date* in order to visualise the analysis procedure, which aims to identify the best departure date. This process involves finding the smallest required impactor mass for the given departure dates. To achieve this, the relation $\Delta I = m_{\text{sail}} v_{\text{imp}}$ is applied, allowing to determine the corresponding sail mass. In this context, Figure 7.6 shows the respective required impactor masses which result from the according impact velocity achievement and momentum transfer requirement, over the range of applied *departure dates*. Upon analysing both figures, it becomes evident that the most efficient trajectory - among the other calculated trajectories within InTrance - for the KEI implementation is

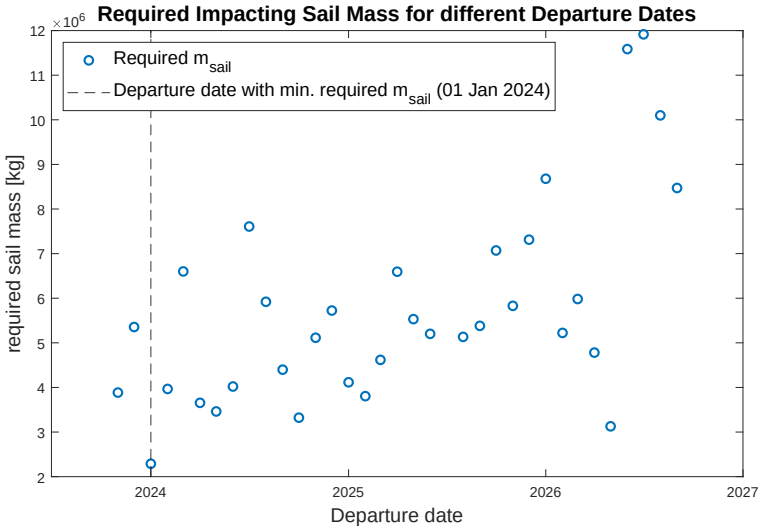

Figure 7.6: Visualisation of the required sail mass to deflect asteroid 2023 PDC, determined from the required momentum transfer and the according achievable impact velocity. The black line marks the departure date on 01 January 2024 with the assigned lowest required impactor mass.

achieved with a departure date on 01 January 2024, resulting in an impact velocity of 15.93 km/s for an impact date on 06 February 2025. The respective launch and impact date is marked within the Figures 7.5 and 7.6 by the black, dashed line. The, from the chosen launch window determined, trajectory requires a minimum sail mass of $m_{\text{sail}} = 2.29 \times 10^6$ kg which corresponds to a number of 28263 single impacting sunshade sailcraft.

These mission parameters determined by the launch window analysis provide a specific framework for for the design of a deflection mission concerning the application of the sunshade sailcraft arrangement 1.

Deflection Efficiency for the Chosen Launch Window

Since the achieved deflection distance is a central parameter for this study, the corresponding mass-specific deflection efficiency for this case is also calculated and shown in Figure 7.7. The figure shows the course of the achieved deflection distance for an impacting sailcraft mass of 1 kg, while the respective asteroid mass is incrementally increased like conducted in Section 7.1.2. Hence, the impact velocity of 15.93 km/s determined from the launch window analysis is used to assess the effectiveness of the selected impact trajectory.

By comparing this mission configuration with the previous results from Section 7.1.2, an improvement in the achieved impact mass-specific deflection distance can be observed for the scenario, which is determined within the launch window analysis. The specific deflection efficiency for this scenario is higher by a **factor of 6.6**, resulting in a value of about **10 m/kg**. Given that this case presents the best option among the investigated

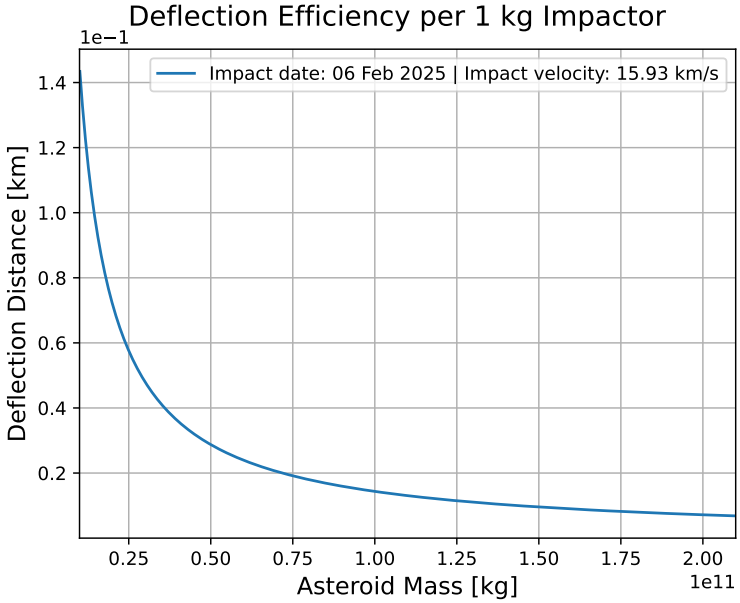

Figure 7.7: The achieved deflection distance $\Delta\xi$ for an increasing asteroid mass in the KEI application for the optimised impact scenario on 06 February 2025 for the sailcraft arrangement 1.

trajectories, it serves as the basis for the further deflection mission design. An overview of the parameters defining the chosen mission scenario can be taken from Table 7.1.

Table 7.1: Boundary conditions for the chosen deflection scenario (sunshade sailcraft arrangement 1).

Departure date	01 January 2024
Impact date	06 February 2025
Time of flight [d]	402
Impacting sail mass [kg]	2.29×10^6
Impact velocity [km/s^2]	15.93
Deflection efficiency [m/kg]	10

Validation of the Launch Window Selection

For the sailcraft arrangement 1, the KEI implementation scenario demonstrates an improved deflection efficiency compared to the previous analysis, where the sailcraft orbits are analytically approximated in order to generate a preliminary overview[2]. However, it is essential to note that achieving an earlier impact date results in a longer

[2]See Section 7.1

deflection time, which is the time from the kinetic impact until the predicted collision date with Earth. Therefore, to assess the impact effectively, a comparison between the two KEI scenarios, one with analytically approximated impact trajectories and the other with the impact velocity resulting from the best transfer trajectory[3], is conducted for the *same impact date* on 06 February 2025. Furthermore, the KEI mission for the analytically approximated case with an impact on 22 October 2026 is conducted to show the actual efficiency enhancement resulting from the previous conducted launch window analysis.

The deflection course of the deflection efficiency is again calculated through the implementation of a KEI mission using a 1 kg heavy impacting sailcraft. Figure 7.8 illustrates that the significant enhancement in deflection efficiency is not solely due to the earlier impact date. The impact velocity combined with the respective required momentum transfer also plays a crucial role in achieving the desired deflection distance. The difference between the orange line (impact date: 06 February 2025) and the green

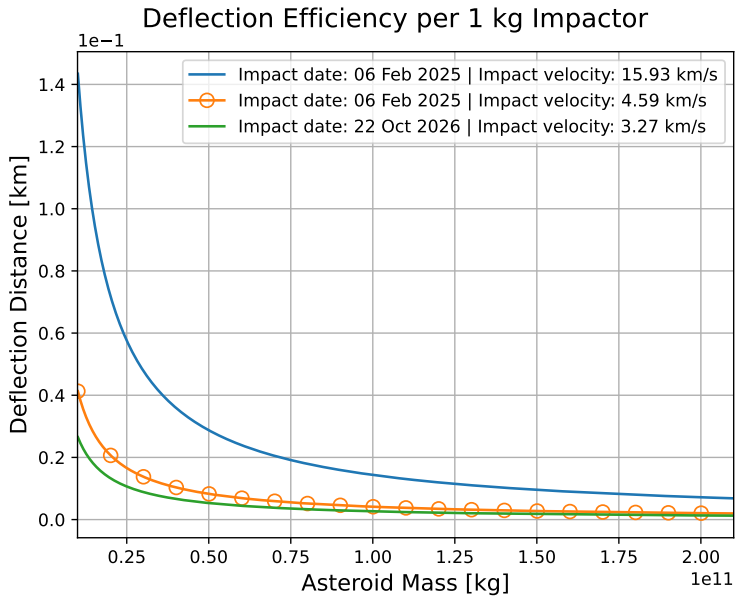

Figure 7.8: Comparison of the deflection efficiencies for 1 kg impactor mass for three cases: (1) the scenario with the best transfer trajectory among the investigated cases for an impact date on 06 February 2025, (2) the analytically approximated mission design with the same impact date, and (3) for an impact date on the 22 October 2026.

line (impact date: 22 October 2026) primarily stems from the variation in deflection time between the two analytically approximated mission designs. The scenario with the earlier impact date on 06 February 2025 involves a longer deflection time, resulting in a higher deflection efficiency for a given asteroid mass compared to the case with the impact date on 22 October 2026. Furthermore, it can be seen that the trajectory which

[3]The best impact trajectory which results from the conducted analysis considering the achieved impact velocity and the required momentum transfer according to a specific launch and impact date.

emerges from the launch window analysis has a significant higher mass specific deflection efficiency. The value for this case approximates 10 m/kg, where the analytically designed mission scenarios approximate 3 m/kg and 1.5 m/kg.

Therefore, the validation process shows that the launch window analysis provides evidence for significant enhancements in deflection efficiency.

Discussion

In conclusion, the findings from the KEI implementation for sailcraft arrangement 1 underscore the important role of the launch window analysis in significantly enhancing deflection efficiency. The comparison between scenarios using analytically approximated impact trajectories and those informed by the launch window analysis demonstrates a substantial improvement.

Furthermore, the validation process emphasises the substantial impact of trajectory selection on mass-specific deflection efficiency. The selected trajectory for the specific launch window not only benefits from an earlier impact date but also leverages higher impact velocity and the corresponding required momentum transfer. As a result, the deflection efficiency of the chosen trajectory from the launch window analysis is markedly higher. This trajectory achieves a mass-specific deflection efficiency of around 10 m/kg, while the analytically designed mission scenarios approximate values of 3 m/kg and 1.5 m/kg.

These outcomes collectively underscore the importance of the launch window analysis and trajectory optimisation in kinetic impactor deflection missions. By considering optimal departure dates and impact trajectories, the deflection efficiency can be significantly enhanced, allowing for more effective deflection of potentially hazardous asteroids. Moreover, the effectiveness of a KEI implementation tends to increase with earlier execution, primarily due to the longer deflection time. In many cases, taking action at an early stage is often challenging due to the complexities of policy formulation, scientific decision-making, and the discovery time of the asteroid. Therefore, optimisation processes like the one discussed hold significant importance in mission planning and design. They allow for the identification of additional local optima, enhancing the likelihood of a successful deflection outcome by exploring a broader range of possibilities.

7.2.2 Sunshade Sailcraft Arrangement 2

In contrast to the first sunshade arrangement, the second configuration embodies a sailcraft design that closely aligns with contemporary achievable state-of-the-art technology. Sailcraft featuring a characteristic acceleration in the vicinity of 0.21 mm/s^2 exemplify a technological benchmark that is close to today's standards. As a result, the focused examination of the sails within this second arrangement holds particular significance.

Similar to the initial arrangement, the second configuration involves the incorporation of distinct sailcraft attributes into the InTrance calculation. This process generates an array of diverse trajectories, each optimised for the time of flight. This evaluation provides

the the best trajectory (among the investigated scenarios) in terms of deflection efficiency and therefore facilitates the identification of the precise departure date harmonising with the specific sailcraft properties.

By examining the impact velocity and time of flight across various simulated departure dates with one month intervals for the second sunshade sailcraft arrangement, a notable difference emerges (Figure 7.9). It becomes evident that the average transfer

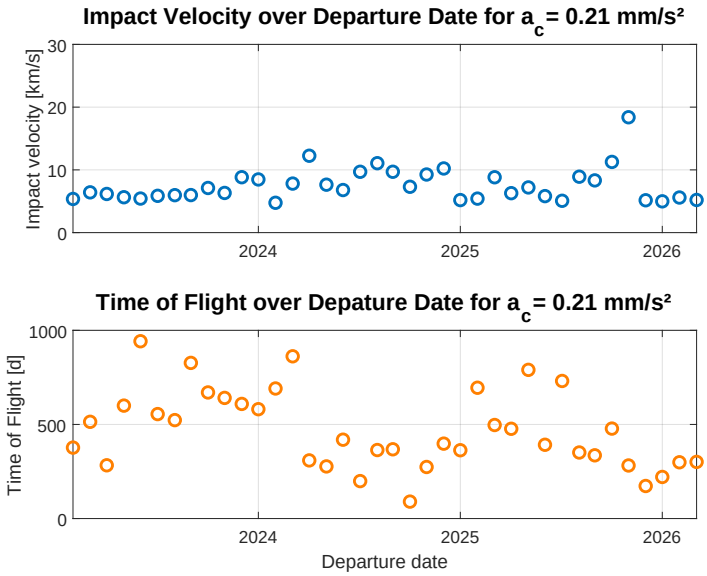

Figure 7.9: Visualisation of time of flight and impact velocity over several departure dates from August 2023 to September 2026 for the sunshade sailcraft arrangement 2 ($a_c = 0.21\,\mathrm{mm/s^2}$).

time associated with the characteristic acceleration of $0.21\,\mathrm{mm/s^2}$ is considerably greater compared to the first arrangement with $a_c = 0.9\,\mathrm{mm/s^2}$. The data depicted in Figure 7.9 yields an average TOF of 467 days and an average impact velocity of 7.5 km/s, while the values for the first sailcraft arrangement amount to 344 days for the average TOF and 8.67 km/s for the average v_{imp}. Consequently, to guarantee the discovery of a TOF-optimised trajectory for every departure date by InTrance, it is required to establish a maximum mission duration of 1000 days for the simulation input. Figure 7.10 shows the overlay of the achieved impact velocities resulting from the TOF-optimised trajectories and the required momentum transfer to deflect 2023 PDC. The figure visually illustrates that by applying a similar approach as that for the first sailcraft arrangement to find the best trajectory, the evaluation of achieved impact velocities in relation to the required momentum transfer showcases the departure date on 01 October 2024 as striking the best balance. This trade-off between necessary momentum transfer and achieved v_{imp} is attained. Consequently, the corresponding mass required for a kinetic impact to successfully deflect 2023 PDC under this specific scenario totals 3.3 $\times 10^6$ kg. This corresponds to an assemblage of 60000 individual sailcraft impacts, each with a mass per sail of 55 kg for this particular arrangement (Figure 7.11). As a result, the corresponding departure date for this scenario is 01 October 2024, which represents

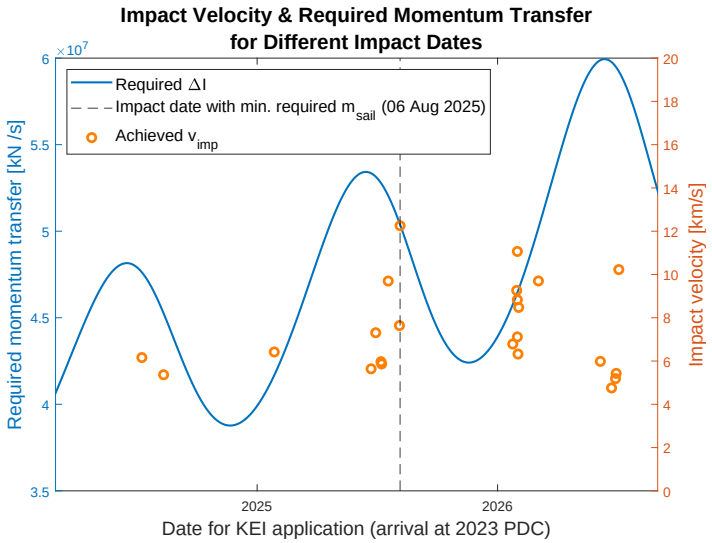

Figure 7.10: Visualisation of the variation of impact velocities determined from InTrance and the corresponding required momentum transfer to deflect 2023 PDC with $a_c = 0.21$ mm/s^2. The values are presented in relation to the impact (or arrival) date and the black line marks the impact date with the assigned lowest required impactor mass.

a shift of the sailcraft launch by 10 months compared to the first arrangement. The achieved impact velocity for this scenario amounts to 12.25 km/s, with a transfer time to the asteroid of 309 days. Since this mission scenario reveals as the best among the investigated cases, it is taken as basis for the further analysis of the KEI implementation for this specific sailcraft arrangement.

Deflection Efficiency for the Chosen Launch Window

Through the use of this specific scenario, a mass-specific deflection efficiency can be calculated, as depicted in Figure 7.12. The attained deflection distance per kilogramme of impacting sail mass for an asteroid like 2023 PDC is approximately **5 m/kg** for this case. The corresponding values for the determined mission scenario can be taken from Table 7.2.

Validation of the Launch Window Selection

The process of validating the analysis methodology, with the objective of finding the best trajectory among the investigated scenarios, is likewise conducted for the sailcraft arrangement 2. This extension allows for an evaluation of the specific deflection efficiency in relation to the mission scenarios where sailcraft orbits are analytically approximated. The primary aim is to determine whether the trajectory design chosen for this sailcraft arrangement exhibits a higher deflection distance per 1 kg of impacting sail mass, extending beyond the influence of a longer deflection time. To ensure the validity of the chosen trajectory for sailcraft arrangement 2, a comparison is again performed involving

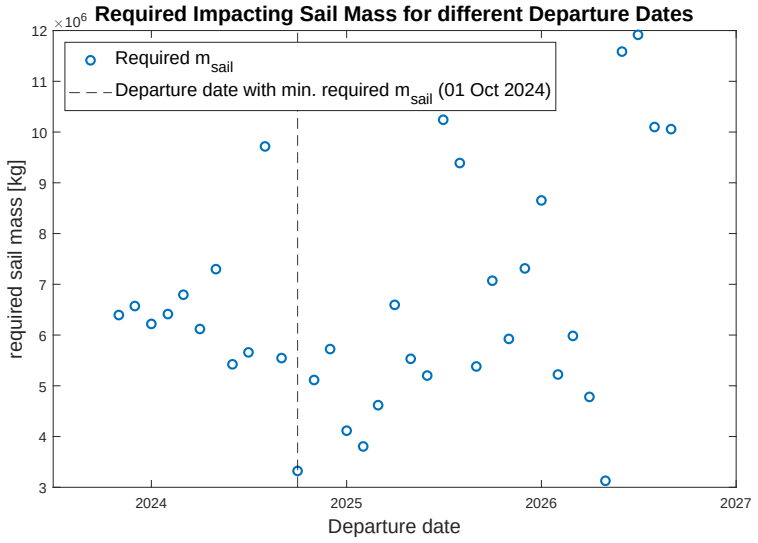

Figure 7.11: Visualisation of the required sail mass to deflect asteroid 2023 PDC, determined from the required momentum transfer and the according achievable impact velocity. The black line marks the Departure date on 01 October 2024 with the assigned lowest required impactor mass.

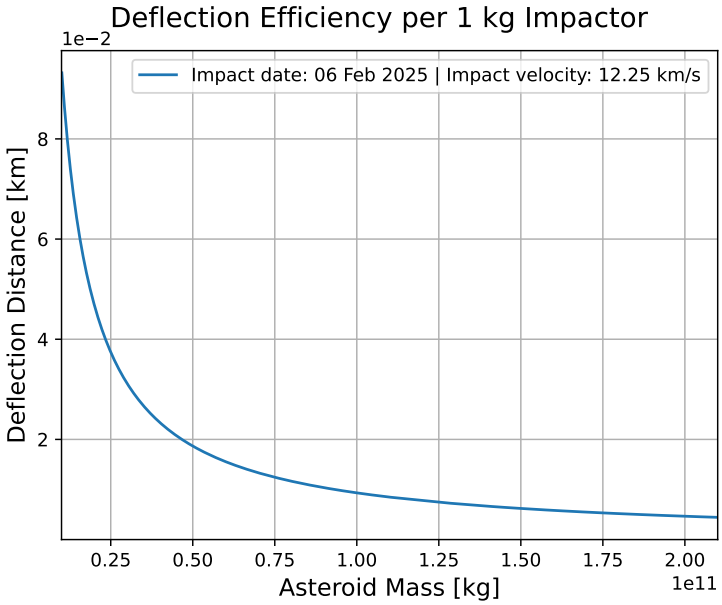

Figure 7.12: The achieved deflection distance $\Delta\xi$ for an increasing asteroid mass in the KEI application for the optimised impact scenario on 06 August 2025 for the sailcraft arrangement 2.

Table 7.2: Boundary conditions for the chosen deflection scenario (sunshade sailcraft arrangement 2).

Departure date	01 October 2024
Impact date	06 August 2025
Time of flight [d]	309
Impacting sail mass [kg]	3.3×10^6
Impact velocity [km/s^2]	12.25
Deflection efficiency [m/kg]	5

three distinct cases: The trajectory selected based on the launch window analysis, which showcases the trajectory design that aligns with the sailcraft arrangement 2 properties and two the scenarios involving analytical approximations for the impact date of 06 August 2025 and the case considering the impact date of 22 October 2026, see Figure 7.13. For both the impact date of 06 August 2025 and that of 22 October 2026, the

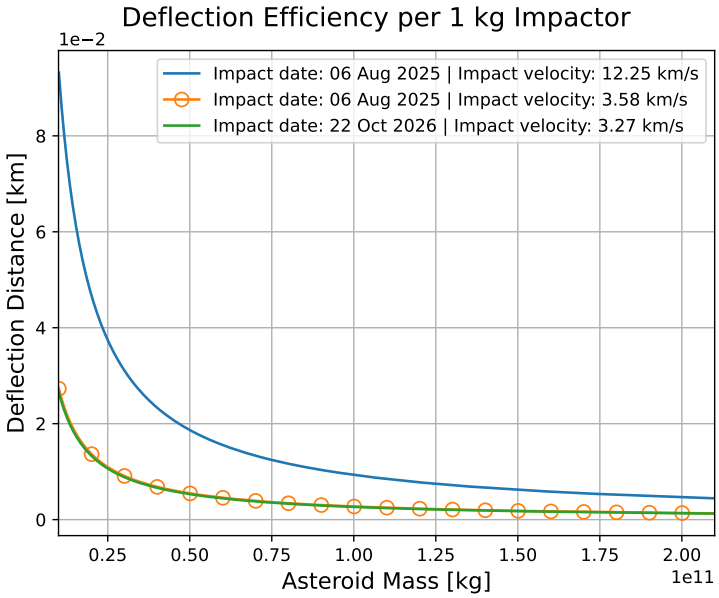

Figure 7.13: Comparison of the deflection efficiencies for 1 kg impactor mass for three cases: (1) the scenario with the best transfer trajectory among the investigated cases for an impact date on 06 August 2025, (2) the analytically approximated mission design with the same impact date, and (3) for an impact date on the 22 October 2026.

analytically approximated impact velocities of 3.58 km/s and 3.27 km/s only slightly differ. This small difference in the deflection efficiencies is visually depicted in the graph, where the curves representing the two analytically approximated scenarios (depicted by the orange and green line) nearly coincide, converging to an approximate impactor

efficiency of 1.5 m/kg. In contrast, the trajectory specifically chosen from the analysed options, which requires the lowest impactor mass and is characterised by an impact velocity of 12.25 km/s (depicted by the blue line), showcases a substantially enhanced deflection efficiency. This trajectory's curve converges toward a value of approximately 5 m/kg, indicating a significant deflection enhancement. Therefore an offset of 4.5 m/kg concerning the approximation values emerges.

Although the absolute deflection efficiency appears relatively lower in comparison to the results from the first sailcraft arrangement, it is important to recognise that the analysis process effectively identifies a trajectory for this sailcraft constellation, which enables an increase in the achieved mass-specific deflection distance.

Discussion

The investigation into the second sunshade sailcraft arrangement, which features a characteristic acceleration of $0.21\,\mathrm{mm/s^2}$, highlights its alignment with current state-of-the-art technological capabilities. The analysis process in order to find the best mission scenario for this arrangement is successful in identifying a trajectory that yields a significantly improved mass-specific deflection distance compared to the analytically approximated trajectory design. Through a comparison involving various scenarios, including the chosen trajectory, analytically approximated alternatives for impact dates on 06 August 2025 and 22 October 2026, a clear trend emerges.

The trajectories with analytically approximated impact velocities for both considered impact dates exhibit only marginal discrepancies. The resultant deflection efficiencies for these cases converge around an approximate value of 1.5 m/kg, indicating a relatively moderate enhancement. However, the trajectory selected from the analysed options, is characterised by an impact velocity of 12.25 km/s and requires the lowest impactor mass, showcases a considerably improved deflection efficiency. This trajectory's curve converges towards a value of approximately 5 m/kg, which is half of the achieved deflection efficiency concerning the chosen mission scenario for sailcraft arrangement 1. This reduction of a factor 2 is relatively modest, especially when taking into account the difference in characteristic accelerations between the two sailcraft arrangements. This finding underscores that sailcraft with a characteristic acceleration of $0.2, \mathrm{mm/s^2}$ can still achieve a significant impact within the context of the analysed mission scenario.

Moreover, despite the initial appearance of a lower absolute deflection efficiency, the analysis successfully identifies a trajectory that significantly enhances the overall deflection efficiency for this particular sailcraft arrangement by 4.5 m/kg compared to the first analytically approximated approach.

7.3 Deflection Mission Design

Now that the framework conditions for the KEI deflection mission is established, the focus shifts towards the detailed analysis of the mission design. This section describes the trajectory properties specific to asteroid 2023 PDC as calculated by InTrance for both cases studied. Subsequently, an adapted KEI implementation is simulated, aiming to

achieve the successful deflection of 2023 PDC. By examining these aspects, the goal is to develop an efficient and viable strategy for deflecting asteroids like 2023 PDC using the described sunshield sailcraft arrangements.

7.3.1 Sunshade Sailcraft Arrangement 1

With the results from the launch window analysis in Section 7.2, a deflection mission scenario for the application of sunshade sailcraft arrangement 1 can be derived. Among the determined trajectories within InTrance, the trajectory with a departure date on 01 January 2024 is chosen for this specific case. Assuming that the sunshade configuration is already implemented by this time and that 2023 PDC was discovered approximately one year ago on 10 January 2023, this departure date becomes feasible with a fast action and decision-making at the scientific and political level.

The determined hyperbolic excess velocity at this point amounts to $v_\infty = 1.32\,\mathrm{km/s}$ ($C_3 = 1.75\,\mathrm{km^2/s^2}$). Figure 7.14 displays the trajectory calculated by InTrance for this specific case. The temperature range throughout the mission is between -83°C (190 K)

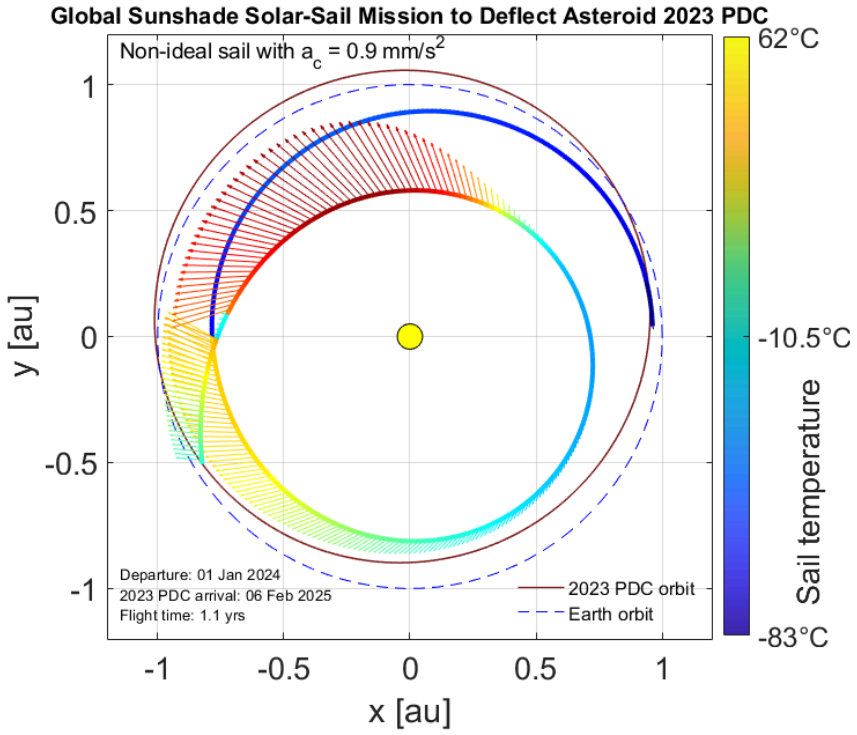

Figure 7.14: Sailcraft trajectory to the asteroid 2023 PDC for a departure date at 01 January 2024, TOF optimised within InTrance.

and 62°C (336 K). The colour of the trajectory line represents the respective temperature, revealing information about the orientation and steering within the optimisation process of InTrance. The lower temperature ranges (dark blue) indicate when the sailcraft's

normal vector is perpendicular to the Sun line ($\alpha \approx 90°$), while the higher temperature regions (orange to red) indicate the sailcraft's surface facing the Sun ($\alpha \approx 0°$). Figure 7.15 provides a detailed view of the sail cone angle over the first 150 days of flight time. During this period, the sail cone angle ranges from 70° to 80°, corresponding to the low-temperature region observed in Figure 7.14. The low temperatures occur when the sailcraft's normal vector is nearly perpendicular to the Sun line, resulting in minimal solar radiation absorption. Regarding the orbital elements, which are depicted in Figure 7.16, it can be seen that the initial values fit well with the implemented launch position. The inclination of 0.01° and the eccentricity measuring below 0.01 as well as the semi-major axis of 0.89 au collectively indicate an initial orbit that closely aligns with a slightly eccentric path within the ecliptic plane, starting at a position close to L_1. At

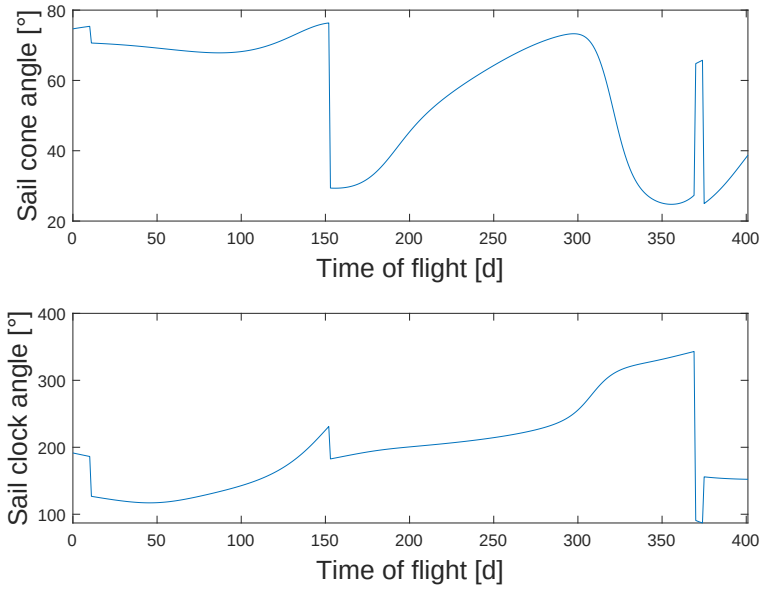

Figure 7.15: Course of the sail cone angle and sail clock angle over the entire mission duration concerning the chosen deflection mission scenario to approach 2023 PDC with $a_c = 0.9$ mm/s^2.

approximately 150 days into the mission, a significant and abrupt change in the sailcraft's orientation occurs. The sail cone angle suddenly decreases to $\alpha = 28°$, accompanied by a change in the sail clock angle δ from 230° to 180°. This orientation shift leads to an instantaneous temperature rise from -80°C to about 25°C, as shown in Figure 7.14, until the sail cone angle increases again to 73°. This shift in orientation causes the sailcraft's surface to face the Sun more directly, resulting in a substantial temperature increase on the sail membrane.

Subsequently, from the 300th to the 350th day of flight, the sail cone angle decreases again to 20°. During this phase, the semi-major axis of the trajectory decreases to 0.67 au, and the orbital eccentricity increases to $e = 0.36$. These changes result in the closest solar

distance encountered throughout the entire trajectory, as shown in Figure 7.16. This also shows that an TOF-optimised transfer trajectory to 2023 PDC exists that does not require to exploit the temperature limitations of the sails, which would occur at a perihelion of approximately 0.4 au. As a consequence, the sail experiences the maximum temperature

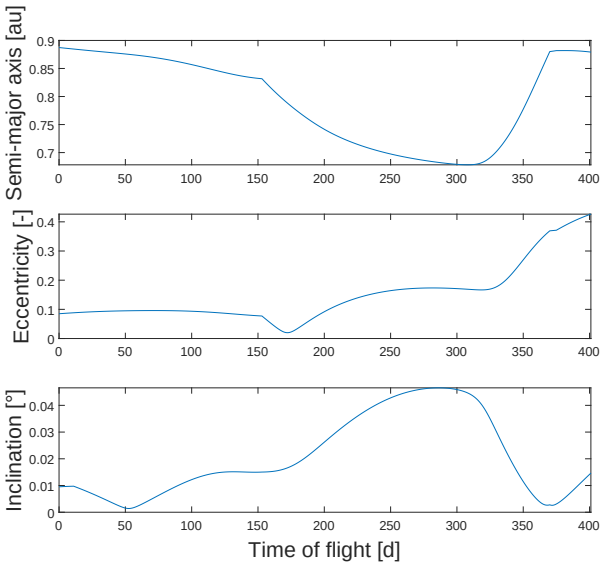

Figure 7.16: Variation of the orbital elements for the chosen mission scenario to approach 2023 PDC with $a_c = 0.9$ mm/s^2.

(T_{max}) of 62°C during this phase of the mission. Towards the end of the mission, there is another rise in the sail cone angle to about 70°, which includes an nearly instantaneous increase in the sail clock angle from 60° to 150°. This change in orientation leads to an increase in the semi-major axis of the orbit, bringing the sailcraft closer to the orbit of 2023 PDC in order to approach the asteroid for the KEI implementation.

Consequently, the chosen departure date of 01 January 2024 allows the sailcraft to achieve a trajectory with a hyperbolic excess velocity of $v_\infty = 1.32$ km/s. The trajectory is analysed, and the steering parameters are adjusted within the InTrance software to define and describe the sailcraft's path. This specific path leads to the according impact velocity of 15.93 km/s, which is selected based on the launch window analysis conducted in the previous section.

Implementation of Accumulated Impacts

Due to the considerable impactor mass of 2.29×10^6 kg required for a single instantaneous impact, a sequenced impact scenario is explored for the optimised case by distributing the impacts over several days (Figure 7.17). The aim is to investigate the feasibility and efficiency of this approach while addressing the challenges posed by the required impactor mass. To perform the accumulated impact analysis, it would provide a higher accuracy to determine the impact velocity for each day within the mission period. A detailed analysis

considering various factors, such as the specific trajectory, steering parameters, and SRP effects, can lead to significant variations in impact velocity over time (as shown in Figure 7.5). However, due to time and resource constraints, conducting a comprehensive analysis

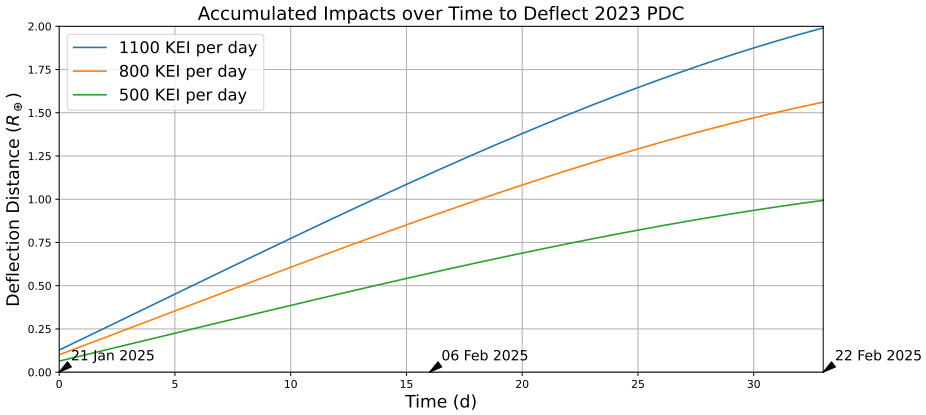

Figure 7.17: Accumulated impact deflection strategy for the optimised case concerning Sunshade Sailcraft Arrangement 1 with a mass of 81 kg per sail.

to determine the impact velocity for each day is not applied within this work. Instead, a simplified approach is adopted, assuming a constant impact velocity of 15.93 km/s for all days in the sequenced impact scenario[4]. Similar to the process detailed in Section 7.1.3, in this context as well, multiple kinetic impactor events are simulated each day by adjusting the impactor mass accordingly. This simulation is carried out over a series of days until a deflection distance of $2R_\oplus$ is achieved.

The results in Figure 7.17 show that by applying this average impact velocity over 33 days, with the middle impact date set as 06 February 2025, 1100 KEI per day are required to achieve a safe deflection distance of $2R_\oplus$. This implies approximately 46 impacts per hour. A deflection distance of 1 Earth radius can be achieved with the application of 500 KEI per day (20 impacts per hour). This demonstrates that the current sequenced impact scenario with the, within the launch window analysis chosen, trajectory and constant impact velocity of 15.93 km/s allows for a substantial reduction in the required number of KEI compared to the initial sequenced impact scenario described in Section 7.1.3. For the same deflection distance achieved over a 12 days shorter time span, the current scenario requires 3100 fewer KEI than the initial analytically approximated scenario.

It is important to acknowledge that the constant impact velocity assumption simplifies the analysis and may lead to deviations from the actual trajectory. Therefore, the results should be interpreted with consideration of these limitations.

Discussion

In conclusion, the analysis of sunshade sailcraft arrangement 1 results in a feasible deflection mission scenario. The trajectory, set to commence on 01 January 2024,

[4]See Section 7.3.3 for a further explanation concerning the chosen simplifications.

effectively aligns with the discovery date of the 2023 PDC, which occurred on 10 January 2023. Throughout its course, the trajectory maintains a relatively stable temperature range between -83°C and 62°C. To address the substantial challenge posed by the required impactor mass, a strategic solution involving the distribution of impacts over 33 days has been devised. With a deflection goal of $2R_{\oplus}$, this approach is premised on assuming a constant impact velocity of 15.93 km/s. Consequently, this scenario necessitates approximately 1100 kinetic impactor events per day, roughly translating to an hourly impact frequency of 46.

In essence, the chosen trajectory from the launch window analysis, combined with the strategic distribution of impact events, underscores the effectiveness of the proposed deflection mission scenario for addressing the deflection of an asteroid like 2023 PDC.

7.3.2 Sunshade Sailcraft Arrangement 2

Similar to the analysis conducted for sunshade sailcraft arrangement 1, an in-depth deflection mission is carried out to assess the application of sunshade sailcraft arrangement 2. By using the boundary conditions specified in Table 7.2, a detailed trajectory analysis was conducted using InTrance. The resulting trajectory is illustrated in Figure 7.18, where the sail's temperature ranges from -46°C (227 K) to -4°C (269 K). Notably, despite the second sailcraft arrangement exhibiting a shorter average transfer time, the time of flight for this particular scenario, to reach 2023 PDC, is 93 days less than the optimised case for sailcraft arrangement 1. It is worth mentioning the relatively low hyperbolic excess velocity of 0.16 km/s ($C_3 = 0.0256\,\mathrm{km^2/s^2}$) associated with the departure date on 01 October 2024. With a TOF of 309 days, the transfer duration is shorter than the regular heliocentric orbital period of the target asteroid. Analysing the orbital characteristics depicted in Figure 7.18, the trajectory extends beyond the orbit of 2023 PDC. The sailcraft experiences its highest temperature of -4°C during the initial 20 days of the journey when the sail cone angle ranges from 15° to 0° (Figure 7.19). Subsequently, α gradually increases to approximately 20° until day 55. Notably, the temperature then reduces to a minimum of approximately -46°C, remaining relatively stable between days 200 and 280. The sail cone angle undergoes significant changes primarily within the first 100 days of flight. Initially rotating from 240° to 300° in the initial 50 days, it then gradually decreases to 290° by day 100. An abrupt 70° rotation (from 300° to 230°) occurs around day 95. Examining the evolution of orbital elements throughout the transfer, an outward spiralling pattern can bee seen in the course of the semi-major axis, which increases until day 100 (see Figure 7.20). After this, the semi-major axis gradually decreases again in order to align with the orbit of 2023 PDC at a distance of 0.86 au. The eccentricity and inclination of the trajectory experience moderate increases as the sailcraft progresses from the L_1 position to match the orbital parameters of 2023 PDC.

Implementation of Accumulated Impacts

Similar to the analysis conducted for sunshade sailcraft arrangement 1, an investigation of the cumulative impacts approach is also carried out for sunshade sailcraft arrangement 2.

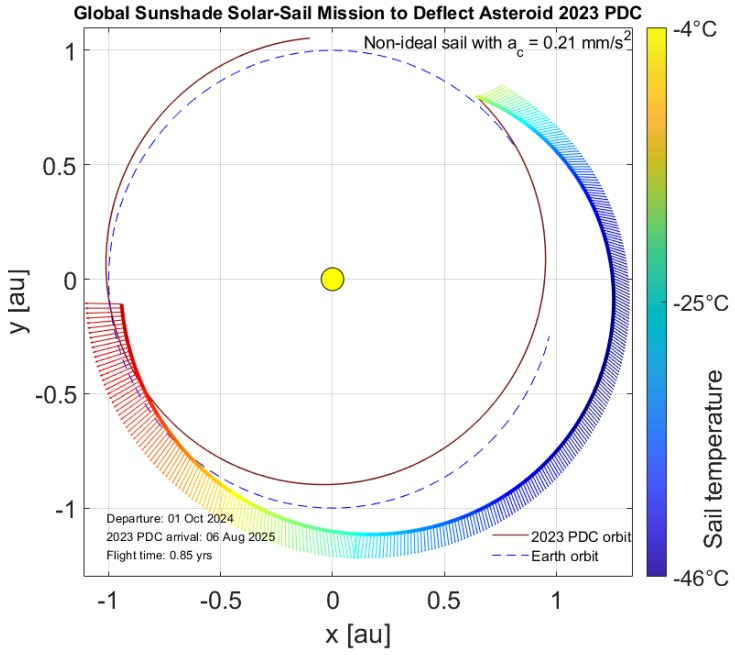

Figure 7.18: Sailcraft trajectory to the asteroid 2023 PDC for a departure date at 01 October 2024, TOF optimised within InTrance.

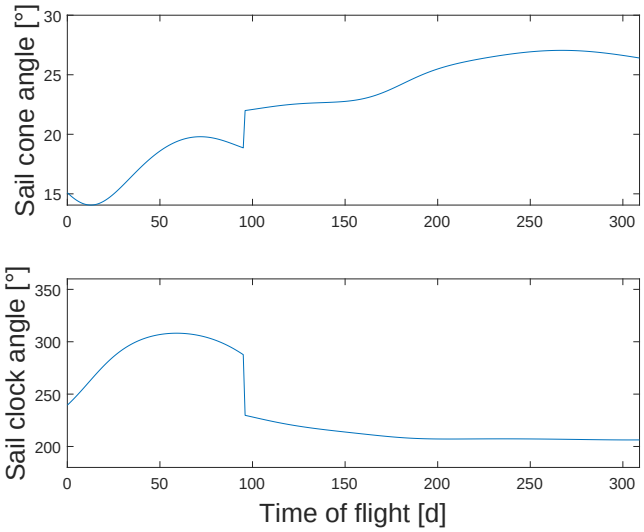

Figure 7.19: Course of the sail cone angle and sail clock angle over the entire mission duration concerning the chosen deflection mission scenario to approach 2023 PDC with $a_c = 0.21\,\mathrm{mm/s^2}$.

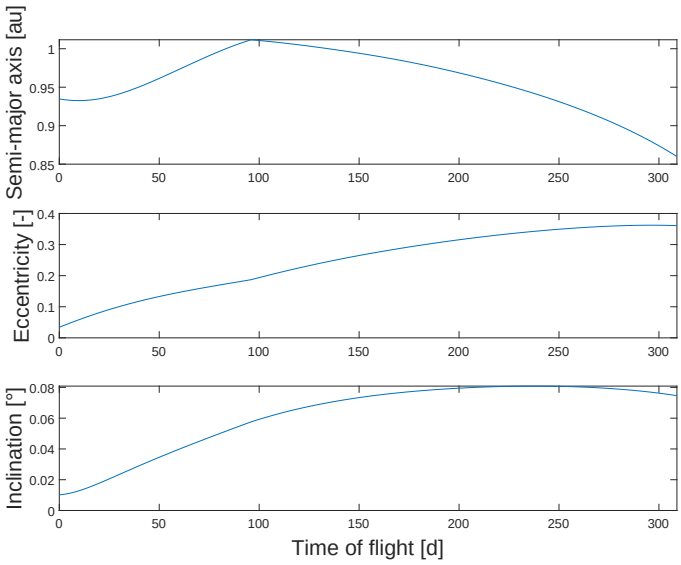

Figure 7.20: Variation of the orbital elements for the chosen mission scenario to approach 2023 PDC with $a_c = 0.21$ mm/s^2.

The impact date determined through the optimisation process, which falls on 06 August 2025, is again chosen as the central date for this evaluation. The average impact velocity of 12.25 km/s, previously derived during the optimal launch window analysis, is applied over the specified time span.

With these established boundary conditions for a sequenced KEI implementation, the results depicted in Figure 7.21 reveal that for this specific scenario with sunshade sailcraft arrangement 2, a number of 2250 KEI per day are required over a 30-day duration to successfully deflect asteroid 2023 PDC by a safe deflection distance of $2R_\oplus$. Achieving a

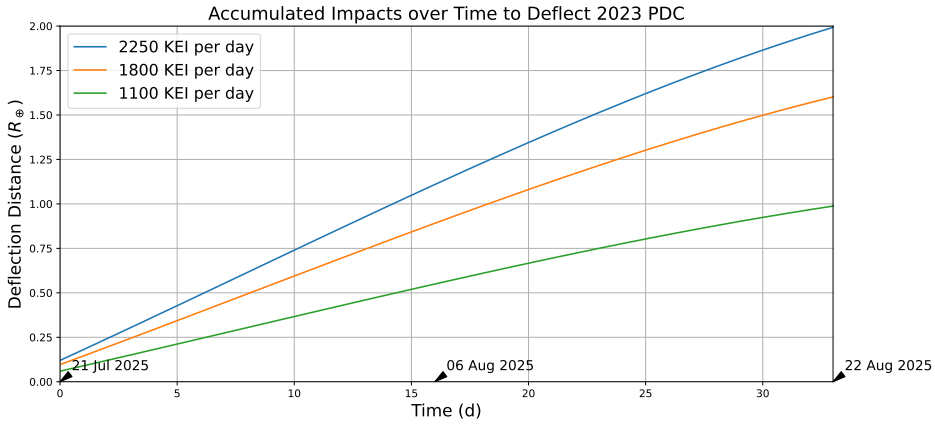

Figure 7.21: Accumulated impact deflection strategy for the optimised case concerning Sunshade Sailcraft Arrangement 2 with a mass of 55 kg per sail.

deflection distance of one Earth radius necessitates the impact of 1100 sunshade sailcraft. It is important to note that a key distinction of this sailcraft arrangement compared to the

first one is the smaller mass per sailcraft. This particular attribute introduces a challenge as a higher number of sails must be coordinated to achieve a successful deflection due to the lower individual mass of each sailcraft.

Discussion

A corresponding mission design for the implementation of the accumulated impact approach is devised for the second sailcraft arrangement. The trajectory, requiring 309 days for transfer to 2023 PDC, results in a final impact velocity of 12.25 km/s. Also here, the outcome of the launch window analysis shows significant enhancements by the application of the accumulated impact approach over several days. For this implementation the lower mass of the sailcraft within this configuration represents a significant disadvantage for the KEI efficiency, which nonetheless, is effectively addressed through the applied analysis process. Notably, despite the sails of the second arrangement being less massive than those of arrangement 1, the from the launch window analysis determined scenario demands 1950 less impacting sailcraft from arrangement 2 than arrangement 1 does in the analytically approximated KEI mission, see Figure 7.3a. Furthermore, the observation underscores the unique paradigm shift introduced by the prospect of deploying a vast number of sailcraft. The possibility of deploying a large number of sailcraft not only disrupts conventional optimisation and mission design strategies but also transforms the anticipated outcomes concerning the specific sailcraft characteristics.

7.3.3 Deflection Strategy Assessment

Throughout the analysis, it becomes apparent that while the sequenced impact scenario allows for a reduction in the required impactor mass per day, it introduces complexities and imperfections in the calculation of the deflection process. One of the main challenges represents the assumption of a constant impact velocity for each day, which may not fully reflect the actual variations in impact velocity that could occur due to the trajectory's sensitivity to steering parameters and solar radiation pressure effects. The impact velocity is significantly dependent on the specific trajectory, and small variations in the sailcraft's orientation and position relative to the Sun can lead to significant changes in v_{imp}. As a result, the assumed constant impact velocity might not fully capture the dynamics of the deflection process, potentially slightly affecting the overall deflection efficiency and accuracy of the mission.

The constant v_{imp} approach is employed to facilitate the analysis, considering the limitations of resources and time constraints. However, it is essential to recognise that this simplification may lead to deviations from the most accurate results. Furthermore, variations in the impact velocity can influence the momentum transfer and deflection efficiency for each impact. Inaccuracies in the assumed v_{imp} values could impact the overall cumulative deflection achieved by the sequenced impacts.

Another important aspect to consider is the operational challenges posed by the sequenced impact scenario. Coordinating and executing a series of impacts over multiple

days necessitates precise planning and coordination of the sunshade sailcraft. Deviations from the planned schedule or disturbances during the mission could affect the accuracy of the deflection process.

Despite these imperfections and complexities, the accumulated impact analysis provides valuable insights into the potential feasibility and efficiency of the sequenced impact scenario. The results provide a foundational understanding of the cumulative deflection achieved through this approach, serving as a initial step for further exploration and refinement. This includes the potential implementation of an actual simulation optimised for maximum deflection using InTrance.

Chapter 8

Conclusion

8.1 Summary

This thesis explores the use of planetary sunshade sailcraft as kinetic impactors for the deflection of potentially hazardous asteroids, with a specific focus on the case of 2023 PDC as outlined in the Planetary Defence Conference 2023 scenario. These planetary sunshade sailcraft, designed by the Planetary Sunshade Foundation, are intended for space-based geoengineering, positioned near the Sun-Earth Lagrange Point 1.

Two distinct sunshade sailcraft arrangements, introduced and designed in [32], are employed for the kinetic impactor implementation. Both arrangements exhibit a TRL ranging from 3 to 4 by today's standards. The second arrangement, although requiring less research time and capacity for realisation, offers similar potential as the first one. Remarkably, both arrangements would consist of a high number ranging from one hundred million to over one billion individual units. The investigation reveals that due to this substantial quantity of available sails in interplanetary orbit, the application of accumulated sailcraft kinetic impacts holds considerable promise for the deflection of potentially hazardous asteroids. To optimise the mission design for sequenced impacts, trajectory analysis is performed within InTrance, exploring various time-of-flight-optimised trajectories to reach asteroid 2023 PDC. The corresponding impact velocities and arrival dates are determined and related to the required momentum transfer for deflecting 2023 PDC by two Earth radii.

Considering both the necessary momentum transfer and the achieved impact velocity, an optimal mission design is established among the analysed scenarios. For sailcraft arrangement 1, the launch date of 01 January 2024, with a corresponding impact velocity of 15.93 km/s, yields the best scenario, arriving at the asteroid on February 6, 2025. For sailcraft arrangement 2, the launch date of 01 October 2024, with a corresponding impact velocity of 12.25 km/s, emerges as the optimal scenario, reaching the asteroid on 06 August 2025.

Validation of the optimisation process involves comparing the mass-specific deflection efficiency between analytically designed impact orbits and optimised mission designs. The outcomes highlight a substantial enhancement for both sailcraft arrangements through

the applied optimisation process. For an asteroid of 2023 PDC's mass magnitude, sailcraft arrangement 1 achieves a deflection efficiency of 10 metres per kilogram, while arrangement 2 achieves 5 metres per kilogram. In contrast, the analytical case demonstrates an efficiency of 1.5 metres per kilogram. Furthermore, the validation process underscores that the enhancement of deflection efficiency is not solely reliant on extended deflection time; the optimisation process exerts additional influence. Consequently, the analysis underscores that planetary sunshade sailcraft offer not only a promising strategy against global warming but also an opportunity for deflecting potentially hazardous asteroids, due to their substantial mass presence in interplanetary space.

By applying the conducted optimisation process, it becomes evident that such a mission can be markedly improved by optimising trajectories based on achieved impact velocities and arrival dates. InTrance, in this context, proves invaluable, facilitating the discovery of specific trajectories and the development of an apt mission design for impactor sailcraft.

8.2 Outlook

The research conducted in this thesis opens avenues for further exploration and development in the field of planetary defence and space-based geoengineering. Several key areas present potential directions for future research and application:

- **Advanced Trajectory Optimisation**: While this thesis demonstrates the efficiency of using planetary sunshade sailcraft as kinetic impactors for asteroid deflection, there remains room for further refinement in trajectory optimisation techniques. Future research could focus on more sophisticated algorithms and computational methods to identify even more optimal trajectories, potentially leading to enhanced deflection efficiencies and reduced mission costs. Additional improvements within the optimisation process will also contribute to a more precise mission design, particularly in areas such as accurately determining the impact velocities for each day of a sequenced kinetic impact mission.

- **Multi-Sailcraft Coordination**: The use of multiple sailcraft in coordinated formations holds promise for increasing deflection capabilities. Investigating the dynamics and control strategies of sailcraft constellations could lead to innovative methods for diverting larger and more complex asteroids.

- **Technology Advancements**: As technology continues to evolve, advancements in materials science, propulsion systems, and autonomous control could revolutionise the design and deployment of planetary sunshade sailcraft. Exploring novel materials with improved strength-to-weight ratios and developing more efficient propulsion mechanisms could contribute to more effective deflection missions.

- **Asteroid Erosion and Deflection Dosage**: Further exploration into the erosion of asteroids due to numerous impacts could provide valuable insights. Additionally,

the concept of measuring the deflection of the target asteroid could enable precise dosing of impactors to avoid keyholes and fine-tune the deflection trajectory. Unused sailcraft in a kinetic impactor scenario could potentially be redirected to maximise miss distance, avoiding dust coma interactions, and then return to the sunshade. This approach could simplify decision-making, decouple the mission timeline from orbital dynamics, and enable parallelisation.

- **New Paradigms in Mission Design**: The unique challenges posed by the potential for numerous sailcraft open up new paradigms in optimisation and mission design. This is inherent to sailcraft, where continuous acceleration is possible due to the absence of fuel consumption, a departure from traditional Δv minimisation. The added dimension of a large number of spacecraft and the concept of "decision after departure" further contribute to the emerging landscape of mission design.

In conclusion, the findings and insights gained from this work provide a foundation for future research endeavours aimed at refining and expanding our capabilities in planetary defence. The exploration of the outlined areas of future research enable working towards safeguarding planet Earth from potential asteroid impacts and advancing our understanding of space-based technologies for the greater benefit of humanity.

Appendix A

Reference Frames

A.1 Cartesian Coordinate Systems

Essential for characterising the motion of an object is the establishment of a coordinate system. Initially, we consider the Cartesian coordinate system, illustrated in Figure A.1, which is a right-handed, orthogonal inertial frame featuring the origin $\mathcal{O}$ and the three Cartesian unit vectors $\{\hat{\boldsymbol{x}}, \hat{\boldsymbol{y}}, \hat{\boldsymbol{z}}\}$. The vector $\boldsymbol{r}$ serves as an illustration of the current position of an object in three-dimensional space. The components of $\boldsymbol{r}$, namely $\{x, y, z\}$, correspond to its respective coordinates [25].

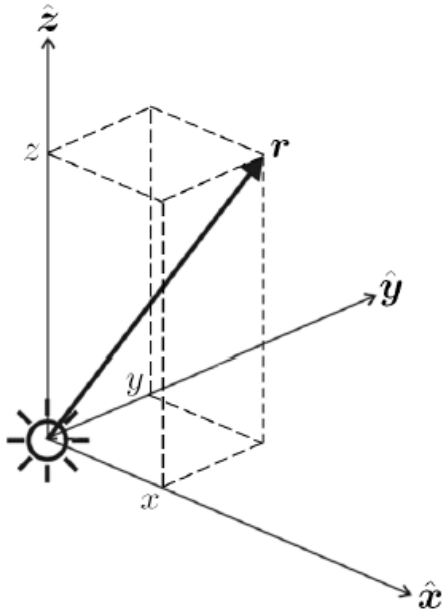

Figure A.1: Cartesian coordinate system. [25]

$$\boldsymbol{r} = \begin{pmatrix} x \\ y \\ z \end{pmatrix} \tag{A.1}$$

A.2 Spherical Coordinate Systems

In the context of astrodynamics, the utilisation of a *spherical coordinate system* is crucial. The spherical coordinates consist of the *azimuth angle* φ, the *elevation angle* θ, and the *position vector* $\boldsymbol{r}$. The three spherical unit vectors are $\hat{\boldsymbol{r}}, \hat{\boldsymbol{\varphi}}, \hat{\boldsymbol{\theta}}$, and they are determined by the following relationships:

$$\hat{\boldsymbol{\theta}} = \hat{\boldsymbol{r}} \times \hat{\boldsymbol{\varphi}} \tag{A.2}$$

Here, $\hat{\boldsymbol{r}}$ represents the unit vector pointing in the direction of $\boldsymbol{r}$, as depicted in Figure A.2 [25]. When observed from the initial Cartesian reference frame, the components of the spherical unit vectors are can be expressed by the following coherences.

$$\hat{\boldsymbol{r}} = \begin{pmatrix} \cos\varphi\cos\theta \\ \sin\varphi\cos\theta \\ \sin\theta \end{pmatrix} \tag{A.3}$$

$$\hat{\boldsymbol{\varphi}} = \begin{pmatrix} -\sin\varphi \\ \cos\varphi \\ 0 \end{pmatrix} \tag{A.4}$$

$$\hat{\boldsymbol{\theta}} = \begin{pmatrix} -\cos\varphi\sin\theta \\ -\sin\varphi\cos\theta \\ \cos\theta \end{pmatrix} \tag{A.5}$$

Hence, the position ($\boldsymbol{r}$), velocity ($\dot{\boldsymbol{r}}$), and acceleration ($\ddot{\boldsymbol{r}}$) of the celestial body under consideration in spherical coordinates are determined by

$$\boldsymbol{r} = r\hat{\boldsymbol{r}} \tag{A.6}$$

$$\dot{\boldsymbol{r}} = \dot{r}\hat{\boldsymbol{r}} + r\dot{\varphi}\cos\theta\hat{\boldsymbol{\varphi}} + r\dot{\theta}\hat{\boldsymbol{\theta}} \tag{A.7}$$

$$\begin{aligned} \ddot{\boldsymbol{r}} = {} & (\ddot{\boldsymbol{r}} - r\dot{\theta}^2 - r\dot{\varphi}^2\cos^2\theta)\hat{\boldsymbol{r}} \\ & +(2\dot{r}\dot{\varphi}\cos\theta + r\ddot{\varphi}\cos\theta - 2r\dot{\varphi}\dot{\theta}\sin\theta)\hat{\boldsymbol{\varphi}} \\ & +(2\dot{r}\dot{\theta} + r\ddot{\theta} + r\dot{\varphi}^2\sin\theta\cos\theta)\hat{\boldsymbol{\theta}} \end{aligned} \tag{A.8}$$

A.3 Polar Orbit Reference Frames

The rotating polar orbit reference frame is illustrated with the components $\hat{\boldsymbol{r}}, \hat{\boldsymbol{t}}, \hat{\boldsymbol{h}}$. The unit vector $\hat{\boldsymbol{r}}$ indicates the direction from the central body to the orbiting asteroid, while $\hat{\boldsymbol{h}}$ points in the direction of the asteroid's angular momentum, perpendicular to the orbit plane [25]. Additionally, $\hat{\boldsymbol{t}}$ represents the transversal unit vector,

$$\hat{\boldsymbol{h}} = \hat{\boldsymbol{r}} \times \hat{\boldsymbol{t}}\,, \tag{A.9}$$

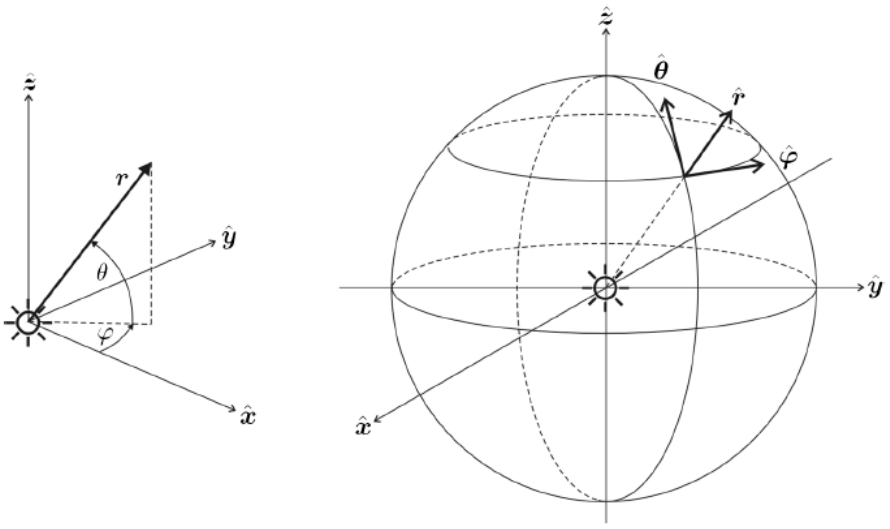

Figure A.2: Spherical coordinates [25].

where the right-handed coordinate system satisfies the relationship.

Appendix B

3D Orbit Parameters

Orbital mechanics relies on various parameters to define orbits in three-dimensional space (Figure B.1). For a *two-body problem*, the velocity vector $\boldsymbol{v}$, the distance vector $\boldsymbol{r}$ between

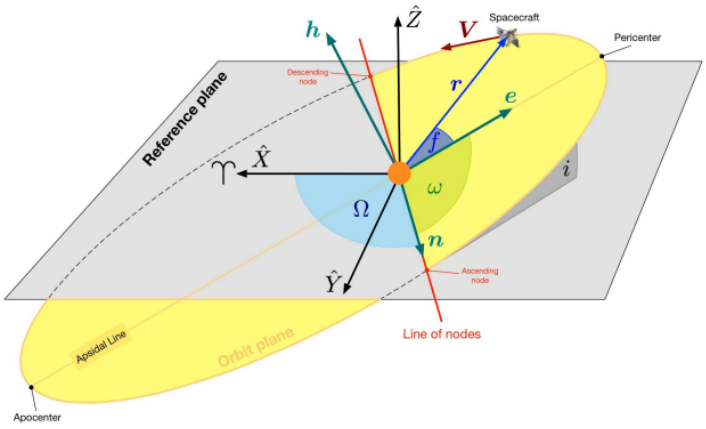

Figure B.1: Orbit in three-dimensional space [25].

the central and orbiting body, and the reference time t define an orbit completely [82]. The distance vector $\boldsymbol{r}$ represents a position within the orbit and is mathematically described by r, where p denotes the *semi-latus rectum*. Additionally, the specific angular momentum $\boldsymbol{h}$ and the specific *orbital energy* E are significant parameters, with the latter being a function of a and μ.

$$E = -\frac{\mu}{2a} \tag{B.1}$$

The magnitude of the orbit velocity v can be determined fundamentally by the so-called *vis-viva equation* (B.2).

$$v = \sqrt{\frac{2\mu}{r} - \frac{\mu}{a}} \tag{B.2}$$

Of interest in orbital mechanics is the *orbital period* P, which represents the time taken by an object to complete a full orbit around its central body. Additionally, there are six other scalars that define the shape and orientation of an orbit (see Figure B.1). The primary

parameters a, e, f capture the motion of an object within the orbital plane. The *semi-major axis* (a) determines the size of the orbit and, consequently, the orbital period. The radii r_p and r_a denote the distances from the central body to the *pericenter* and *apocenter* (also known as periapsis and apoapsis) of the orbit, respectively. The eccentricity e characterizes the orbital shape, while the angle f (known as the *true anomaly*) describes the position of the orbiting body within the orbital plane [25]. In certain cases, it is more beneficial to determine the *mean anomaly* numerically with $M = E - e \sin E$, which is the Kepler equation when E is defined as the *eccentric anomaly*. The remaining three parameters Ω, ω, i describe the orientation of the orbit. *The longitude of the ascending node* (Ω) determines the orientation of the orbital plane [25]. The value of ω, also known as the *argument of pericenter*, specifies the orbit's orientation relative to the orbital plane. Lastly, the *orbital inclination* (i) represents the tilt of the orbit with respect to the orbital plane [25]. To analyse the motion of asteroids within the solar system, the *ecliptic plane*[1] is often selected as the *reference plane*.

B.1 Shapes of Orbits and Interplanetary Trajectories

Celestial bodies can follow various types of flight paths represented by *conic sections* [25] (Figure B.2). Kepler's first law established that almost all orbits are ellipses [67], making the elliptic orbit a fundamental geometric description for the motion of planets and celestial objects around their central body. A special case of an ellipse is the circular orbit, both of which are considered *closed* paths or *orbits*. In contrast, *opened* shapes such as parabolic and hyperbolic paths are referred to as *trajectories* [25]. To escape from a closed orbit, a S/C must achieve the minimum required escape velocity $v_\infty = \sqrt{\frac{2\mu}{r}}$, which occurs when the total orbital energy (equation (B.1)) equals zero [16]. The

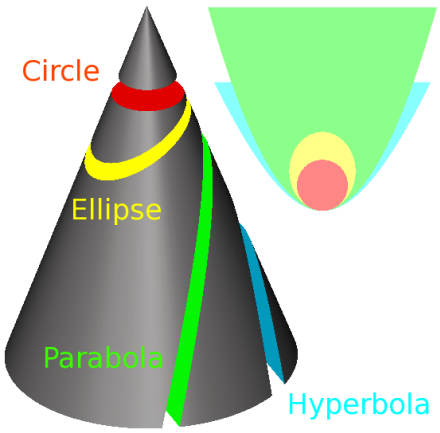

Figure B.2: Conic sections [30].

[1] The ecliptic plane corresponds to the orbital plane of the Earth around the Sun [82].

fundamental parameters, required for a precise orbit construction, can be determined by the earlier discussed equations from section B.1. With respect to these parameters, the most important adjusted formulae are embodied in Table B.1.

Table B.1: The orbit formulae.

	e	**r**	**a**	**V**	**E**	**P**
Circle	$e = 0$	$p = \frac{h^2}{\mu} = \text{const.}$	r	$\sqrt{\frac{\mu}{r}}$	$-\frac{\mu}{2r}$	$2\pi\sqrt{\frac{r^3}{\mu}}$
Ellipse	$0 \leq e \leq 1$	$\frac{p}{1+e\cos f}$	$\frac{r_\mathrm{p}+r_\mathrm{a}}{2}$	$\sqrt{\frac{2\mu}{r} - \frac{\mu}{a}}$	$-\frac{\mu}{2a}$	$2\pi\sqrt{\frac{a^3}{\mu}}$
Parabola	$e = 1$	$\frac{p}{1+\cos f}$	-	$\sqrt{\frac{2\mu}{r}}$	0	-
Hyperbola	$e > 1$	$\frac{p}{1+e\cos f}$	$\frac{p}{1-e^2}$	$\sqrt{\frac{2\mu}{r} - \frac{\mu}{\lvert a\rvert}}$	$-\frac{\mu}{2\lvert a\rvert}$	-

Appendix C

Further Deflection Possibilities

The concepts discussed below outline theoretical possibilities and ideas for asteroid deflection. However, for the purpose of this work, they are not substantially relevant and will be briefly touched upon:

C.1 Gravity Tractor

The concept of the gravity tractor revolves around deploying a spacecraft in close proximity to an asteroid and utilizing its gravitational attraction to induce a gradual alteration in the asteroid's trajectory. Through the spacecraft's gravitational pull, a gentle yet persistent force is exerted, enabling long-term deflection. However, it is important to note that this approach necessitates maintaining extended proximity to the asteroid over a considerable period of time to achieve the desired deflection. [6] [79].

C.2 Solar Collector

This concept exploits solar energy to deflect asteroids. By using a large mirror or concentrator, sunlight is focused onto the asteroid's surface. The absorbed energy creates a jet of vaporized material that acts as a thruster, causing the asteroid to deviate from its original trajectory. [45].

C.3 Ion Beam Shepherd

The ion beam method operates by directing ions towards the surface of an asteroid, leading to a transfer of momentum and a resultant "pushing effect" [8]. To facilitate the necessary push, the implementation of this technique necessitates the utilization of two ion engines [8]. Consequently, employing two engines reduces the risk of fragmentation.

C.4 Smart Clouds

The utilisation of smart clouds for asteroid deflection is a concept that revolves around the deployment of a substantial cloud consisting of small particles. These particles impact the surface of the Near-Earth Asteroid (NEA), resulting in a transfer of momentum to the asteroid itself [34]. Similar to the ion beam shepherd method, this technique carries a slight risk of potential asteroid fragmentation [34].

C.5 Laser Ablation

A laser is employed to heat up the surface of the asteroid, resulting in the evaporation of material from the asteroid's surface. This material ejection generates the required momentum to alter the orbit of the NEA [77]. This method operates on the same underlying physical principle as the Solar Collector technique.

C.6 Nuclear Explosive Devices

In this approach, a nuclear explosive device is strategically positioned near the surface of the Near-Earth Asteroid (NEA) and detonated at an altitude adjusted to the composition of the asteroid. The intention is not to completely destroy the asteroid but rather to mitigate the threat it poses. As the released energy is converted into thermal heat, an additional deflection effect takes place, similar to the phenomenon observed in laser ablation [9].

C.7 Painting the Asteroid

In general, this deflection technique is founded on the physical principle known as the Yarkovsky effect. The objective is to coat the asteroid with a specialized paint, which serves to influence the impact of solar radiation pressure and generate a kinetic momentum through the interaction with the painted surface [61].

Bibliography

[1] European Space Agency. *The NEOCC is ESA's centre for computing asteroid and comet orbits and their probabilities of Earth impact).* 2023. URL: https://neo.ssa.esa.int/.

[2] R. P. Binzel et al. "Apophis 2029: Decadal Opportunity for the Science of Planetary Defense". In: *Planetary Science and Astrobiology Decadal Survey 2023-2032* (2020). DOI: http://newton.mines.edu/paul/meetings/decadal2020/decadal2020Apophis.pdf.

[3] C. M. Baum, S. Low, and B. K. Sovacool. "Between the sun and us: Expert perceptions on the innovation, policy, and deep uncertainties of space-based solar geoengineering". In: *Renewable and Sustainable Energy Reviews* 158 (2022), p. 112179. ISSN: 13640321. DOI: 10.1016/j.rser.2022.112179.

[4] R. Bewick, J. P. Sanchez, and C. R. McInnes. "The feasibility of using an L1 positioned dust cloud as a method of space-based geoengineering". In: *Advances in Space Research* 49.7 (2012), pp. 1212–1228. ISSN: 02731177. DOI: 10.1016/j.asr.2012.01.010.

[5] R. Bewick et al. "Heliotropic dust rings for Earth climate engineering". In: *Advances in Space Research* 51.7 (2013), pp. 1132–1144. ISSN: 02731177. DOI: 10.1016/j.asr.2012.10.024.

[6] S. Bhaskaran. "Deflection Assessment for a Gravity Tractor Spacecraft". In: *2017 AAS/AIAA Astrodynamics Specialist Conference, Stevenson, Washington, August 20-24, 2017* (2017). URL: http://hdl.handle.net/2014/47538.

[7] J. Blackstock et al. "Climate Engineering Responses to Climate Emergencies". In: *Novim* (2009). URL: /files/tkg/files/119.blackstock.etal_.climateengresptoclimemerg.e.pdf.

[8] C. Bombardelli and J. Pelaez. "Ion Beam Shepherd for Asteroid Deflection". In: *Journal of Guidance, Control, and Dynamics* 34.4 (2011), pp. 1270–1272. ISSN: 0731-5090. DOI: 10.2514/1.51640.

[9] M. Bruck Syal, D. S.P. Dearborn, and P. H. Schultz. "Limits on the use of nuclear explosives for asteroid deflection". In: *Acta Astronautica* 90.1 (2013), pp. 103–111. ISSN: 00945765. DOI: 10.1016/j.actaastro.2012.10.025.

[10] C. Chapman. "The hazard of near-Earth asteroid impacts on Earth. Earth Planetary Science Letters". In: *Earth and Planetary Science Letters* 222 (2004), pp. 1–15. DOI: 10.1016/j.epsl.2004.03.004.

[11] A. F. Cheng et al. "AIDA DART asteroid deflection test: Planetary defense and science objectives". In: *Planetary and Space Science* 157 (2018), pp. 104–115. ISSN: 00320633. DOI: 10.1016/j.pss.2018.02.015.

[12] A. F. Cheng et al. "Asteroid Impact and Deflection Assessment mission". In: *Acta Astronautica* 115 (2015), pp. 262–269. ISSN: 00945765. DOI: 10.1016/j.actaastro.2015.05.021.

[13] A. F. Cheng et al. "DART mission determination of momentum transfer: Model of ejecta plume observations". In: *Icarus* 352 (2020), p. 113989. ISSN: 00191035. DOI: 10.1016/j.icarus.2020.113989.

[14] Andrew F. Cheng et al. "Momentum transfer from the DART mission kinetic impact on asteroid Dimorphos". In: *Nature* 616.7957 (2023), pp. 457–460. DOI: 10.1038/s41586-023-05878-z.

[15] D. Conte and D. Spencer. "Targeting the Martian Moons via Direct Insertion into Mars' Orbit". In: 2015.

[16] H. D. Curtis. *Orbital mechanics for engineering students*. Third edition. MATLAB examples. Amsterdam: Butterworth-Heinemann/Elsevier, 2014. ISBN: 978-0080977478. URL: http://www.sciencedirect.com/science/book/9780080977478.

[17] J. Olympio D. Izzo and C. H. Yam. *Asteroid Deflection Theory: fundamentals of orbital mechanics and optimal control*. 2009. URL: https://www.esa.int/gsp/ACT/doc/MAD/pub/ACT-RPR-MAD-2009-AstDeflection.pdf.

[18] B. Dachwald. "Advanced Space Dynamics". In: *Lecture Script* (2021). FH Aachen.

[19] B. Dachwald. "Advanced Space Propulsion". In: *Lecture Script* (2021). FH Aachen.

[20] B. Dachwald. "Low-Thrust Trajectory Optimization and Interplanetary Mission Analysis Using Evolutionary Neurocontrol". In: (2004). URL: http://www.spacesailing.net/paper/Dachwald_PhDThesis.pdf.

[21] B. Dachwald. "Low-thrust trajectory optimization and interplanetary mission analysis using evolutionary neurocontrol". In: *Doktorarbeit, Institut für Raumfahrttechnik, Universität der Bundeswehr, München* (2004).

[22] B. Dachwald. "Optimal Solar Sail Trajectories for Missions to the Outer Solar System". In: *Journal of Guidance, Control, and Dynamics* 28.6 (2005), pp. 1187–1193. ISSN: 0731-5090. DOI: 10.2514/1.13301.

[23] B. Dachwald. "Optimization of very-low-thrust trajectories using evolutionary neurocontrol". In: *Acta Astronautica* 57.2-8 (2005), pp. 175–185. ISSN: 00945765. DOI: 10.1016/j.actaastro.2005.03.004.

[24] B. Dachwald. "Physikalische Grundlagen der Raumfahrttechnik". In: *Lecture Script* (2019). FH Aachen.

[25] B. Dachwald. “Spaceflight Mechanics”. In: *Lecture Script* (2019). FH Aachen.

[26] B. Dachwald and R. Kahle. “Head-On Impact Deflection of NEAs: A Case Study for 99942 Apophis”. In: *Planetary Defense Conference 2007, Wahington D.C., USA, 05-08 March 2007* (2007). ISSN: 0731-5090. URL: https://citeseerx.ist.psu.edu/viewdoc/download?doi=10.1.1.487.4572&rep=rep1&type=pdf.

[27] J. M. A. Danby and T. M. Burkardt. “The solution of Kepler’s equation, I”. In: *Celestial Mechanics* 31.2 (1983), pp. 95–107. ISSN: 0008-8714. DOI: 10.1007/BF01686811.

[28] *Defending planet Earth: Near-Earth object surveys and hazard mitigation strategies*. Washington, D.C.: National Academies Press, 2010. ISBN: 0-309-14968-1.

[29] N. S. Diffenbaugh and C. B. Field. “Changes in ecologically critical terrestrial climate conditions”. In: *Science (New York, N.Y.)* 341.6145 (2013), pp. 486–492. DOI: 10.1126/science.1237123.

[30] Duk. *Conic sections*. No changes - CC Attribution-Share Alike 3.0 Unported - (https://creativecommons.org/licenses/by-sa/3.0/deed.en). 2005. URL: https://en.wikipedia.org/wiki/File:Conic_sections_3.png.

[31] J. D. Feldhacker et al. “Shape Dependence of the Kinetic Deflection of Asteroids”. In: *Journal of Guidance, Control, and Dynamics* 40.10 (2017), pp. 2417–2431. ISSN: 0731-5090. DOI: 10.2514/1.G002270.

[32] C. Fuglesang and M. G. de Herreros Miciano. “Realistic sunshade system at L1 for global temperature control”. In: *Acta Astronautica* 186 (), pp. 269–279. ISSN: 00945765. DOI: 10.1016/J.ACTAASTRO.2021.04.035. URL: doi:10.1016/J.ACTAASTRO.2021.04.035.

[33] L. Gasperini et al. “A possible impact crater for the 1908 Tunguska Event”. In: *Terra Nova* 19.4 (2007), pp. 245–251. ISSN: 0954-4879. DOI: 10.1111/j.1365-3121.2007.00742.x.

[34] A. Gibbings. “A smart cloud approach to asteroid deflection”. In: *62nd International Astronautical Congress 2011, IAC 2011* 2 (2011), pp. 1351–1361.

[35] B. Govindasamy and K Caldeira. “Geoengineering Earth’s radiation balance to mitigate CO 2 -induced climate change”. In: *Geophysical Research Letters* 27.14 (2000), pp. 2141–2144. ISSN: 00948276. DOI: 10.1029/1999GL006086.

[36] J. T. Grundmann et al. “Capabilities of Gossamer-1 derived small spacecraft solar sails carrying Mascot-derived nanolanders for in-situ surveying of NEAs”. In: *Acta Astronautica* 156 (2019), pp. 330–362. ISSN: 00945765. DOI: 10.1016/j.actaastro.2018.03.019.

[37] H.-O. Pörtner, D.C. Roberts, M. Tignor, E.S. Poloczanska, K. Mintenbeck, A. Alegría, M. Craig, S. Langsdorf. “IPCC, 2022: Climate Change 2022: Impacts, Adaptation and Vulnerabilit: Contribution of Working Group II to the Sixth Assessment Report of the Intergovernmental Panel on Climate Change”. In: *Cambridge University Press, Cambridge, UK and New York, NY, USA* (2022), 3065 p.p. URL: doi:10.1017/9781009325844.

[38] T. Heberling et al. “Calculating the momentum enhancement factor for asteroid deflection studies”. In: *Procedia Engineering* 204 (2017), pp. 124–129. ISSN: 18777058. DOI: 10.1016/j.proeng.2017.09.764.

[39] D. Hestroffer et al. “Small Solar System Bodies as granular media”. In: *The Astronomy and Astrophysics Review* 27.1 (2019). ISSN: 0935-4956. DOI: 10.1007/s00159-019-0117-5.

[40] K. A. Holsapple and K. R. Housen. “Momentum transfer in asteroid impacts. I. Theory and scaling”. In: *Icarus* 221.2 (2012), pp. 875–887. ISSN: 00191035. DOI: 10.1016/j.icarus.2012.09.022.

[41] K.R. Housen and K.A. Holsapple. “DEFLECTING ASTEROIDS BY IMPACTS: WHAT IS BETA?” In: *43rd Lunar and Planetary Science Conference* (2012).

[42] International Academy of Astronautics. “IAA PLANETARY DEFENSE CONFERENCE 2023”. In: (2023). URL: https://iaaspace.org/event/8th-iaa-planetary-defense-conference-2023/.

[43] L. Johnson et al. “Solar Sails: Technology And Demonstration Status”. In: *International Journal of Aeronautical and Space Sciences* 13.4 (2012), pp. 421–427. ISSN: 2093-274X. DOI: 10.5139/IJASS.2012.13.4.421.

[44] R. Kahle. “Modelle und Methoden zur Abwendung von Kollisionen von Asteroiden und Kometen mit der Erde”. Doctoral Thesis. Berlin: Technische Universität Berlin, Fakultät V - Verkehrs- und Maschinensysteme, 2005. DOI: 10.14279/depositonce-1226. URL: http://dx.doi.org/10.14279/depositonce-1226.

[45] R. Kahle et al. “Physical limits of solar collectors in deflecting Earth-threatening asteroids”. In: *Aerospace Science and Technology* 10.3 (2006), pp. 256–263. ISSN: 12709638. DOI: 10.1016/j.ast.2005.12.004.

[46] R. G. Kennedy, K. I. Roy, and D. E. Fields. “Dyson Dots: Changing the solar constant to a variable with photovoltaic lightsails”. In: *Acta Astronautica* 82.2 (2013), pp. 225–237. ISSN: 00945765. DOI: 10.1016/j.actaastro.2012.10.022.

[47] S. J. Koppal. “Lambertian Reflectance”. In: *Computer Vision*. Ed. by Katsushi Ikeuchi. Boston, MA: Springer US, 2014, pp. 441–443. ISBN: 978-0-387-30771-8. DOI: 10.1007/978-0-387-31439-6{_}534.

[48] L. Wheeler. *Probabilistic Asteroid Impact Risk Assessment: 2023 PDC Hypothetical Impact Exercise Epoch 3*. 2023. URL: https://cneos.jpl.nasa.gov/pd/cs/pdc23/PDC23-ImpactRisk-Epoch3.pdf (visited on 2023).

[49] NASA Jet Propulsion Laboratory. “Orbits of Potentially Hazardous Asteroids (PHAs)”. In: (). URL: https://www.jpl.nasa.gov/images/orbits-of-potentially-hazardous-asteroids-phas.

[50] Dr. Gregory L. Matloff. “Solar-Sail Earth Defense (SOSED) from NEO Impacts”. In: *57th International Astronautical Congress*. Reston, Virigina: American Institute of Aeronautics and Astronautics, 2006. ISBN: 978-1-62410-042-0. DOI: 10.2514/6.IAC-06-C4.6.04.

[51] C. R. McInnes. *Solar Sailing: Technology, Dynamics and Mission Applications*. Astronomy and Planetary Sciences. London and s.l.: Springer London, 1999. ISBN: 1447139925. DOI: 10.1007/978-1-4471-3992-8.

[52] C.R. McInnes. "Minimum mass solar shield for terrestrial climate control". English. In: *Journal of the British Interplanetary Society* 55.9-10 (2002), pp. 307–311. ISSN: 0007-084X.

[53] C.R. McInnes. "Minimum mass solar shield for terrestrial climate control". English. In: *Journal of the British Interplanetary Society* 55.9-10 (2002), pp. 307–311. ISSN: 0007-084X.

[54] J. Melosh, I. Nemchinov, and Y. Zetzer. "Non-nuclear strategies for deflecting comets and asteroids". In: -1 (1994), pp. 1111–1132. URL: https://www.researchgate.net/publication/234347108_Non-nuclear_strategies_for_deflecting_comets_and_asteroids.

[55] Patrick Michel, Francesca E. DeMeo, and William Frederick Bottke, eds. *Asteroids IV*. The University of Arizona space science series. Tucson and Houston: The University of Arizona Press and Lunar and Planetary Institute, 2015. ISBN: 9780816532131.

[56] Stefano Mottola et al. "The DLR AsteroidFinder for NEOs". In: *38th COSPAR Scientific Assembly*. Vol. 38. Jan. 2010, p. 7.

[57] NASA Jet Propulsion Laboratory. "NASA JPL Horizons System". In: (2023). URL: https://ssd.jpl.nasa.gov/horizons/.

[58] NASA Jet Propulsion Laboratory. "NASA/JPL NEO Deflection App". In: (2023). URL: https://cneos.jpl.nasa.gov/nda/nda.html.

[59] Joris T. Olympio. "Optimal Control of Gravity-Tractor Spacecraft for Asteroid Deflection". In: *Journal of Guidance, Control, and Dynamics* 33.3 (2010), pp. 823–833. ISSN: 0731-5090. DOI: 10.2514/1.46378.

[60] P. Chodas. *The 2023 PDC Hypothetical Impact Scenario: Overview of Asteroid Deflection Issues at Epoch 1*. 2022. URL: https://cneos.jpl.nasa.gov/pd/cs/pdc23/PDC23-Deflection1.pdf (visited on 2023).

[61] S. W. Paek. *A multi-functional paintball cloud for asteroid deflection*. 2012. DOI: 10.13140/RG.2.1.2569.6801.

[62] S. W. Paek et al. "Optimization and decision-making framework for multi-staged asteroid deflection campaigns under epistemic uncertainties". In: *Acta Astronautica* 167 (2020), pp. 23–41. ISSN: 00945765. DOI: 10.1016/j.actaastro.2019.10.042.

[63] Planetary Sunshade Foundation. *Reversing Global Warming*. 2023. URL: https://www.planetarysunshade.org/.

[64] E. S.G. Rainey et al. "Impact modeling for the Double Asteroid Redirection Test (DART) mission". In: *International Journal of Impact Engineering* 142 (2020), p. 103528. ISSN: 0734743X. DOI: 10.1016/j.ijimpeng.2020.103528.

[65] R. S. Ribeiro et al. “Alternative approach to the DART mission by the use of gravity assist maneuvers with the Moon and solar sails”. In: *Scientific reports* 13.1 (2023), p. 6937. DOI: 10.1038/s41598-023-33680-4.

[66] A. S. Rivkin and A. F. Cheng. “Planetary defense with the Double Asteroid Redirection Test (DART) mission and prospects”. In: *Nature communications* 14.1 (2023), p. 1003. DOI: 10.1038/s41467-022-35561-2.

[67] A. E. Roy. *Orbital motion*. Fourth Edition. Boca Raton, London, and New York: CRC Press, 2005. ISBN: 0750310154.

[68] S. Fix. “Feasibility study of a sunshade in the vicinity of the Sun Earth L1 Lagrange Point”. In: 2021. URL: https://static1.squarespace.com/static/60d495bac7a14f7e7507d20b/t/610862ec0ef29060d75365dc/1627939568010/Fix-2021.pdf.

[69] J.-P. Sánchez and C. R. McInnes. “Optimal Sunshade Configurations for Space-Based Geoengineering near the Sun-Earth L1 Point”. In: *PloS one* 10.8 (), e0136648. DOI: 10.1371/journal.pone.0136648. URL: doi:10.1371/journal.pone.0136648.

[70] N. Schmidt, ed. *Planetary Defense: Global Collaboration for Defending Earth from Asteroids and Comets*. Space and Society. Cham: Springer International Publishing, 2019. ISBN: 9783030010003. DOI: 10.1007/978-3-030-01000-3. URL: http://dx.doi.org/10.1007/978-3-030-01000-3.

[71] W. Seifritz. “Mirrors to halt global warming?” In: *Nature* 340.6235 (1989), p. 603. DOI: 10.1038/340603a0.

[72] A. M. Stickle et al. “Modeling impact outcomes for the Double Asteroid Redirection Test (DART) mission”. In: *Procedia Engineering* 204 (2017), pp. 116–123. ISSN: 18777058. DOI: 10.1016/j.proeng.2017.09.763.

[73] J. L. Tonry. “An Early Warning System for Asteroid Impact”. In: *Publications of the Astronomical Society of the Pacific* 123.899 (2011), pp. 58–73. ISSN: 00046280. DOI: 10.1086/657997.

[74] J. Torppa et al. “Asteroid shape and spin statistics from convex models”. In: *Icarus* 198.1 (2008), pp. 91–107. ISSN: 00191035. DOI: 10.1016/j.icarus.2008.07.014.

[75] Y. Tsuda et al. “Achievement of IKAROS — Japanese deep space solar sail demonstration mission”. In: *Acta Astronautica* 82.2 (2013), pp. 183–188. ISSN: 00945765. DOI: 10.1016/j.actaastro.2012.03.032.

[76] P. Vernazza et al. “VLT/SPHERE imaging survey of the largest main-belt asteroids: Final results and synthesis”. In: *Astronomy & Astrophysics* 654 (), A56. ISSN: 0004-6361. DOI: 10.1051/0004-6361/202141781. URL: doi:10.1051/0004-6361/202141781.

[77] M. Vetrisano, C. Colombo, and M. Vasile. “Asteroid rotation and orbit control via laser ablation”. In: *Advances in Space Research* 57.8 (2016), pp. 1762–1782. ISSN: 02731177. DOI: 10.1016/j.asr.2015.06.035.

[78] G. Vulpetti, L. Johnson, and G. L. Matloff. *Solar sails: A novel approach to interplanetary travel*. New York, NY: Copernicus Books Springer, 2008. ISBN: 0387344047.

[79] B. Wie. "Dynamics and Control of Gravity Tractor Spacecraft for Asteroid Deflection". In: *Journal of Guidance, Control, and Dynamics* 31.5 (2008), pp. 1413–1423. ISSN: 0731-5090. DOI: 10.2514/1.32735.

[80] B. Wie. "Hovering control of a solar sail gravity tractor spacecraft for asteroid deflection". In: *Advances in the Astronautical Sciences* 127 (Jan. 2007).

[81] P. Wiegert. "On the Delivery of DART-ejected Material from Asteroid (65803) Didymos to Earth". In: *The Planetary Science Journal* 1.1 (2020), p. 3. ISSN: 0004-637X. DOI: 10.3847/PSJ/ab75bf.

[82] William E. Wiesel. *Spaceflight dynamics*. 3rd ed. Beavercreek, Ohio: Aphelion Press, 2012. ISBN: 978-1452879598.

[83] R. Willnecker. "Erforschung und Nutzung des Weltraums". In: *Lecture Script* (2019). FH Aachen.

[84] Y. Sugimoto. "Hazardous asteroid mitigation: campaign planning and credibility analysis". In: 2014. URL: http://theses.gla.ac.uk/5388/14/2014sugimotophd.pdf.

[85] D. Yeomans et al. "Deflecting a Hazardous Near-Earth Object 1 st IAA Planetary Defense Conference: Protecting Earth from Asteroids 27-30 April 2009 Granada, Spain". In: (Aug. 2020). URL: https://cneos.jpl.nasa.gov/doc/PDC_proceedings_062009.pdf.

[86] P. Zhao, Chenchen WU, and Yangmin LI. "Design and application of solar sailing: A review on key technologies". In: *Chinese Journal of Aeronautics* 36.5 (2023), pp. 125–144. ISSN: 10009361. DOI: 10.1016/j.cja.2022.11.002.

Declaration

I hereby affirm that I have written this thesis independently and have not used any sources other than those listed in the bibliography.
Passages that have been taken literally or analogously from published or not yet published sources are marked as such.
The pictures or illustrations in this work have been made by myself or are accompanied by a corresponding reference.
This thesis has not yet been submitted in the same or a similar form to any other examination office.

Bremen, August 2023

Fabienne Seibert